Autoignition Studies Of Gasoline Surrogate Fuels

In The Advanced Fuel Ignition Delay Analyzer

by

Drew Morales Cameron

B.S., Seattle University, 2015

A thesis submitted to the

Faculty of the Graduate School of the

University of Colorado in partial fulfillment

of the requirement for the degree of

Master of Science

Department of Mechanical Engineering

2017

This thesis entitled:
Autoignition Studies Of Gasoline Surrogate Fuels
In The Advanced Fuel Ignition Delay Analyzer
written by Drew Morales Cameron
has been approved for the Department of Mechanical Engineering

_____

Professor John Daily

_____

Professor Peter Hamlington

_____

Professor Nicole Labbe

Date_____

The final copy of this thesis has been examined by the signatories, and we find that both the
content and the form meet acceptable presentation standards of scholarly work in the above
mentioned discipline.

Abstract

Drew Morales Cameron (M.S., Mechanical Engineering)

Autoignition Studies Of Gasoline Surrogate Fuels In The Advanced Fuel Ignition Delay

Analyzer

Thesis directed by Professor John Daily and Dr. Bradley Zigler (NREL)

Improving vehicle efficiency is a substantial way to reduce $CO_2$ emissions from the transportation sector. The most limiting factor of spark ignition (SI) gasoline engine efficiency is the phenomenon known as knocking. The current methods to characterize fuel knock resistance are with the Research Octane Number (RON) and Motor Octane Number (MON) methods. However, it has been shown that these engine-based test methods do not directly predict knock resistance in modern direct injection (DI) gasoline engines, especially under boosted conditions. Alternative test devices have been used to more directly study ignition kinetics. Constant volume combustion chambers (CVCCs) have been used to obtain valuable autoignition data at a broader ranger of pressure and temperature conditions than the single point engine operating conditions of the RON and MON tests. This study uses a new CVCC to study gasoline range fuels at engine relevant conditions to collect autoignition data on a set of simple gasoline surrogate fuels and correlate these data to the fuel chemistry and properties. A set of nine gasoline surrogates, with and without oxygenates were tested in the Advanced Fuel Ignition Delay Analyzer (AFIDA). The main outputs of this study are 3D surfaces of autoignition (ignition delay time) as a function of pressure and temperature. These data more completely characterize ignition delay at a wide range of engine relevant conditions, providing more insight than the RON and MON tests. Linear regression was performed between the ignition delay time and the fuel composition and properties, however significant correlations were not found. This study paves the way for more

complex, full-boiling range gasoline fuels to be characterized in the AFIDA, fuels which are too

complex to model with chemical kinetics.

Dedication

This thesis is dedicated this to my parents Denise Morales and Don Cameron whose love, support, and scientific encouragement helped me accomplish my goals. I also dedicate this thesis in memory of David Helete who made me the scientist I am today. I could not have done this with out any of you.

## Acknowledgments

# Contents

# Tables

# Figures

# Acronym List

AFIDA: Advanced Fuel Ignition Delay Analyzer

ASTM: American Society for Testing and Materials

AVFL: Advanced/Vehicles/Fuels/Lubricants

BDC: Bottom Dead Center

CN: Cetane Number

CRC: Coordinating Research Council

DCN: Derived Cetane Number

DHA: Detailed Hydrocarbon Analysis

DI: Direct Injection

FACE: Fuels for Advanced Combustion Engines

G-CN: Generic Cetane Number

GHG: Greenhouse Gas

HPLC: High Performance Liquid Chromatography

ID: Ignition Delay

IQT: Ignition Quality Tester

LLNL: Lawrence Livermore National Laboratory

LTHR: Low-Temperature Heat Release

MON: Motor Octane Number

NREL: National Renewable Energy Laboratory

NTC: Negative Temperature Coefficient

ON: Octane Number

PRF: Primary Reference Fuel

RCM: Rapid Compression Machine

RON: Research Octane Number

S: (Octane) Sensitivity

SI: Spark Ignition

TDC: Top Dead Center

TRF: Toluene Reference Fuel

TSF: Toluene Standardization Fuel

CHAPTER 1

Introduction

## 1.1 Motivation

In the United States, the transportation sector consumes a significant amount of petroleum (see Figure 1 and Figure 2), and is therefore a significant contributor of greenhouse gas (GHG) emissions [1]. Light duty vehicles dominate the transportation sector (see Figure 3), and the majority of those vehicles are powered by spark ignition (SI) internal combustion engines [2,3]. It is crucial to increase efficiency of SI engines to reduce these emissions.
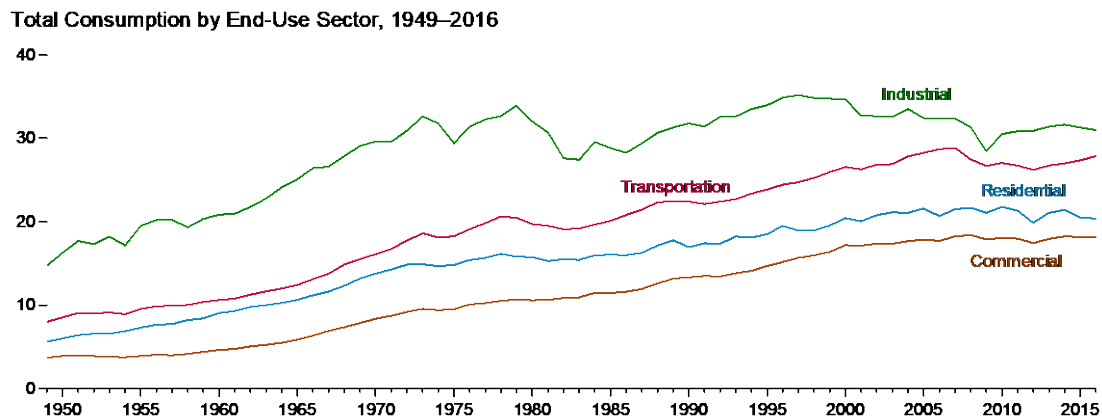
Figure 1: United States total energy consumption by end-use sector, 1949-2016 in Quadrillion ($10^{15}$) British Thermal Units (BTUs) [1].
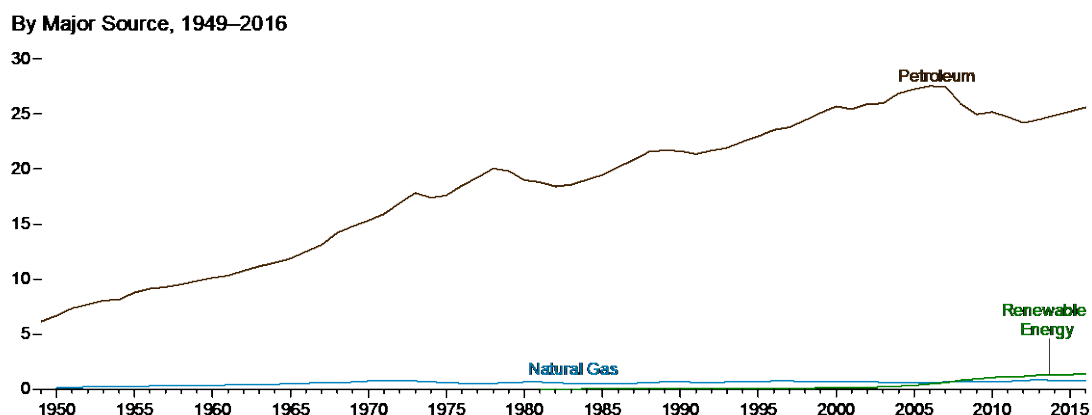
Figure 2: United States total transportation sector energy consumption by major source, 1949-2016 in Quadrillion BTUs [1].
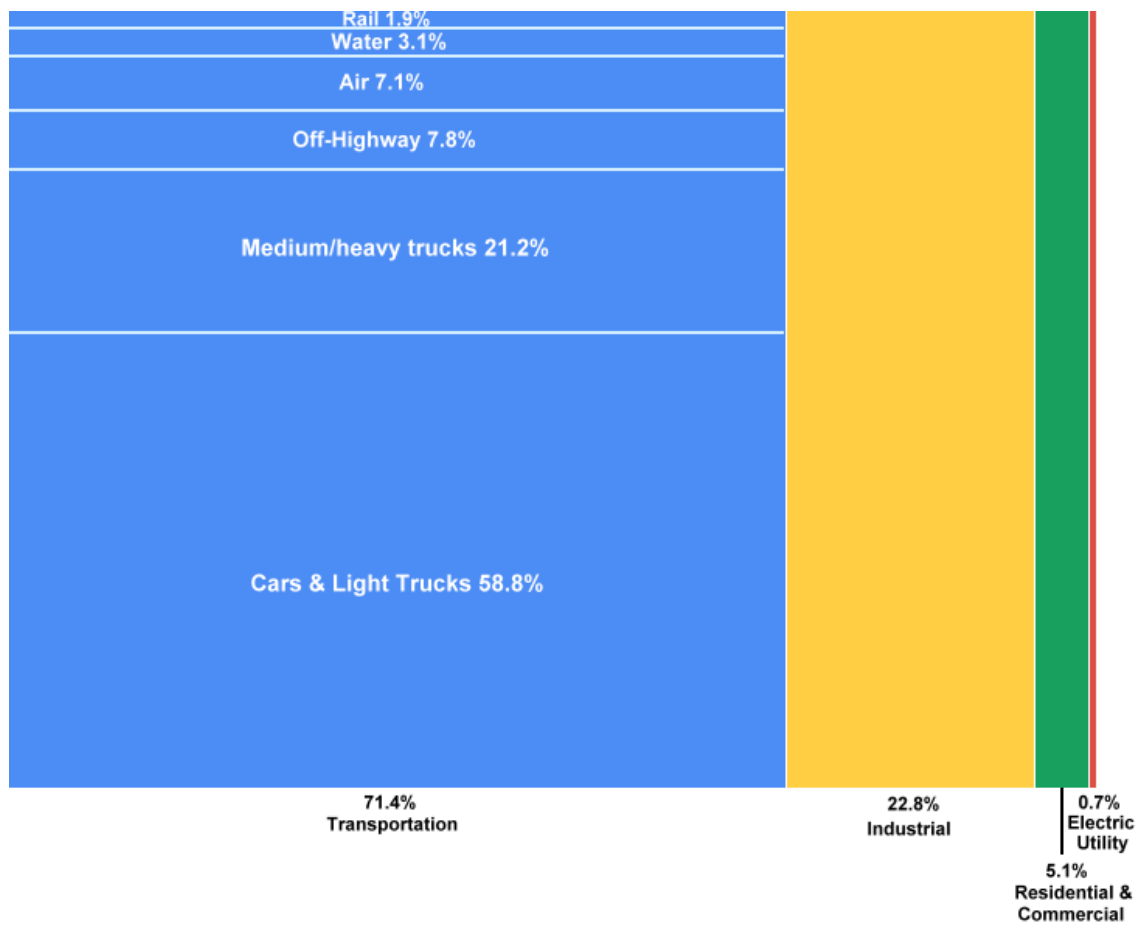
Figure 3: United States total petroleum consumption by sector, 2016 [2].

The phenomena of knock, has long been a limiting factor of SI engine efficiency [4]. Fuel knocking refers to the autoignition of unburned gasoline fuel/air mixture (endgas) as the flame front propagates across the combustion chamber [5]. Figure 4 is a visual representation of a normal combustion event in an SI engine (A) to a knocking event (B). It is named fittingly as extreme knocking is signified by the loud sound of an unintentional combustion event, which can cause extensive engine damage. Smaller knocking events cause a decrease in efficiency and interference with the engine cycles. In SI engines, efficiency is limited by the compression ratio, which is the ratio of the volume of the cylinder when the piston is at bottom dead center (BDC) to the volume of the cylinder when the piston is at top dead center (TDC) [6]. Compression ratio is related to the Carnot cycle efficiency by Equation (1.1), where r is the compression ratio and k

is the specific heat ratio [6]. For the advancement of SI engines the knocking propensity of fuels

must be accurately characterized at modern engine relevant conditions.

$$\eta = 1 - \frac{1}{r^{k-1}} \tag{1.1}$$
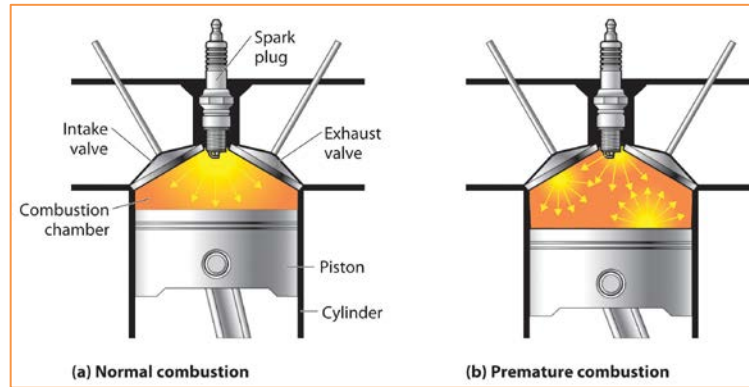


Figure 4: Comparison of a normal combustion event (A), to a knocking, or premature combustion event in (B) in an SI engine [7].

## 1.2 Background

As automotive companies employ novel technologies such as down-sizing, down-

speeding, and turbocharging to increase efficiency, all of which rely on increased combustion

temperatures and pressures, it is critical to accurately characterize the knocking potential of fuels

[8]. The current method to characterize the knocking potential is known as the octane number

(ON), which corresponds to the fuel's resistance to knocking autoignition. The two related

methods used for gasoline fuels are, Research Octane Number (RON) and Motor Octane Number

(MON) [9,10], the average of which is commonly shown on commercial gasoline fuel pumps. In

these tests the fuel's knocking quality is compared to that of Primary Reference Fuels (PRFs),

which are volumetric mixtures of iso-octane and n-heptane. The PRFs define the octane rating.

Iso-octane is the definition of ON 100 and n-heptane is the definition of ON 0. The RON and

MON tests are conducted at specific engine conditions, lower intake temperatures and slower

engine speeds, versus higher intake temperatures and faster engine speeds respectively [11]. The

difference between RON and MON is known as the octane sensitivity (S), which indicates the difference in performance at different engine conditions. The RON and MON octane rating methods involve engine testing with technology dating to the 1920s, and have been shown to no longer directly predict knock resistance in modern SI engines, especially those with gasoline direct injection [2,8]. The RON and MON tests also fail to evaluate significant fuel chemistry effects that biofuels have in resisting knock [12,13]. The engine research and development community requires more accurate methods of quantifying a fuel's knock resistance to support advanced SI engine development with simultaneous changes in fuel blend composition.

## 1.3 Current Work

Significant work has been carried out in shock tubes, rapid compression machines (RCMs), and chemical kinetic simulations to characterize fuels and examine the ignition delay (ID) times in these various set-ups. ID time is the time it takes for a fuel to combust after it has been introduced to the system and is frequently used to measure the ignitability of the fuel. Studies in the Ignition Quality Tester (IQT), a constant volume combustion chamber (CVCC) or similar devices can be used to compliment RCM, and shock tube work. While the capabilities of RCM and shock tube devices are improving they have previously been limited to homogenous mixtures, and high-volatility fuels [14, 15, 16, 17]. Additionally these tests have long set-up/testing times, making it difficult to test large fuel sets efficiently [18]. While these tests are valuable there is a need to characterize high quantities of lower-volatility fuels in CVCCs like the IQT.

Similar kinetics data can be obtained in single-cylinder engines, however these tests are complex and typically less repeatable [18]. Additionally large volumes of fuel are required for these engine tests compared to the hundreds of mL or less, which is required to run extensive

testing in most CVCCs. The small volume of fuel required for CVCCs make them ideal for screening new fuels that are not available in high quantities. While there are many competing methods for characterizing fuels the IQT and similar devices provide important information and can be helpful both in screening new fuels, but also in providing validation of chemical kinetic models for complex fuel mixtures [19]. CVCCs also have the advantage of providing purely quiescent ambient conditions, which are not obtainable in flow devices such as shock tubes, RCM, and engines [20]. The higher ID times in the IQT allows for the mixture to reach a quasi-homogenous state, which allows the fuel chemistry effects on ignition delay to be studied with minimal interference from the fuel spray physics [19].

## 1.4 Research Plan

The goal of this research is to develop a methodology to evaluate the ignition behavior of gasoline surrogate fuels (both simple and complex) using a research CVCC and subsequently develop correlations between fuel properties, composition, and autoignition characteristics. This research was conducted at the National Renewable Energy Laboratory (NREL) with the use of the IQT and newer CVCC, the Advanced Fuel Ignition Delay Analyzer (AFIDA). The original goal was to study a set of 19 complex surrogate gasoline blends in cooperation with the Coordinating Research Council, who developed the fuels and studied them extensively in both direct injection (DI) and port fuel injection SI engines. The fuels would be analyzed in the IQT and correlations developed with the fuel properties, as well as chemical makeup to follow. However, the course of research was altered and a reduced set of simpler gasoline surrogate fuels was studied in the AFIDA instead.

These parametric ignition delay studies of gasoline surrogates in the AFIDA will help enable a bridge to link differences in fuel chemistry and how those differences impact engine

knock limits and thus, engine efficiency. The current standard for evaluating knocking potential of gasoline, RON and MON no longer describe knock performance in direct terms for modern DISI engines. Octane sensitivity (S), the difference between RON and MON has become more relevant and indicative of knocking potential than RON or MON alone [11]. Higher S, and lower MON actually helps efficiency in boosted DI engines, counter-intuitive to logic that a higher MON and RON rating equates to higher auto ignition, or knock, resistance. This study will more fully describe knock resistance than RON or MON alone, as these tests will be conducted over a broad ranger of parametric space of temperature and pressure compared to the single operating points of RON and MON tests. This study will also pave the way for further autoignition studies of complex gasoline range blends relevant to engine operating conditions, as shock tubes and most RCMs tend to operate at higher temperatures and lower pressures than engines. Although improvements have been made in these more fundamental devices for ignition kinetics measurements, shock tubes and RCMs are still challenging to operate with wide boiling range fuels. This research will also enable the AFIDA to provide support in validating chemical kinetic mechanisms. Currently chemical kinetic mechanisms are available to model simple fuels blends; some of the components this study uses, such as iso-octane, and n-heptane have well-established models. However blending effects (especially with oxygenates) have not been extensively studied under engine-relevant conditions. More importantly, more realistic, complex gasoline surrogates and real, full-boiling range gasolines are not currently modeled with detailed kinetic mechanisms. This study is establishing the groundwork with simple surrogate blends that will enable NREL to transition to full-boiling range gasolines, which are not simple to model, and would need well-controlled, engine-relevant experimental validation which the AFIDA can support.

CHAPTER 2

Experimental

## 2.1 Fuel Sets

The Coordinating Research Council (CRC) is a non-profit organization that directs

studies on the interaction between automotive/other mobility equipment and petroleum products

[21]. The Advanced Vehicles/Fuels/Lubricants 20 (AVFL-20) study investigates efficiency

advantages for increased octane number fuels that may be available from ethanol or other blend

components in modern light-duty vehicles [22]. For this study the CRC developed a fuel matrix

to allow exploration of a wide range of ethanol content (10 to 30 vol. %), RON (91 to 102), and

sensitivity (S=RON-MON) (6 to 7 and 10 to 12) [22]. Further studies with this AVFL-20 fuel set

have been conducted as part of the AVFL-30/31 project. The objective of this project is to

evaluate combustion properties of the AVFL-20 test fuel set using a laboratory ignition

characterization method to develop correlations between fuel properties, composition, and

autoignition characteristics [22]. The CRC shared the fuel set with NREL for this study to be

conducted in NREL's research CVCCs.

After initial testing on the AVFL-20 fuel matrix and working through experiments and

equipment setbacks, a different set of fuels as seen in Table 1 was eventually chosen for testing

and correlation work instead. The new set of fuels is publicly available and does not require CRC

panel permission for publication thus expediting the research process. This fuel set had been

used in a previous single cylinder research engine study of knock limited engine performance

and particulate matter emissions at NREL, and was designed to vary heat of vaporization (HOV)

while keeping RON and S close to constant [23]. The fuel set, with the exception of FACE

research gasoline B, consists of simple surrogate blends with up to six different components,

toluene, iso-octane, n-heptane, ethanol, anisole, and p-cresol. Toluene, iso-octane, and n-heptane were blended into Primary Reference Fuels (PRF), Toluene Standardization Fuels (TSF), and Toluene Reference Fuel (TRF) with ethanol, anisole, and p-cresol blended by volume percent as noted (i.e. E25=25 vol. % ethanol) [24, 25]. Before either set of fuels was tested in a CVCC initial screening was done with a fuel from CRC AVFL-24. AVFL-24 developed a set of fuels known as the Fuels for Advanced Combustion Engines (FACE) research gasolines [26]. The FACE gasoline matrix is composed of 10 fuels designed around the four properties of aromatic content, RON, S, and normal-paraffin content [26]. These fuels were designed by the CRC FACE working group, produced by Chevron Philips Chemical Company, and made available in research quantities to enable advanced combustion researchers to make comparison of results from different laboratories of the same, well defined fuel set [26]. Due to the large quantity of these fuels, and the similarities in properties (fuel boiling point, RON) to the AVFL-30 fuels, FACE B was selected from the matrix to conduct initial screening with until the test procedure was vetted. While the original AVFL-20 fuel set consists of gasoline range fuels and would be interesting to analyze due to the available detailed hydrocarbon analysis (DHA), span of RON, span of S, and span of ethanol content, the new fuel set in Table 1 is ultimately a better fit for this study, with more tractable data and simple chemical compositions with which to correlate.

Table 1: Properties of fuel set.

| Fuel | Density (g/mL) | RON | S | HOV (kj/kg) |
|---|---|---|---|---|
| PRF 100 | 0.692 | 100 | 0 | 303 |
| TSF99.8 | 0.820 | 99.8 | 11.1 | 390 |
| E25 in TRF88 | 0.754 | 101.6 | 10.7 | 489 |
| E40 in TRF71 | 0.770 | 99.2 | 12.2 | 595 |
| E20 + 2% p-cresol in TRF88 | 0.757 | 101.1 | 9.4 | 472 |
| E20 + 6% anisole in TRF88 | 0.769 | 99.9 | 9.6 | 472 |
| TRF88 | 0.742 | 87 | 5.2 | 348 |

| E25 in FACE B | 0.720 | 105.6 | 11.8 | 485 |
|---|---|---|---|---|
| FACE B | 0.697 | 95.8 | 3.4 | 340 |

## 2.2 Ignition Quality Tester

2.2.1 Ignition Quality Tester: Design

The Ignition Quality Tester (IQT) is a CVCC with a spray injection system, intended to measure the combustion propensity of diesel fuels [27, 28, 29, 30]. The Derived Cetane Number (DCN) is the metric for rating the propensity of a fuel to ignite, analogous to how the ON rates the anti-knocking propensity of gasoline fuels [31]. The DCN is mathematically derived, by relating a measured ignition delay time to a cetane number measured by ASTM D613 single cylinder engine-based method [32]. The IQT was designed to run samples of diesel fuels to determine the DCN. The IQT is intended to control chamber temperature, chamber pressure, and air-fuel ratio, while the ignition delay time and the DCN are measured. The IQT holds pressure and temperature constant, while the fuel is injected into the chamber. Under these conditions the fuel will autoignite; the time from start of injection to rapid pressure rise, and thus combustion of the fuel is called the ignition delay (ID) time measurement, and is on the order of ones to hundreds of milliseconds.

The IQT consists of a 3 main components, which can be seen in Figure 5: a heated chamber (1), a fuel injection system (2), and computer (3) that runs the software to control the tests and analyze the results. The fuel injection system consists of a pneumatically driven mechanical fuel pump with a single-hole S-type delayed (inward-opening) pintle nozzle [19,33]. The injector nozzle is cooled by a closed loop liquid-to-air cooling system [34]. The fuel line is pressurized to 50 psi during tests, and 2600±50 psi during injections.

Figure 5: Ignition Quality Tester device, with 3 main components. 1: Combustion chamber. 2: Fuel delivery system. 3: Computer/software controls [34].

A cross section of the combustion chamber can be seen in Figure 6. The combustion chamber is electrically heated, and thermally insulated. The front end houses the fuel injector, and thermocouples to monitor the nozzle temperature. The back of the combustion chamber houses a pressure transducer. The pressure transducer measures the pressure in the chamber during the injection and the combustion event, to obtain data for the pressure profile. A thermocouple referred to as 'air back temperature' is in close proximity to the pressure transducer to monitor temperature and pressure in the same area of the chamber. Two other thermocouples measure the internal temperature of the chamber, the average of which is reported in the software. Additionally two other thermocouples monitor the outer surface temperature of the combustion chamber.
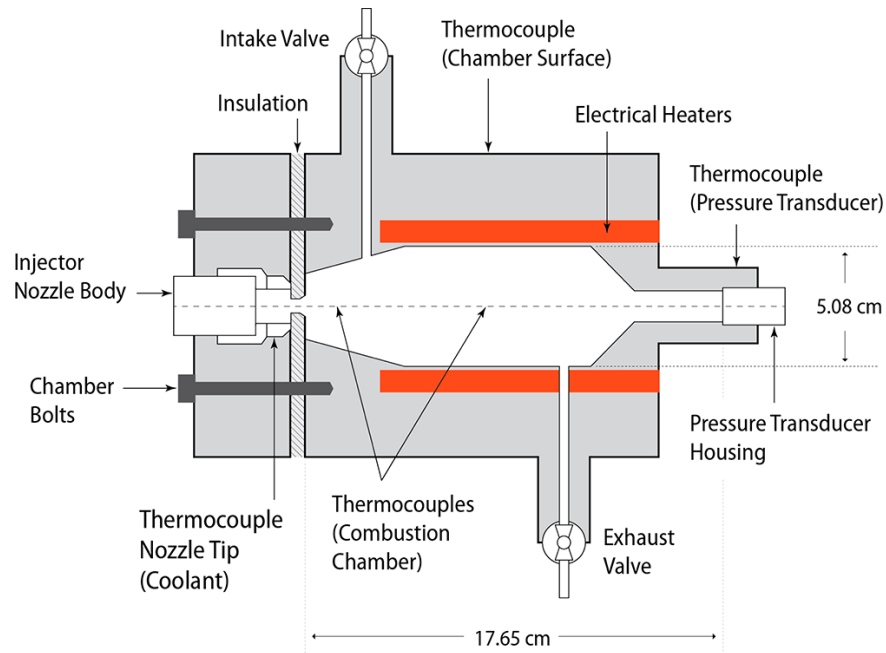
Figure 6: Cross section schematic of the IQT combustion chamber [19].

The software enables the user to control the test, and collects data from the pressure transducer, chamber thermocouples, and needle lift of the injector. While the test is being conducted plots are updated in real time of the needle lift profile and the pressure trace. The needle lift plot essentially shows when and how much fuel is being injected into the chamber. The pressure trace shows the change in chamber pressure over time. The software also processes the data and outputs DCN and ID time measurements. This software defines ID time as the time from the start of injection, to the 'pressure recovery point' (calculates as 138kPa above the initial chamber pressure based on ASTM D6890 conditions) [31, 35]. The software calculates DCN from ID time according to an empirical correlation relating ID time to Cetane Number as measured in the single cylinder cetane rating engine [31, 32].

2.2.2 Ignition Quality Tester: Derived Cetane Number Test

The IQT is designed to run under DCN conditions, using a 20.9% oxygen balance nitrogen diluent at a chamber pressure of 310 psi (~21 bar) [32]. ASTM D6890 requires

verification of IQT calibration each time the instrument is used. The combustion skin

temperature is adjusted so that pure n-heptane has a measured ignition delay of $3.78 \pm 0.03$

milliseconds before DCN measurements begin [32]. The resulting air temperature for DCN

conditions is typically around 545°C. Each test consists of 15 pre-injections to stabilize

conditions and 32 main (measured) injections. The result is an average ID time that is taken over

all 32 main injections. The software calculates DCN from ID according to an empirical

correlation relating ID to Cetane Number as measured in the single cylinder cetane rating engine,

as show in Figure 7 [31, 32].
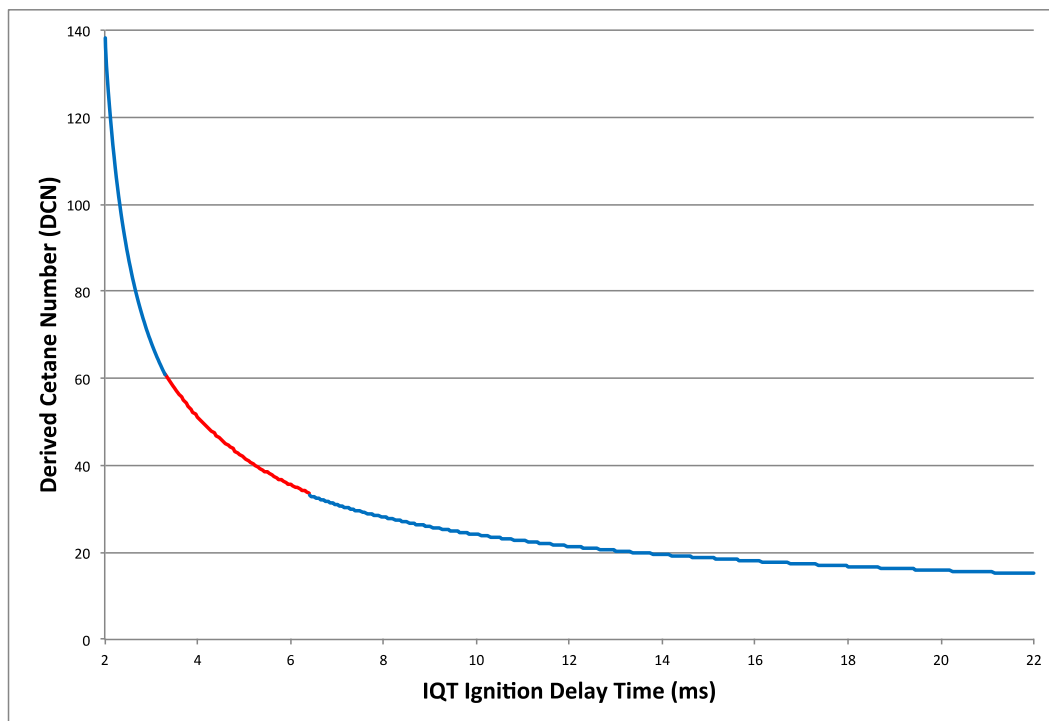


Figure 7: Plot of Derived Cetane Number versus Ignition Delay Time in the IQT. The red portion represents the normal range of DCN values for diesel-like fuels.

2.2.3 Modified Ignition Quality Tester: Temperature Sweep Test

The IQT was originally designed to measure diesel fuels over an ignition delay range

from 3.1 ms to 6.5 ms (64 DCN to 33 DCN), and as such the software's definition of ID time, is

inaccurate for gasoline range fuels [31]. Many diesel fuels ignite in one stage and have short

ignition delay times, where gasoline fuels can have 2-stage ignition defined by low-temperature heat release (LTHR), and then the main ignition event. NREL developed a LabVIEW-based independent control system to allow for much longer ID measurements and to adjust the definition of start of combustion, for gasoline fuels [32]. With the independently controlled system, ID time is calculated by a user defined fixed pressure point, above the initial chamber pressure, to describe the entire ignition event [32]. Prior research conducted by NREL focused on the ability to produce IQT data suitable for kinetic mechanism development feedback, as the ID time from the IQT inherently includes both physical ID effects (spray breakup and evaporation) as well as chemical kinetic ID effects [32,33].

Another unique capability of the NREL's modified IQT is to test fuels across a temperature range, as opposed to a single temperature condition in the DCN tests [32, 35]. For this test the IQT chamber is pressurized to a user specified pressure, typically 10, 20, or 30 bar using 20.9% oxygen in nitrogen balance and heated to approximately 730 °C, as measured by the air back thermocouple in the IQT. The amount of fuel injected is adjusted for each fuel to maintain a fuel-air equivalence ratio ($\phi$) of 1 at an air back temperature of 700 °C, charged to 145 psi. Once the test is started, the heaters are turned off to let the temperature drop gradually throughout the test. This test allows for the collection of chemical kinetic combustion data over a wide range of temperatures. Five pre-injections are done at the beginning of the test. The main injections are allowed to continue until the ignition delay becomes >400 ms or the air back thermocouple temperature reaches approximately 375 °C. The temperature drop from ~700 °C to ~ 375 °C takes around two hours. Main injections are performed about every 30 seconds. The mass of fuel injected is kept constant through this test, however the number of moles in the chamber is increasing as the temperature drops by the ideal gas law as pressure and volume

remain constant, thus creating leaner conditions as the test progresses to low temperatures. The mass of fuel injected is adjusted mechanically by inserting varying thickness of shims that effectively changes the pneumatic pressure intensifier stroke. The process of changing shim is extensive and requires the user to take apart the fuel reservoir while testing is stopped. Thus it is not possible to adjust the mass of fuel injected during the test.

2.2.4 Ignition Quality Tester: FACE B Trials

The IQT has been used to conduct temperature sweep tests in previous studies on gasoline range fuels. However, most studies have been centered on PRFs or surrogate gasoline blends, consisting of a few components. The lower boiling point of gasoline blends compared to PRFs and diesel fuels poses a challenge to conducting tests in the IQT. Since fuel in the IQT reservoir, transfer lines, and injector nozzle is pressurize at 50 psi before the pressure is ramped up to ~2600 psi for an injection event, lower boiling point fuel fractions can begin to boil within the IQT fuel system at high chamber temperatures (and pressures) that increase the heat transfer to the injector tip. Previously gasoline surrogate blends that encounter boiling issues have been run in the IQT at NREL. To remedy this issue in the past, the bleed off valve (A) as seen in Figure 8, which is located near the injector nozzle was opened and closed right before the injection. This expelled the vaporized fuel from the line, and replenished it with un-boiled fuel. For previous gasoline surrogate blends this was successful in maintaining the fuel-air equivalence ratio throughout the test for the surrogate blends, which can be confirmed by the needle lift profile. The area under the needle lift profile represents the mass of fuel injected, thus when significant changes occur in the profile it is clear the global air fuel ratio is changing.

The AVFL-20 gasoline blends, as well as FACE B, have low initial boiling points, thus fuel boiling was expected during these tests in the IQT. The boiling would negatively affect the

amount of fuel injected during the temperature sweep test, and result in an inconsistent fuel-air

ratio. To accommodate the high quantity of AVFL-20 samples (19 different fuel blends) to be

tested in the IQT (57 different tests at 2 hours each) a few options were explored to modify the

IQT and automate a solution to prevent fuel boiling. The first option is to chill the sample and

the second is to automate the opening and closing of the bleed off valve. Unfortunately the fuel

cannot be chilled in the nozzle where the boiling is occuring. The nozzle is in close proximity to

the combustion chamber and to sufficiently cool the fuel, would compromise the constant

chamber temperature requirement. Thus to accommodate the high quantity of gasoline range

AVFL-20 fuels it was decided to design and install an automated bleed off valve.



Figure 8: Image of the IQT device. Of importance is the circled bleed off valve [34].

The ASCO EF8262H006V solenoid valve was chosen for this application. It is rated for

use with fuel and oil, and can withstand pressures of 120 psi. The valve would be situated in line

with the original system, and replace the original bleed off valve. This set up can be seen in

Figure 9. After procuring the parts, installing the system, and coding the controls, by NREL

colleagues Jon Luecke, Riley Abel, and Jon Burton. Tests with FACE B were attempted. This

test revealed that the new automated system did not work. In fact the automated system was not

injecting any fuel into the chamber. A few hypotheses were formulated to explain the lack of injection. One hypothesis is that the seal of the solenoid valve is leaking during the injection event. The pressure in the fuel line increases sharply ~2600 psi when the fuel is injected, this surpasses the 120 psi the valve is rated for, thus causing fuel to bypass the valve and preventing the pressure in the line from reaching the value needed for injection. The other hypothesis is that the volume added to the fuel line with the solenoid valve configuration, could be too large, thus preventing the pressure from being reached and the injection from occurring. Unfortunately it would take time and resources to attempt to fix the solenoid valve system, thus moving forward the tests were conducted while manually purging the bleed off valve.
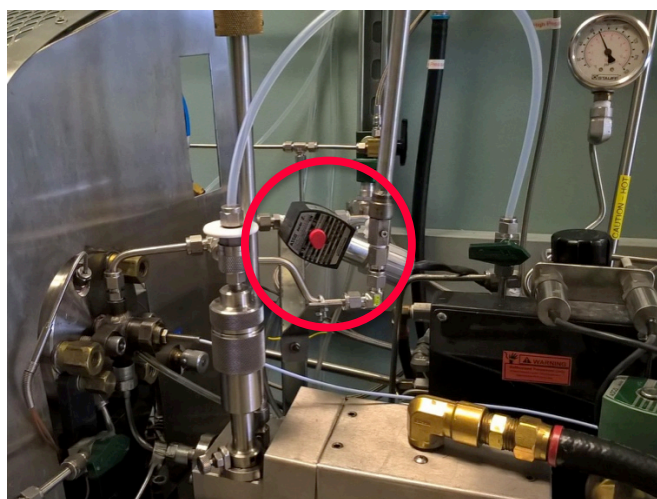


Figure 9: Image of the IQT with the automated solenoid valve replacing the typical manual bleed off valve.

After some initial testing with FACE B in the IQT, which has a similar boiling point to the AVFL-20 samples, it was discovered that the sample was still boiling regardless of the fuel bleed off. As the test continued the needle lift profile of the injected fuel was consistently decreasing. Additionally the fuel reservoir needed to be refueled partway during the tests, as well as opened and evacuated at the end of the test. Each time the fuel reservoir was opened fuel boiling was visibly observable. This study was continued and temperature sweeps were

conducted at 5, 10 and 15 bar, changing the fuel reservoir often and bleeding the fuel off after

each injection to try to mitigate the boiling issues. Figure 10 shows the temperature sweep data

for FACE B at 15 bar, it is clear the ID time is very inconsistent due to fuel boiling, especially at

lower temperatures. The test starts at 725 °C and drops steadily throughout the test until around

400 °C. At the lower temperatures the fuel has been heated in the reservoir for the duration of the

high temperature tests and thus sees more extreme vaporization affecting the fuel-air ratio. It is

clear from this data that the AVFL-20 fuel set cannot be consistently run in the IQT per the

original plan.
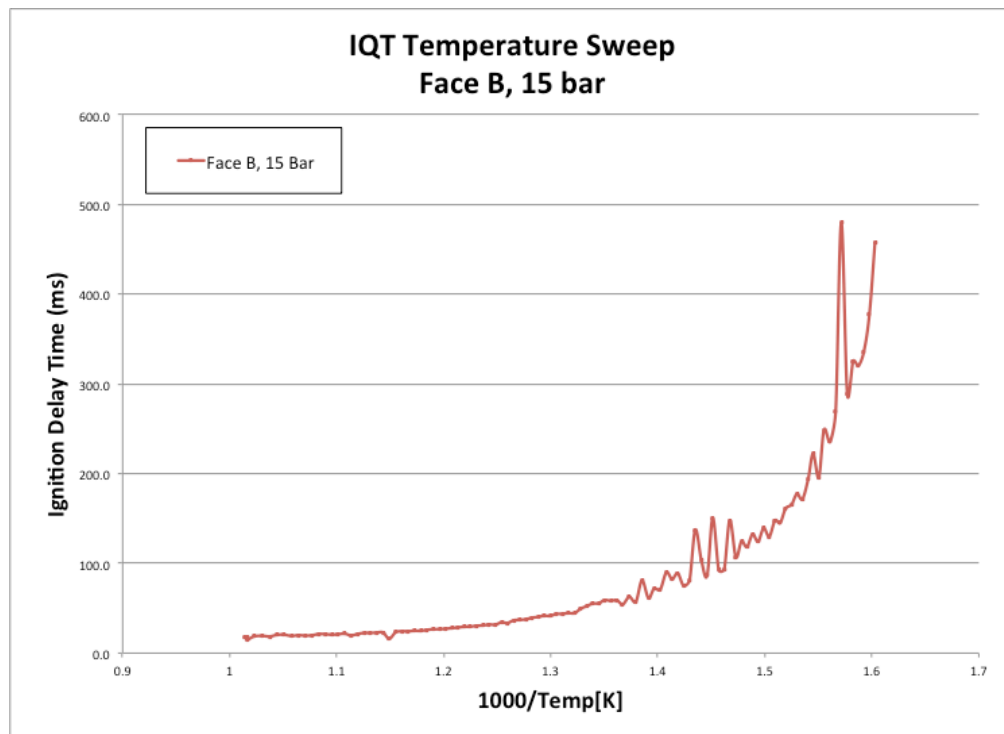


Figure 10: Inverse temperature versus ID time for FACE B conducted at 15 bar in the IQT.

## 2.3 Advanced Fuel Ignition Delay Analyzer

### 2.3.1 Advanced Fuel Ignition Delay Analyzer: Introduction

Upon completion of the FACE B trials in the IQT, the possibility of running the tests in

NREL's new research CVCC the Advanced Fuel Ignition Delay Analyzer (AFIDA) was

explored [36]. In June 2016, NREL acquired the AFIDA 2805, a constant volume research combustion chamber indented to measure Generic Cetane Number (G-CN, similar to DCN) of diesel fuels, in addition to custom parametric studies of ignition delay. This was around the time the FACE B trial experiments were being conducted in the IQT. The AFIDA is ideal for this study since the fuel line is highly pressurized to support a common-rail type piezoelectric fuel injector, which also avoids fuel boiling. The AFIDA was designed for the fully automated determination of the ignition behavior, G-CN and analysis of exhaust gases of diesel fuels [37]. The advantages of testing in the AFIDA include: automated design with a 16-place autosampling carousel, high user control of test parameters, no temperature tuning required for standardized cetane number tests (unlike other constant volume devices), high repeatability, high fuel line pressure using a high-performance liquid chromatography (HPLC) pump, and use of a common rail type piezoelectric fuel injector. The use of the common rail type piezoelectric fuel injector significantly reduces the spray physics dominated portion of overall ID time, allowing greater focus on the chemical kinetics dominated portion of ID. The experiments were not originally planned in the AFIDA, since the device is new both on the market and to NREL, making extensive fuel mapping and device characterization necessary before experiments could be conducted. Still, the AFIDA is ideal for this study since the fuel line can be highly pressurized, up to 2100 bar to avoid fuel boiling. For this reason as well as more precise temperature control, the AFIDA, was chosen to complete the study. NREL's AFIDA is one of four units custom built for non-standard (G-CN), flexible operation, and is currently the only such AFIDA located outside of Europe.

2.3.2 Advanced Fuel Ignition Delay Analyzer: Design

The AFIDA is a fully automated ignition delay analyzer. The device consists of the combustion chamber, fuel delivery system, and computer software that controls the device. The device set up can be seen in Figure 11. Figure 12 shows a schematic of the main components in the AFIDA. The AFIDA has a maximum chamber temperature of 1000 K, a maximum initial charge pressure of 50 bar, and a maximum line pressure of 1200 bar. The fuel delivery system consists of a fully automated sample selection carousel, with a 16 sample capacity at 40 mL per sample. The fuel carousel is capable of heating the fuels, enabling testing of fuels that are solid at room temperature. A high-pressure pump draws the fuel out of the vial and pressurizes it into the curing tube. [37] A Bosch piezoelectric diesel injector injects a precisely defined amount of fuel into the electrically heated and pressurized combustion chamber. Under these conditions the fuel will autoignite, causing a pressure rise in the chamber. A dynamic pressure transducer and multiple thermocouples closely monitor the combustion chamber, the orientation of which can be seen in Figure 12. The AFIDA has very accurate temperature control, and high repeatability compared to the IQT. To achieve temperature conditions in the IQT the temperature dithers around the set point; the heaters are constantly cycling off and on causing the temperature to bouncing above and below the set point. This method is not ideal; as ID time is highly temperature dependent. In contrast the AFIDA has very precise temperature control. The AFIDA ramps the temperature slightly above the set point and then runs the test when the temperature decreases to the set point. The fuel does not inject until the temperature condition is met, even if that means repeating this process. Additionally the AFIDA performs 12 injection cycles at each test condition, with pressure traces evaluated for repeatability.
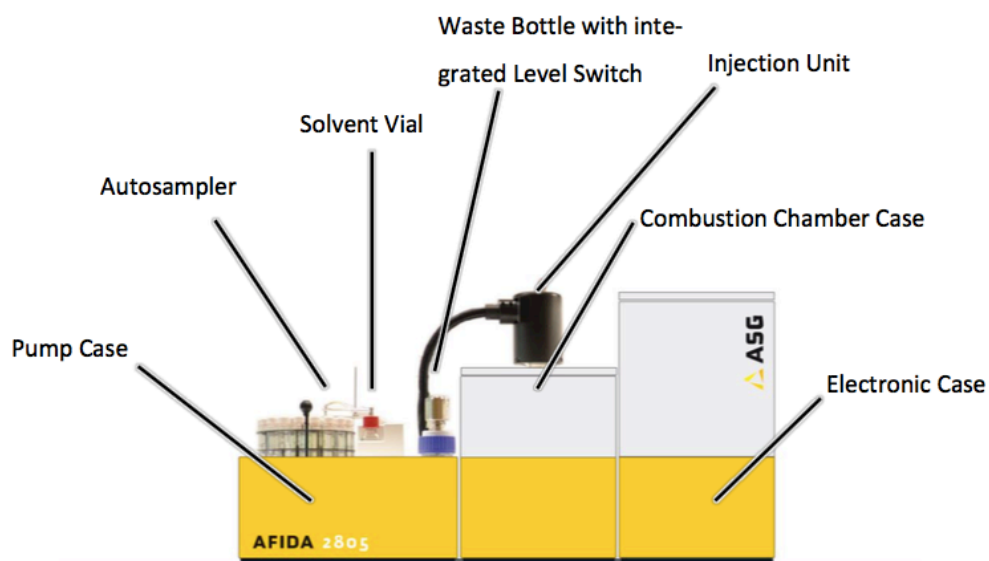
Figure 11: Image of the AFIDA 2805, with the main components identified [37].
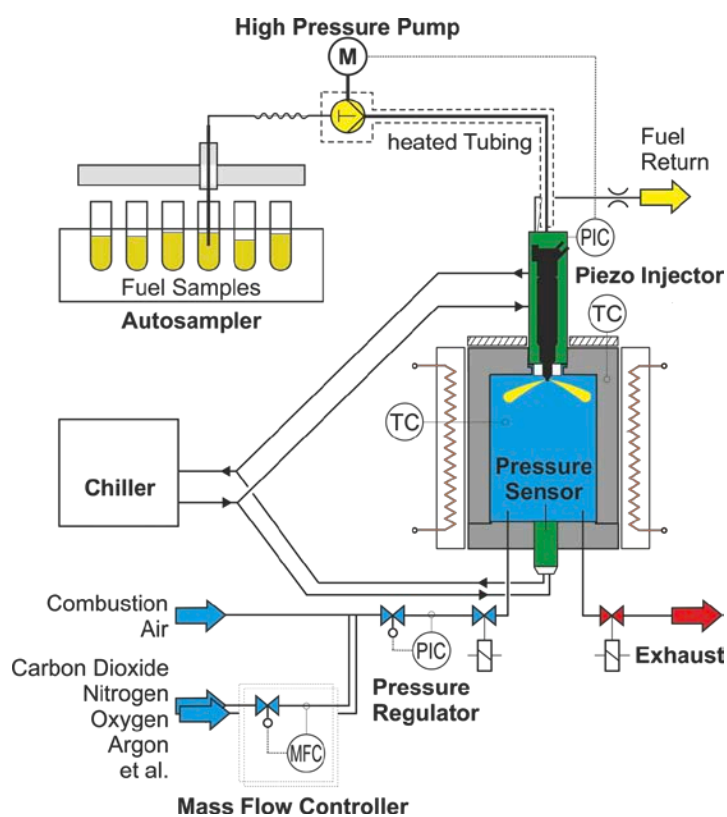


Figure 12: Schematic of the AFIDA, highlighting inputs for the test process with combustion air and fuel input noted, along with the exhaust from the chamber after the test had concluded [37].

2.3.3 Advanced Fuel Ignition Delay Analyzer: Sample Data

The AFIDA performs 12 injections at each temperature and pressure condition, Figure 13 shows the pressure trace for each injection as well as the average for FACE B at 16 bar and 450°C. These data illustrate the repeatability of experiments in the AFIDA. Figure 14 shows what the average pressure trace data at each temperature condition looks like across the entire temperature sweep. LTHR can be seen from 525 °C to 400 °C.
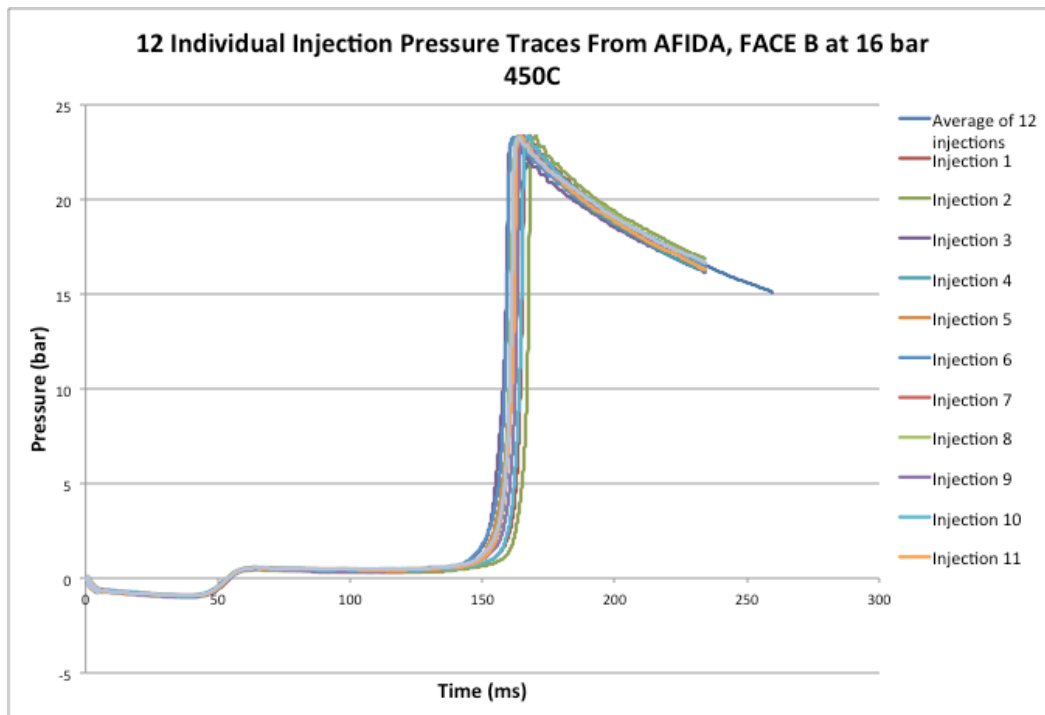


Figure 13: 12 individual pressure traces as well as the average from the AFIDA of FACE B at 16 bar and 450°C.
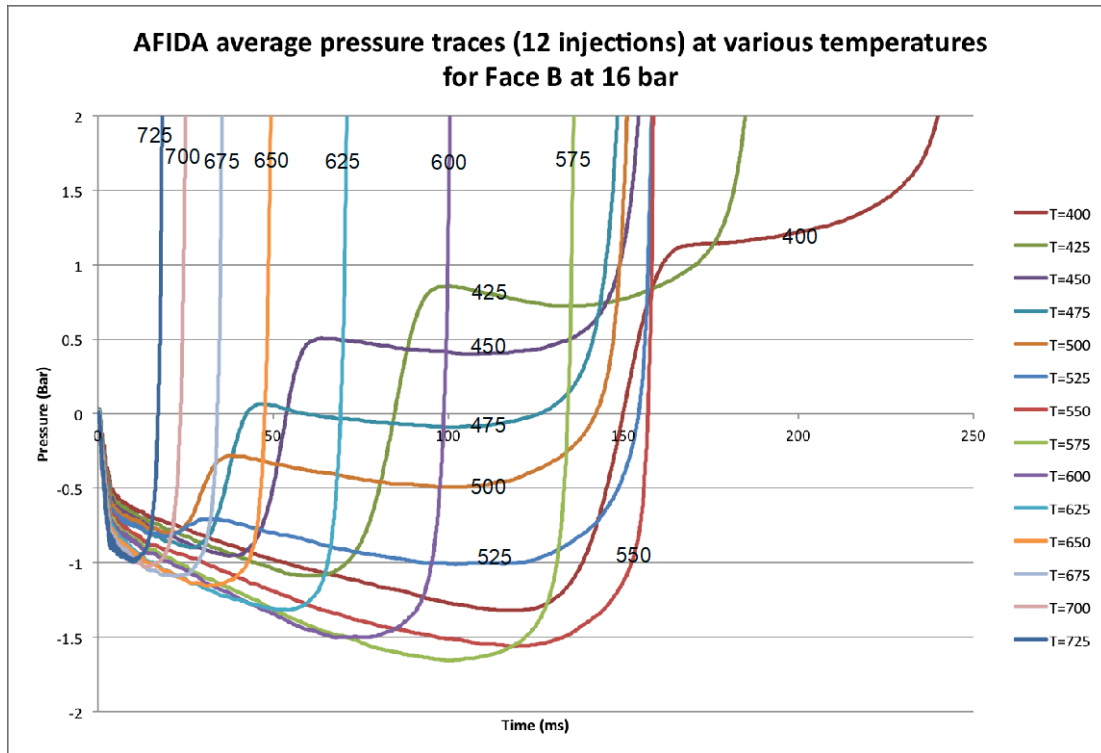
Figure 14: Average pressure trace for each temperature is plotted for FACE B at 16 bar.

2.3.4 Advanced Fuel Ignition Delay Analyzer: ϕ Calculations

In order to run temperature sweeps in the AFIDA, as opposed to the G-CN tests that it is designed to run, extensive characterization was required. Jon Luecke at NREL ran experiments to determine the moles of fuel injected as the injection duration changed, as well as moles of air filling the chamber at different temperature and pressure conditions. These experiments were necessary to determine the fuel-air equivalence ratio of the experiments to be conducted in the AFIDA. The moles of air in the chamber cannot be calculated since the temperature in the chamber is unknown. While thermocouples monitor the chamber temperature, it is only the temperature at one point and does not account for the temperature gradients from the wall to the center of the chamber. The average temperature of the chamber is unknown, thus to determine the moles of air in the chamber experimentally the chamber was filled at 5, 10, and 20 bar pressure conditions at 25 °C, and 400-700 °C in 100 °C increments. Once the chamber stabilized

it was exhausted in an evacuated sampling canister. The canister volume is known, and the pressure was read with a high accuracy pressure gauge. The volume of the canister (about 95% of total volume) was added to the 5% that was left in the chamber (less accurate). The moles of air are calculated with the ideal gas law at room temperature for the canister and at chamber temperature for the 5% remaining volume. While using the temperature of the chamber causes errors, the canister method is highly accurate and accounts for 95% of the total measurement. To determine $O_2$ in the chamber at various pressures, the ideal gas law was used to determine the theoretical moles of air in the chamber. The average theoretical temperature for the experimental number of moles of air in the chamber is taken over the range of pressures 6-26 bar at 5 bar increments. This average theoretical temperature is then linearly correlated to the actual chamber temperature. The linear fit is then used to determine the fuel-air equivalence ratio of a given fuel at a specific temperature pressure condition. The number of moles of $O_2$ is then calculated using the ideal gas law, but instead of chamber temperature, the linear fit equation is used. To calculate the moles of fuel injected, experiments were conducted at different injection durations, and the mass of 60 injections of certification diesel fuel were measured experimentally with 1600 bar fuel pressure at 0-4000 μs in 500 μs increments. The fuel was injected into a tube that was then removed from the injector and weighed. There are some errors associated with this method as fuels have different properties that effect the injection, however testing with a more volatile fuel would result in errors due to fuel evaporation and loss of mass in transferring the tube from the nozzle to the scale. This test was conducted 3 different times at each injection duration condition. The density of the fuel is used to determine the volume of fuel injected. The results were plotted and a correlation was established between the injection duration and the volume of fuel injected. One of the significant challenges of using the AFIDA is attempting to inject stoichiometric

mixtures. The AFIDA was primarily designed for G-CN measurements, and intended for diesel range fuels where the global equivalence ratio would be lean. To study gasoline range fuels, where stoichiometric or slightly lean conditions are of interest, the fuel injector piezo crystal must be energized for long periods of time to inject more fuel. However, fuel pressure drops during injection, as the fuel line volume is small and the HPLC fuel pump cannot quickly ramp up pressure during an injection event to maintain pressure. NREL is working on modifying the AFIDA fuel system for these types of studies, but the work is still early stage. When using an optional fuel line with higher internal volume (to maintain a higher pressurized reservoir to reduce pressure drop during injection) instead of the standard fuel line, the maximum injection duration achievable is 2500 μs, after that the percent error between the measured volume of fuel injected and the curved fit used to predict the volume of fuel injected becomes too high. Between 2500 μs and 3000 μs, the error jumps from -0.15% to -5.23%. With these experiential results the fuel-air equivalence ratio can be determined at each temperature and pressure condition given the fuel injection duration. The fuel-air equivalence ratio is calculated per Equation 2.1, as the ratio of moles of fuel to moles of oxidizer actual, to moles of fuel to moles of oxidizer at stoichiometric conditions.

$$\Phi = \frac{\left(n_{fuel}/n_{ox}\right)_{actual}}{\left(n_{fuel}/n_{ox}\right)_{stoich}} \tag{2.1}$$

A $\phi$ of 1 indicates that there is the exact amount of oxygen needed to react with the fuel, greater than 1 indicates there is excess fuel after the reaction and is referred to as rich, less than 1 indicates there is excess air after the reaction and is referred to as lean.

2.3.5 Advanced Fuel Ignition Delay Analyzer: Iso-octane And N-heptane Mapping

Iso-octane (RON 100) and n-heptane (RON 0) were mapped in the AFIDA by Jon Luecke to examine the differences in ID time as percent oxygen balance in nitrogen diluent, and

pressure varied. The AFIDA chamber volume, 0.4 L, is greater than the 0.2 L volume of the IQT, thus a lower oxygen concentration in nitrogen balance was required to obtain $\phi$ of 1 (calculated per the method in Section 2.2.4), since the AFIDA is fuel limited to maintain stoichiometry. Tests were conducted at with 21%, 10%, and 3% $O_2$. Figure 15 shows a comparison of iso-octane ran at 3% $O_2$, and 10% $O_2$, at 11 bar and $\phi$ of 1. Data were collected from 725 °C - 475 °C. Some data are missing due to insufficient data collection, or exceedingly high ID times. From these data it is clear that the ignition delay times are too long and not relevant to typical engine operating space. Moreover the ID time is in the thousands of ms at a temperature of 475 °C, as further temperature sweeps will test down to 425 °C this will only exacerbate the issue. For this reason, further tests will use 21% $O_2$ and lower $\phi$ values, to obtain quicker and more relevant ID times. Additionally it was discovered that the AFIDA test sequence software cycles the chiller off around 650 ms after the fuel has been injected. This causes a rise in the pressure trace, and then a drop when the chiller comes back on ~100ms later. This interference with the data can be seen in Figure 16. As a result any ignition delay time after 650 ms is not accurate. While ID times past 650 ms are not engine-relevant, this physical issue places an upper limit on the ID time data.
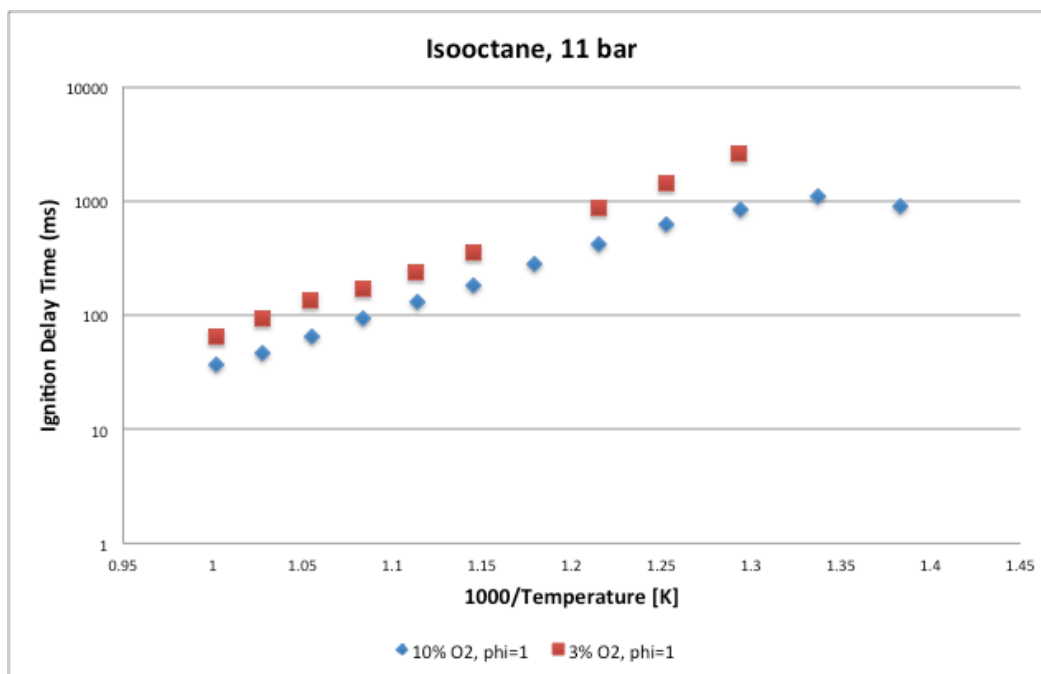
Figure 15: Temperature versus ID time for iso-octane, at 11 bar and a φ = 1, for 3% and 10% O₂.
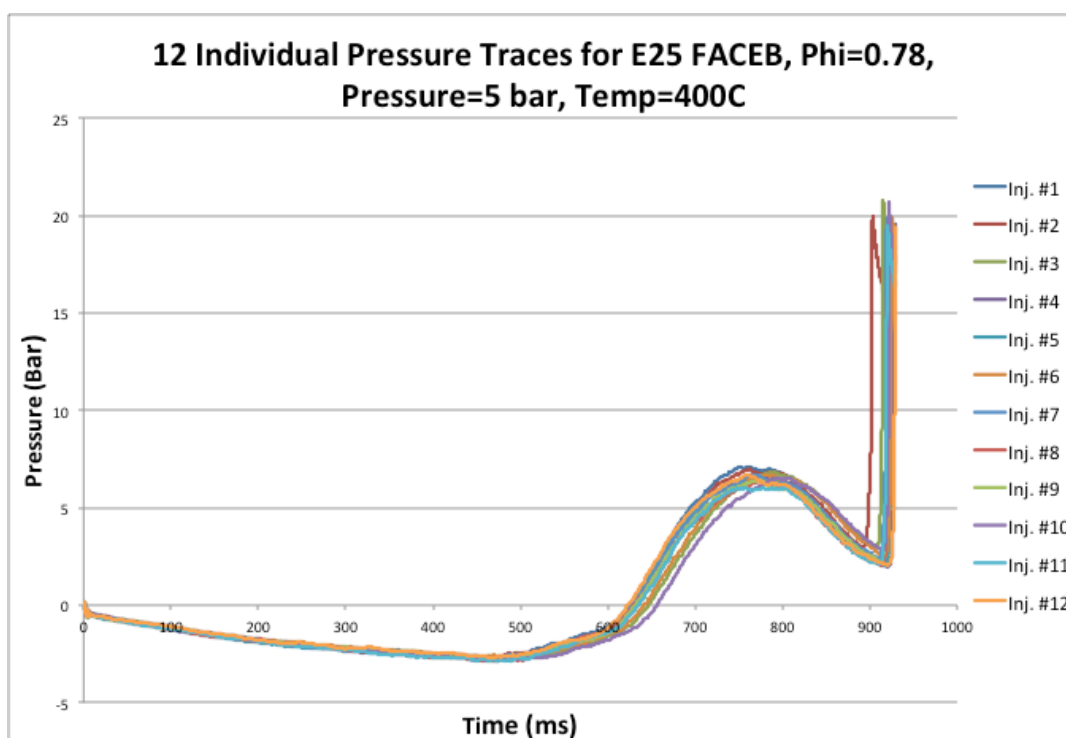


Figure 16: Pressure trace (pressure versus time) for FACE B at 400 °C and 5 bar. The data show the pressure rise and then drop caused by the cycling off, then on, of the chiller.

2.3.6 Advanced Fuel Ignition Delay Analyzer: Gasoline in Piezoelectric Diesel Injector

While the AFIDA was designed to test diesel fuels, NREL intended to study both diesel

and gasoline range fuels in the device. The AFIDA uses a commercially available Bosch diesel

piezoelectric injector (a common production part used in the Audi/VW/Porsche 3.0L V6 diesel).

A schematic of the injector can be seen in Figure 17. The nozzle control is opened and closed by

the piezoelectric stack. The stack is housed in the injector, and expands and contracts with an

electronic signal. This technology enables a fast response time with multiple injection events per

engine cycle. However, the force and displacement from the piezo crystal stack is not great

enough to open the needle. To generate the necessary force the piezo stack is coupled with a

hydraulic amplification system [38]. The piezo stack exerts a force on a smaller fuel chamber

within the injector, and the pressure differential causes the pintle to open.
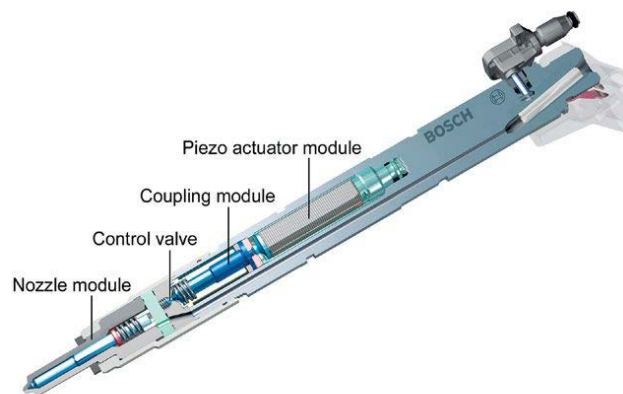
Figure 17: Schematic of Bosch piezoelectric injector. The device consists of a piezo actuator, a
coupling module to amplify the force, a control valve, and the nozzle [38].

The function of the injector relies on the fuel that is to be injected. When tests were

conducted with iso-octane and n-heptane, leakage back from injector bypass into the AFIDA

waste reservoir was observed. While the leak was not significant, even a small amount of

internal leakage in the control valve would affect the mass of fuel injected into the chamber. At

first the cause of this leak was thought to be a broken backpressure regulator on the AFIDA.

However after this part was replaced leaking continued with lower viscosity fuels. While some injectors functioned better than others, likely due to differences in manufacturing tolerances, which only become apparent with less viscous fuels compared to diesel fuels. Discussions with colleagues at Argonne National Laboratory working on gasoline compression ignition engine research (using common rail injectors) showed that they had to add a diesel fuel lubricity additive to prevent wear on the high pressure pump with low lubricity gasoline range fuels [39]. While the issue with the AFIDA was not the same, discussions with the AFIDA developer, Philipp Seidenspinner and ASG Analytik-Service Gesellschaft mbH, as well as engineers at Bosch, revealed that a related issue could be causing the AFIDA issue, where the control valve within the piezo injector may be sticking. Without the lubricity of diesel fuel, the control valve was essentially sticking; this caused the control valve to not open as desired, to stick open, or to not open at all. As a result 1500 ppm of Infineum R655 lubricant additive is mixed into every low lubricity (gasoline range) sample. While this treat rate may be higher than most related applications, it is not common to run gasoline fuels though diesel injectors. Additionally the additive accounts for less than 0.15% of the fuel composition. This is a conservative treat rate, to avoid complications with the injector. Determining the minimum treat rate that can be used is ongoing at NREL, but outside the scope of this project. The acid-based Infineum R655 lubricity additive is expected to have little effect on ignition delay time; even so it is likely affecting all fuels equally in this study.

## 2.4 Fuel Set Composition and Preparation

This fuel set had been utilized in previous single cylinder research studies of knock limited engine performance and particulate matter emissions at NREL, and was designed to vary HOV while keeping RON and S close to constant. The basis of the fuel set is renewable

oxygenates blended into gasoline surrogate BOBs, with the exception of FACE B [23]. The

gasoline BOB surrogates can be seen in Table 2 and are mixtures of toluene, iso-octane, and n-

heptane. The entire fuel set can be seen in Table 3 with the volume percent of each chemical

component in the fuel. The majority of these fuels were blended in large batches as part of that

study. The fuels were splash blended which refers to the process of blending the fuel and

oxygenates by pouring, the sample is not actively mixed. E20 + 6% anisole in TRF88, as well as

E25 in TRF88 were blended in small batches by adding the desired oxygenates to premixed

TRF88 per the previous study.

Table 2: Surrogate BOB, standardization fuel compositions from detailed hydrocarbon analysis
by ASTM D6729, before oxygenate blending [23].

| Fuel | toluene (vol. %) | iso-octane (vol. %) | n-heptane (vol. %) |
|---|---|---|---|
| TRF88 (nominally 30 vol. % toluene in PRF70) | 28.3 | 50.4 | 21.2 |
| TRF71 (nominally 40 vol. % toluene in PRF32) | 41.2 | 18.5 | 40.3 |
| TSF99.8 (nominally 74 vol. % toluene in PRF38.5) | 73.6 | 10.3 | 16.1 |

Table 3: Fuel test set by percent volume of each component in the fuel.

| Fuel | toluene (% by vol.) | iso-octane (% by vol.) | n-heptane (% by vol.) | ethanol (% by vol.) | anisole (% by vol.) | p-cresol (% by vol.) | FACE B (% by vol.) |
|---|---|---|---|---|---|---|---|
| PRF100 | 0 | 100 | 0 | 0 | 0 | 0 | 0 |
| TSF99.8 | 74 | 10 | 16 | 0 | 0 | 0 | 0 |
| E25 in TRF88 | 22.5 | 36.75 | 15.75 | 25 | 0 | 0 | 0 |
| E40 in TRF71 | 24 | 11.52 | 24.48 | 40 | 0 | 0 | 0 |
| E20 + 2% p-cresol in TRF88 | 23.4 | 38.22 | 16.38 | 20 | 0 | 2 | 0 |
| E20 + 6% anisole in TRF88 | 22.2 | 36.26 | 15.54 | 20 | 6 | 0 | 0 |
| TRF88 | 30 | 49 | 21 | 0 | 0 | 0 | 0 |
| E25 in FACE B | 0 | 0 | 0 | 25 | 0 | 0 | 75 |
| FACE B | 0 | 0 | 0 | 0 | 0 | 0 | 100 |

Before the samples were tested in the AFIDA, they were transferred to 40 mL vials, which are compatible with the AFIDA autosampler carousel. During this process 59μL of lubricant Infineum R655 was added to each 40ml of fuel, to achieve 1500 ppm of the additive. The vials were gently rotated to achieve adequate mixing.

## 2.5 Fuel Set Test Preparation

### 2.5.1 Fuel Set: Weight Percent Carbon, Hydrogen, And Oxygen Calculations

Before tests could be conducted the $\phi$ of each fuel needs to be determined per the method outlines in Section 2.3.4. The test conditions are necessary to calculate the $\phi$ at each set of test parameters. Test parameters were planned for 725 °C – 425 °C in 25 °C increments at 5, 10, 20, and 30 bar. The weight percent carbon (C), hydrogen (H) and oxygen (O) in each fuel as well as the density needed to be calculated from the known volume percent of each component in the fuel. The fuel density is calculated as seen in Equation 2.2, which is the sum of the product of percent volume of each component to the density of each component.

$$\rho_{avg} = \sum_i \rho_i * \% \, vol_i \qquad (2.2)$$

The weight percent C, H, and O are calculated from the percent volume, known densities, molecular mass, and chemical equation of each component. The mass fraction of C, H and O in a given compound is calculated by Equation 2.3, where $n_{C,H,O}$ is the number of moles of C H or O in the compound given by the chemical equation, $ma_{C,H,O}$ is the atomic mass of C, H or O respectively, and $MW_{chemical}$ is the molecular weight of the chemical. This calculation is implemented for each chemical component in the surrogate blend.

$$mass \, fraction = \frac{n_{C,H,O} * ma_{C,H,O}}{MW_{chemical}} \qquad (2.3)$$

Next, the mass of each chemical in a 100 mL sample is calculated. Equation (2.4) calculates the

mass in a 100 mL sample, where $\rho_{chemical}$ is the density of the chemical and % vol is the percent

volume of the chemical in the fuel mixture.

$$\text{mass} = \rho_{chemical} * \% \, vol_{chemical} * 100 \tag{2.4}$$

The mass fraction of each chemical in the total fuel mixture is calculated by taking the grams of

each chemical in a 100 mL sample, over the sum of the mass of each chemical in a 100 mL

sample. Finally the mass fraction of C, H and O in each chemical is calculated, by Equation (2.5)

where the mass fraction of each chemical is multiplied by the mass fraction of C, H, and O

respectively. To find the total mass fraction of C, H, and O in the fuel blend, the mass fraction of

C, H, and O of each chemical component is added. From the total C, H, and O mass fraction and

the average density, the $\phi$ can be calculated for each fuel. The total mass fraction of C, H, and O

for each fuel can be seen in Table 4.

$$\text{m fraction}_{C,H,O} = \text{m fraction}_{Chemical} * \text{m fraction}_{C,H,O \, in \, fuel} \tag{2.5}$$

Table 4: Calculated mass fraction of C, H, O, and density of each fuel.

| Fuel | Weight % C | Weight % H | Weight % O | Density (g/ml) |
|---|---|---|---|---|
| PRF 100 (iso-octane) | 84.09 | 15.91 | 0.00 | 0.692 |
| TSF99.8 (74% toluene) | 89.65 | 10.35 | 0.00 | 0.820 |
| E25 in TRF88 (23% toluene) | 77.54 | 13.37 | 9.09 | 0.754 |
| E40 in TRF71 (24% toluene) | 72.87 | 12.89 | 14.24 | 0.770 |
| E20 + 2% p-cresol in TRF88 | 79.13 | 13.22 | 7.64 | 0.757 |
| E20 + 6% anisole in TRF88 | 78.77 | 12.90 | 8.32 | 0.769 |
| TRF88 | 86.55 | 13.45 | 0.00 | 0.742 |
| E25 FACE B | 75.58 | 14.91 | 9.52 | 0.720 |
| FACE B | 84.43 | 15.57 | 0.00 | 0.697 |

Ideally global $\phi$ would be 1, since it is relevant to stoichiometric SI engine operating conditions. However it was determined with tests in Sections 2.3.4 and 2.3.5 that the upper limit on $\phi$ is imposed by the maximum amount of fuel that can be injected (2500 μs) and the $O_2$ concentration required to get relevant ignition delay times (21% $O_2$). To determine the highest $\phi$ that could be achieved for the test set, the $\phi$ of each fuel was calculated at the maximum duration (2500 μs) and 21% $O_2$. E40 in TRF71 was the fuel with the lowest $\phi$, thus each fuel was recalculated with lower durations in order to match the $\phi$ of TRF71, and attain constant $\phi$ conditions between fuels. Ideally $\phi$ would be constant for every test condition, however this was not possible with the AFIDA in its current state. Instead target $\phi$ is held constant at each pressure among the set of 9 fuels. Target $\phi$ refers to the $\phi$ at the highest temperature condition for each pressure. $\phi$ is not consistent through the tests, as the injection duration is held constant and thus the $\phi$ is allowed to drift lean as the chamber temperature decreases (and $O_2 + N_2$ mass, therefore, increases). The change in $\phi$ as temperature drops can be seen in Table 5. The main reason for allowing the $\phi$ to drift lean is to be able to run the highest $\phi$s possible. It is worth noting that while the AFIDA has a high pressure fuel injection system that promotes better mixing than the IQT, it is still expected that $\Phi$ gradients exist within the chamber at these timescales and reported $\Phi$ is an assumed global average. NREL is working to characterize and model the spray process with $\Phi$ and T gradients, but that is ongoing and outside the scope of this thesis project. Past research with the IQT indicates a quasi-homogenous state develops with locally rich gradients where ignition originates, and similar processes likely develop within the AFIDA [33, 35, 40].

Table 5: Calculated $\phi$ at each temperature and pressure condition.

| Chamber Temperature (°C) | $\phi$ at 5 bar | $\phi$ at 10 bar | $\phi$ at 20 bar | $\phi$ at 30 bar |
|---|---|---|---|---|
| 725 | 1.04 | 0.57 | 0.39 | 0.20 |
| 700 | 1.02 | 0.56 | 0.29 | 0.20 |

| 675 | 1.00 | 0.55 | 0.29 | 0.19 |
|-----|------|------|------|------|
| 650 | 0.98 | 0.54 | 0.28 | 0.19 |
| 625 | 0.96 | 0.52 | 0.27 | 0.19 |
| 600 | 0.94 | 0.51 | 0.27 | 0.18 |
| 575 | 0.92 | 0.50 | 0.26 | 0.18 |
| 550 | 0.90 | 0.49 | 0.26 | 0.17 |
| 525 | 0.88 | 0.48 | 0.25 | 0.17 |
| 500 | 0.86 | 0.47 | 0.25 | 0.17 |
| 475 | 0.84 | 0.46 | 0.24 | 0.16 |
| 450 | 0.82 | 0.45 | 0.23 | 0.16 |
| 425 | 0.80 | 0.44 | 0.23 | 0.15 |

Additionally a previous study was conducted in the IQT, which experimented with letting the $\phi$ drift lean at low temperatures, versus changing the amount of fuel injected in steps to hold $\phi$ near constant (a difficult process requiring manual measurement and adjustment of metal shims to change fuel system pneumatic intensifier stroke) [19]. The results of this study can be seen in Figure 18 .The results of the two tests are very similar even when one test has a constant $\phi$ (black diamond) and the other has a variance of 0.2 $\phi$ (open square). From this previous study in the IQT it was determined that allowing the $\phi$ to drift lean in the AFIDA would have little impact on ID time, compared to temperature or pressure. To hold $\phi$ constant in the AFIDA, the fuel set would need to be run at 0.20 if the $\phi$ was allowed to drift lean throughout the test, or 0.15 if it were not. Even if running at an incredibly lean 0.15 $\phi$ were desirable, it would not be possible to collect data at this point, across every pressure and temperature. For some fuels the ID was already approaching or surpassing the cut off point of 650 ms. If less fuel was injected in order to hold $\phi$ constant, the ID times would be to long to measure for most of the desired temperature sweep conditions.
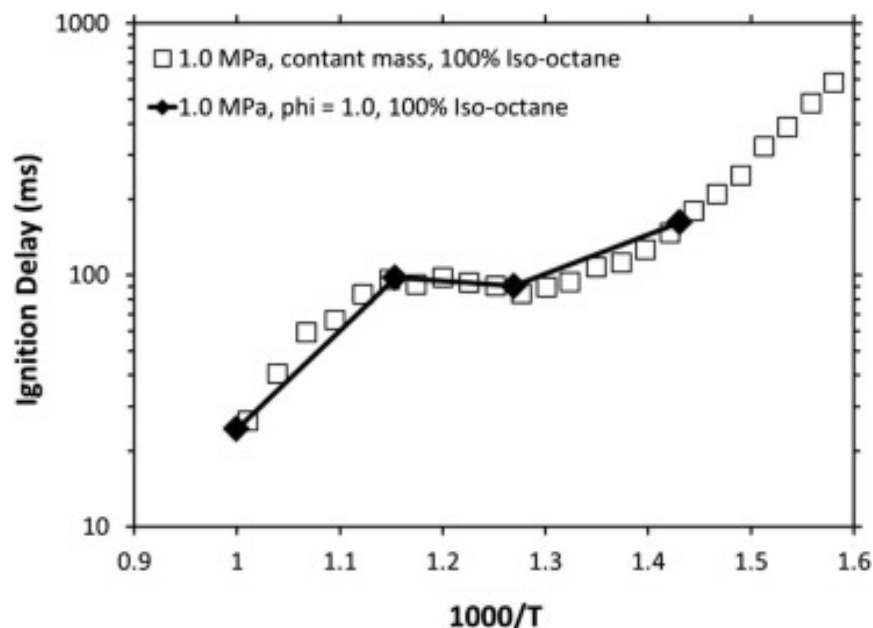
Figure 18: Temperature sweeps at 1.0 MPa. 90 vol.% iso-octane / 10 vol.% ethanol, constant equivalence ratio $\phi = 1.0$ (black diamond), constant mass $0.7 \leq \phi \leq 1.0$ (open square) [19].

2.5.2 Fuel Set: Experimentally And Analytically Determined Properties

For each fuel detailed hydrocarbon analysis (DHA), RON and HOV data were available from a previous study [23]. Neat TRF88 was not originally part of the fuel set, thus data were calculated. For the core fuel set, RON and MON where measured by ASTM D2699 and D2700, respectively [9,10], under subcontract at Southwest Research Institute. HOV was based on chromatographic analysis using ASTM D6729 [41, 42]. For TRF88, the RON was measured according to ASTM D2699 [9]. However, there was no measured value for MON, which is necessary to calculate S. Instead S was estimated based on the method outlined in Morgan et al. [43]. Sensitivity can be predicted from the RON, and percent toluene in the sample. HOV of TRF 88 is calculated based on the DHA data with the help of Earl Christensen at NREL. The properties, experimentally and analytically determined or calculated, of the fuel set can be seen in Table 6.

Table 6: Fuel properties, RON, S, and HOV.

| Fuel | RON | S | HOV |
|---|---|---|---|
| PRF 100 (iso-octane) | 100.0 | 0.0 | 303 |
| TSF99.8 (74% toluene) | 99.8 | 11.1 | 390 |
| E25 in TRF88 (23% toluene) | 101.6 | 10.7 | 489 |
| E40 in TRF71 (24% toluene) | 99.2 | 12.2 | 595 |
| E20 + 2% p-cresol in TRF88 | 101.1 | 9.4 | 472 |
| E20 + 6% anisole in TRF88 | 99.9 | 9.6 | 472 |
| TRF88 | 87.0 | 5.2 | 348 |
| E25- FACE B | 105.6 | 11.8 | 485 |
| FACE B | 95.8 | 3.4 | 340 |

The DHA of each fuel is necessary for later correlation work. Table 7 shows the results

of the DHA for TRF88. TRF 88 is blended with toluene, n-heptane, and iso-octane however, the

DHA shows impurities; trace amounts of other components. For this study trace amounts of

other chemicals were excluded from the correlation work, but a full analysis showing the level of

trace compounds (impurities) is shown in Appendix A. Table 8 shows the results of the DHA

analysis for each fuel, excluding any trace amounts of other chemicals.

Table 7: DHA analysis results for TRF88. TRF88 by definition is 21% n-heptane, 49% iso-octane, and 30% toluene. Analysis gives components in weight, volume, and mole percent, total C, H and O percent, density and particulate matter index (PMI) [44, 45].

| COMPONENT | %WGT | %VOL | %MOL |
|---|---|---|---|
| n-heptane | 19.57 | 21.17 | 20.16 |
| 2-Methylhexane | 0.04 | 0.04 | 0.04 |
| 3-Methylhexane | 0.02 | 0.02 | 0.02 |
| 2,2,4-Trimethylpentane | 47.12 | 50.38 | 42.57 |
| 2,2-Dimethylhexane | 0.03 | 0.03 | 0.03 |
| Toluene | 33.13 | 28.27 | 37.11 |
| Methylcyclohexane | 0.02 | 0.02 | 0.03 |
|  |  |  |  |
| Density (g/ml) at 15C | 0.7439 | | |
| H wt% | 13.6 | | |
| C wt% | 86.4 | | |
| PMI | 0.51 | | |

Table 8: Table of components in each fuel per the DHA analysis. With the exception of FACE B, which is percent of each component in surrogate.

| Fuel | toluene (vol. %) | iso-octane (vol. %) | n-heptane (vol. %) | ethanol (vol. %) | anisole (vol. %) | p-cresol (vol. %) | o-xylene (vol. %) |
|---|---|---|---|---|---|---|---|
| PRF 100 (iso-octane) | 0 | 99.89 | 0 | 0 | 0 | 0 | 0 |
| TSF 99.8 | 73.59 | 8.7 | 16.09 | 0 | 0 | 0 | 0 |
| E25 in TRF88 | 21.63 | 38.55 | 16.2 | 23.49 | 0 | 0 | 0 |
| E40 in TRF71 | 24.95 | 11.23 | 24.45 | 39.44 | 0 | 0 | 0 |
| E20 2pcresol TRF88 | 24.2 | 38.8 | 16.1 | 20.4 | 0 | 2 | 0 |
| E20 6anisole TRF88 | 23.3 | 37.3 | 15.5 | 19.7 | 6.2 | 0 | 0 |
| TRF88 | 28.27 | 50.38 | 21.17 | 0 | 0 | 0 | 0 |
| E25 FACE B | 0 | 65.745 | 5.085 | 25 | 0 | 0 | 4.17 |
| FACE B | 0 | 87.66 | 6.78 | 0 | 0 | 0 | 5.56 |

Correlation work will examine the data set based on percent volume of each component. Seven of the fuels are composed mainly of toluene, n-heptane, iso-octane, ethanol, p-cresol, and anisole (six components). Thus the two fuels with FACE B posed a complexity issue. As shown in Appendix A, Figure A-3 the DHA on FACE B identifies 67 different components, making it difficult to compare to the composition of the rest of the fuels. Even if trace amounts of chemicals were excluded, there would still be twice as many components to consider, than are in the rest of the fuel set. To enable correlation work, Dr. Scott Wagnon at Lawrence Livermore National Laboratory (LLNL) was contacted in hopes of suggesting a surrogate blend for FACE B that could be used in the correlation work instead of the DHA data. Dr. Wagnon, proposed a blend of iso-octane, n-heptane, and o-xylene [46]. The FACE B 3-component surrogate can be seen in Table 9 and gives volume, mass and molar percent of each component. Figure 19

compares the FACE B value (target value) to the surrogate value (current value) for RON, S, and the percent paraffin, iso-paraffin and aromatic content.

Table 9: Table of components in FACE B surrogate blend, in volume, molar and mass percent.

| FACE B Surrogate | Vol % | Molar % | Mass % |
|---|---|---|---|
| n-heptane | 6.78 | 7.42 | 6.60 |
| o-xylene | 5.56 | 7.35 | 6.93 |
| iso-octane | 87.66 | 85.23 | 86.47 |

```
         Target Name      Target Value      Current Value
       ------------------------------------------------------
                  RON            95.8             95.55
                 SENS             3.4             3.883
                   HC           2.197             2.178
          paraffin_vf           0.079           0.06784
      iso-paraffin_vf           0.863            0.8765
          aromatic_vf           0.058           0.05561
```

Figure 19: Comparison of target value properties of FACE B to the current values of the FACE B 3-component surrogate blend [Courtesy of Dr. Wagnon, LLNL].

## 2.6 Advanced Fuel Ignition Delay Analyzer Temperature Sweep Procedure

Initial functional tests in the AFIDA need to be conducted by the user to ensure the device is working properly. Then a test sequence can be entered for the device to run continuously. The AFIDA software has two main tabs: settings and maintenance. The 'Settings' tab is where the user enters in the test sequence to be conducted, which consists of user inputs for chamber temperature, chamber pressure, injection duration (controls $\Phi$), fuel line pressure, fuel name, $\Phi$ value, $O_2$ concentration and data collection time for each fuel. Each fuel was tested from 725 °C $-$ 425 °C in 25 °C increments at 5, 10, 20, and 30 bar with a 21% $O_2$ concentration and a fuel pressure of 1190 bar. Each temperature pressure condition consists of 14 injections comprised of 2 pre-injections and 12 main injections the average of which is used to describe the test. The test sequence is set to start at 725 °C, and run all pressure conditions at that temperature before dropping to the next temperature condition in 25 °C increments until 425 °C. The 'Maintenance' tab is where the user can control the AFIDA functions before a test is started. In

order to prepare for the test of each fuel in the set the AFIDA functioning was examined. The chamber was set to around 600 °C and 20 bar. Then the chamber pressure was monitored to ensure no leakage. Additionally 400 ms or more of certification diesel fuel was run through the fuel line after every fuel test, to insure the low viscosity fuels that were being tested would not be sitting in the fuel line while it was unpressurized and thus risk boiling. Additionally a few injections of certification diesel fuel were run under G-CN conditions, of 17.5 bar and 580 °C to ensure that ID time was consistent between fuel samples [36]. After the proper functioning of the AFIDA was confirmed the 40 mL fuel samples with 1500 ppm Infineum R655 were loaded into the autosampling carousel. A flushing vial is designated to flush the test fuel through the line for 340 ms before the test sequence is initiated. The test sequence for 4 pressures as 13 difference temperature conditions each takes around 10 hours and is automated.

CHAPTER 3

Analysis

## 3.1 AFIDA Data Post Processing

The AFIDA outputs a text file with, pressure transmitter signal data, time, chamber temperature, chamber pressure, injection pressure, injection duration, injection temperature, pressure transmitter temperature, fuel pressure, fuel temperature, and AFIDA software ID time. While the software has its own analysis tool where the user can load a test to be plotted, these plots cannot be exported. The text file must be post processed with an Excel macro created by Jon Luecke at NREL. The macro converts the signals into pressure and time data, as well as smoothens the signal for each of the 12 injections in a test. This code also processed the ID time from the pressure trace data. The ID time definition of the AFIDA (proprietary), is intended for diesel fuels, and like the IQT's ID time definition is typically unable to capture the 2 stage combustion event of gasoline range fuels. The ID time is calculated 4 ways in the macro: maximum dP/dt, 40% of peak pressure, 10% of peak pressure, user defined threshold, and AFDIA definition. Maximum dP/dt finds the time associated with the maximum slope of the pressure trace, defining the greatest rate of pressure rise as the start of combustion, this is calculated for the average pressure trace of the 12 injections. 40% and 10% of peak calculate the ID time based on the time associated with 40 and 10 percent of the maximum pressure in the chamber respectively. This is calculated for each of the 12 injections, and then averaged. User defined, allows the user to choose a threshold pressure much like the NREL designed controls for the IQT defines ID time.

Maximum dP/dt is a commonly accepted definition of ID time. This definition is rooted in the ignition kinetics and relates to the maximum heat release rate. However due to noise this

definition is not always accurate; in these cases 40% of peak is used. 40% of peak is typically

very close to the maximum dP/dt values (typically within 2 ms of maximum dP/dt), thus when

maximum dP/dt fails to properly identify ignition, 40% is used. Figure 20 illustrates an example

of when maximum dP/dt fails to identify ignition; the noise at the beginning of the test causes the

ID time to be very low (~4 ms) when in reality it is more like ~180 ms. Another case where 40%

of peak is used instead of maximum dP/dt is when the maximum rate of pressure rise is at the

very top of the pressure trace which can be seen in Figure 21. In this instance the ID time is more

closely identifying the end of the combustion event, not the beginning. Additionally for some

fuels ignition did not occur before 650 ms, thus some of the fuels are missing data at low

temperatures.
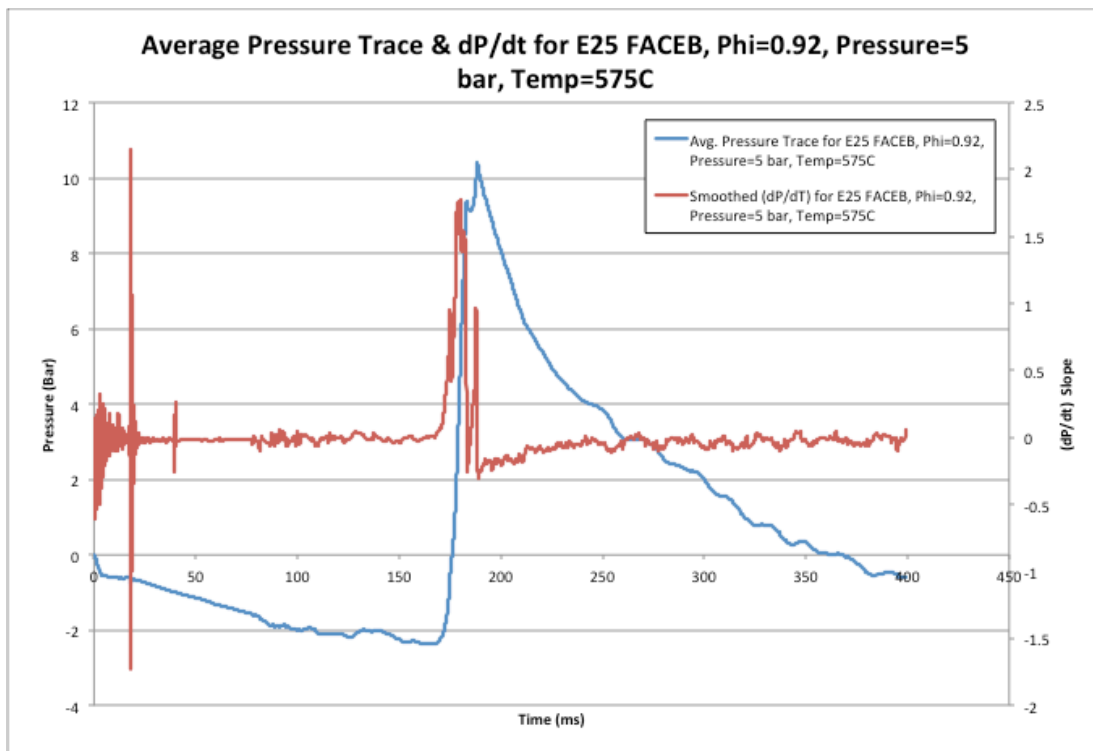


Figure 20: Pressure trace and dP/dt plotted against time for E25 FACE B at a pressure of 5 bar, and temperature of 575 °C.
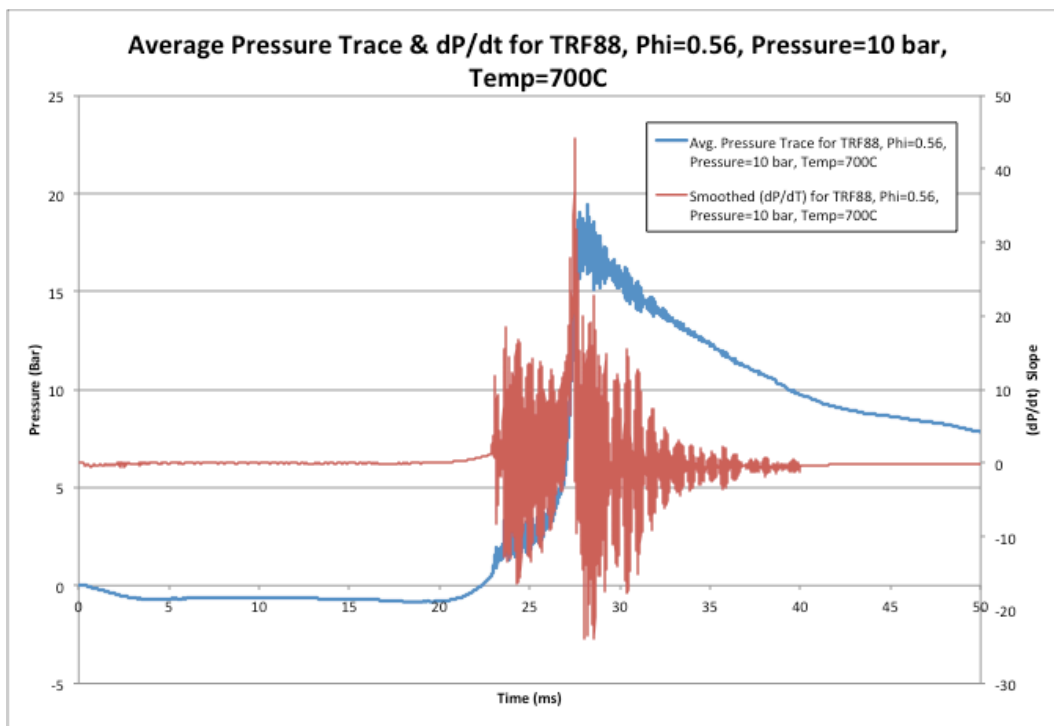
Figure 21: Pressure trace and dP/dt plotted against time for TRF88 at a pressure of 10 bar, and temperature of 700 °C.

## 3.2 Fuel Set Surface Plots

To evaluate the results the data were plotted two different ways. Figure 22, Figure 23, Figure 24, and Figure 25 show a summary of the temperature sweep for every fuel at 5, 10, 20 and 30 bar respectively. The temperature sweep shows ID time (in ms) on a log scale versus the inverse temperature in typical Arrhenius form (1000/T [Kelvin]. The NTC region can be seen for some of the fuels (TRF88, FACE B) on the 5 and 10 bar plots. The NTC region is defined where increases in temperature result in longer ignition delay, due to competing chemical kinetic chain terminating versus chain propagating and branching pathways at that temperature, which is reflected in a negative slope along the ID time curve.
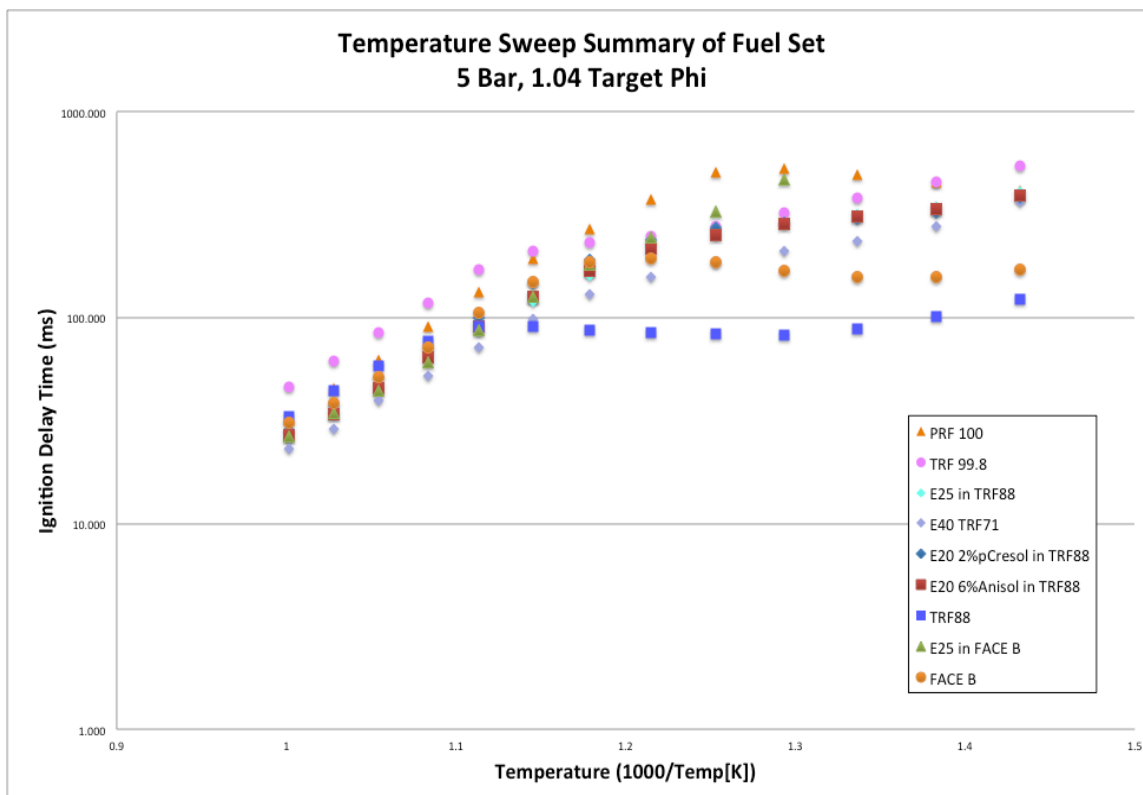
Figure 22: Temperature sweep summary of the fuel set, at 5 bar, with a target Φ of 1.04.
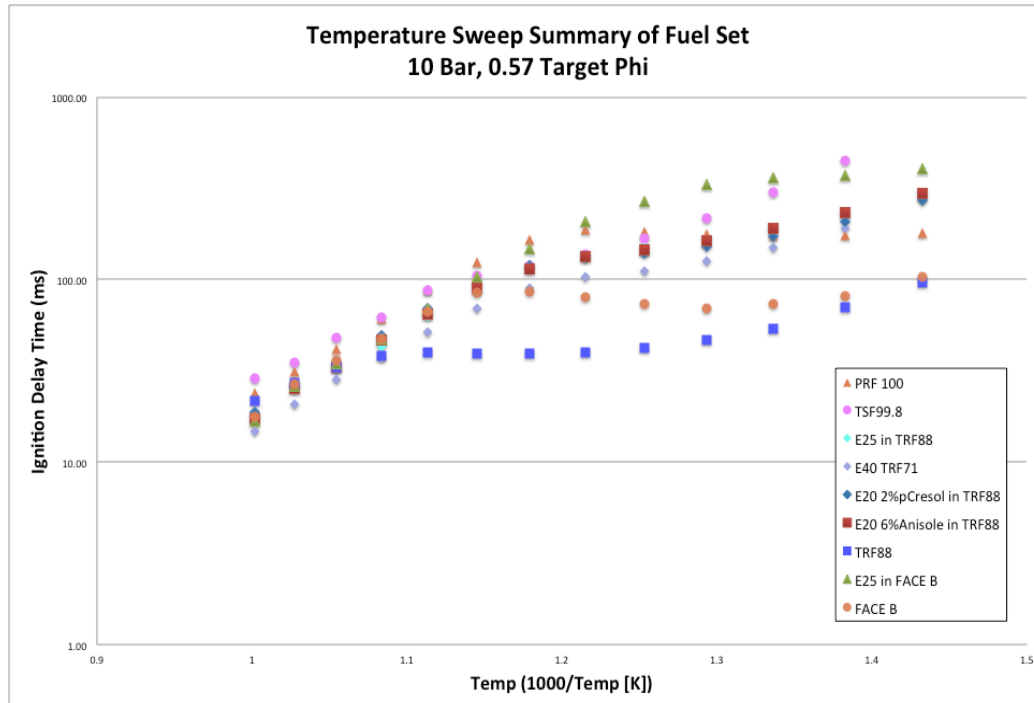


Figure 23: Temperature sweep summary of the fuel set, at 10 bar, with a target Φ of 0.57.
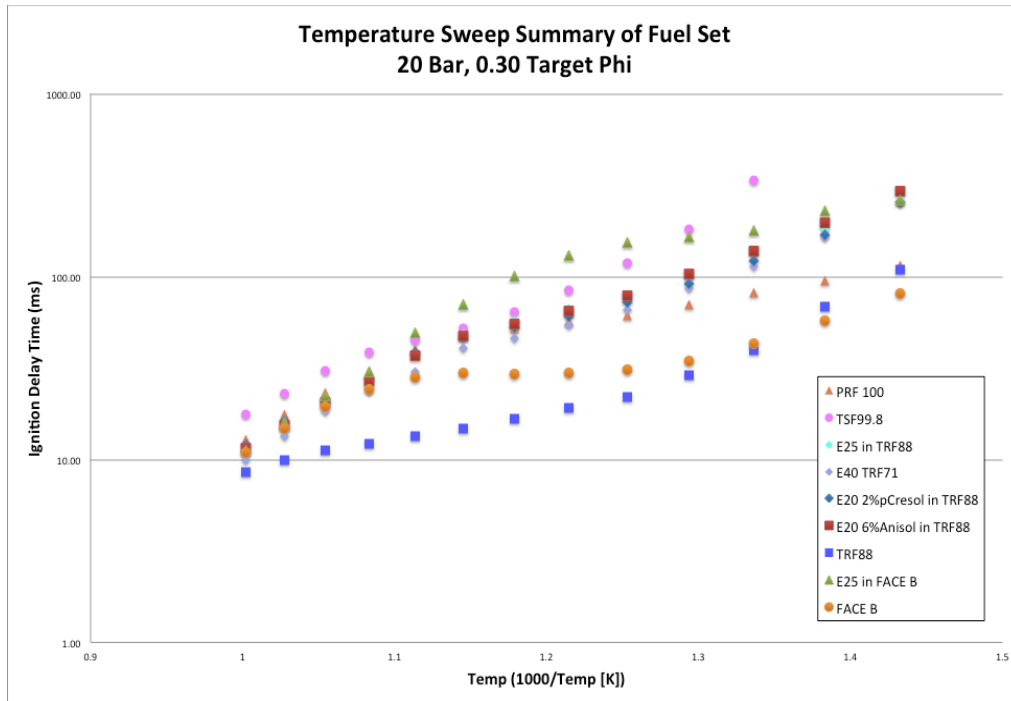
Figure 24: Temperature sweep summary of the fuel set, at 20 bar, with a target Φ of 0.30.
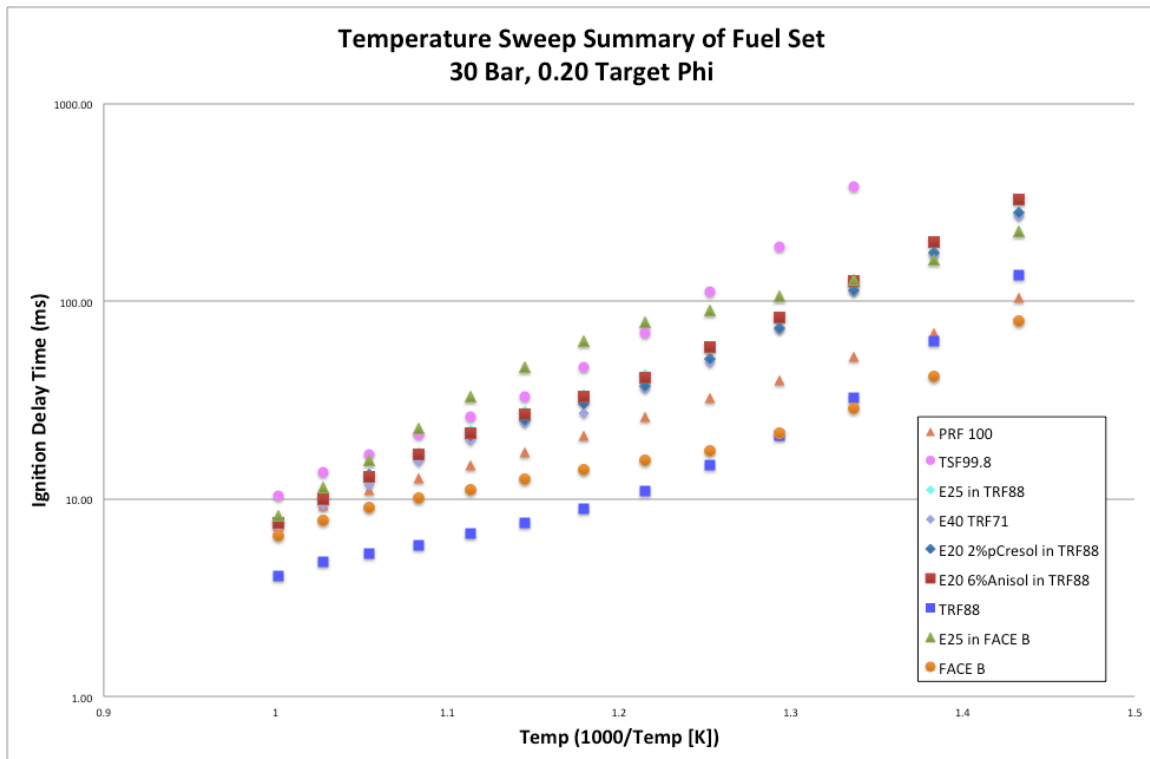


Figure 25: Temperature sweep summary of the fuel set, at 30 bar, with a target Φ of 0.20.

Figure 26, Figure 27, Figure 28 and Figure 29 highlight the differences between TRF88

and E25 in TRF 88; showing the affects of ethanol on the temperature sweep profile at 5, 10, 20

and 30 bar. PRF100 is shown in the background for reference. As the pressure increases the

separation between TRF 88 with and without ethanol becomes more pronounced. At 5 bar in

Figure 27 the high temperature ID times are closer together and the effects of ethanol are not

highly apparent. However, at the lower temperatures the ID time starts to differ and the

difference in S of 5.5 between the two fuels become more pronounces as the fuel with the higher

S (S=10.7) has higher ID times at low temperatures. As the pressure increases the difference in

ID time between the two fuels becomes more noticeable and the E25 blend has higher ID times

at every temperature condition.
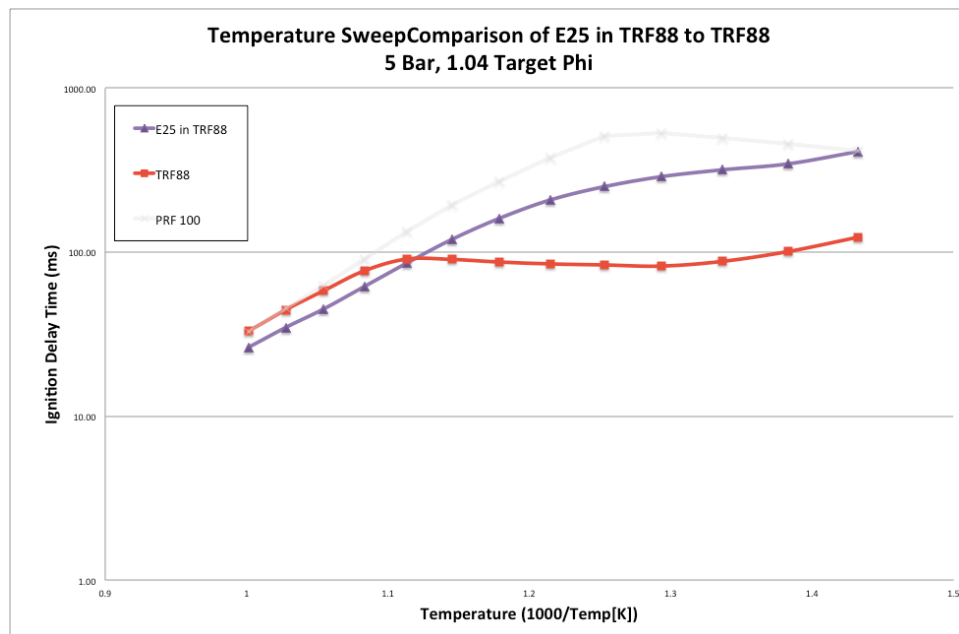


Figure 26: Temperature sweep summary of the TRF88 and E25 TRF88 (with PRF100 in the
background for reference) to compare affects of ethanol, at 5 bar, with a target Φ of 1.04.
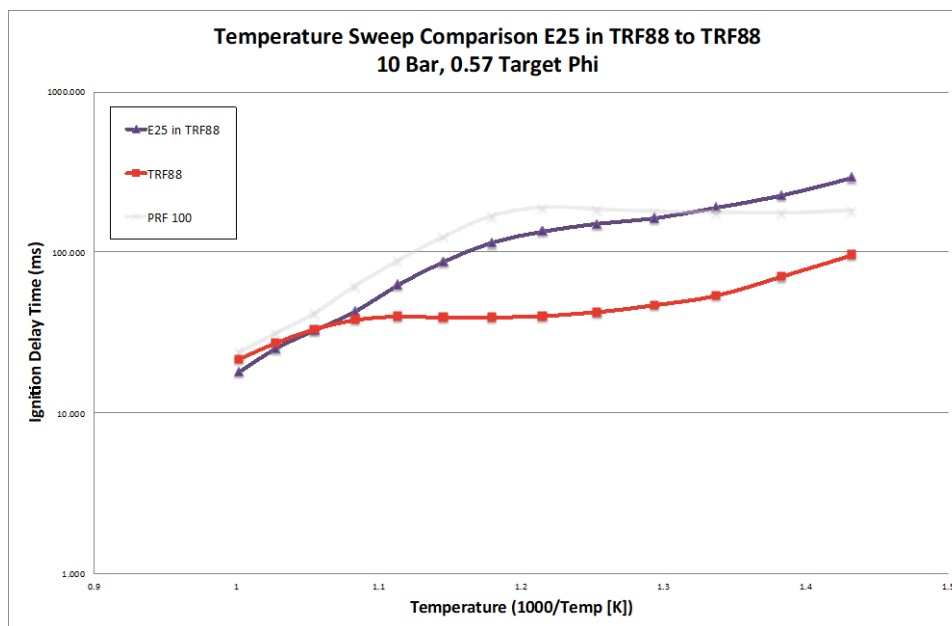
Figure 27: Temperature sweep summary of the TRF88 and E25 TRF88 (with PRF100 in the background for reference) to compare affects of ethanol, at 10 bar, with a target Φ of 0.57.
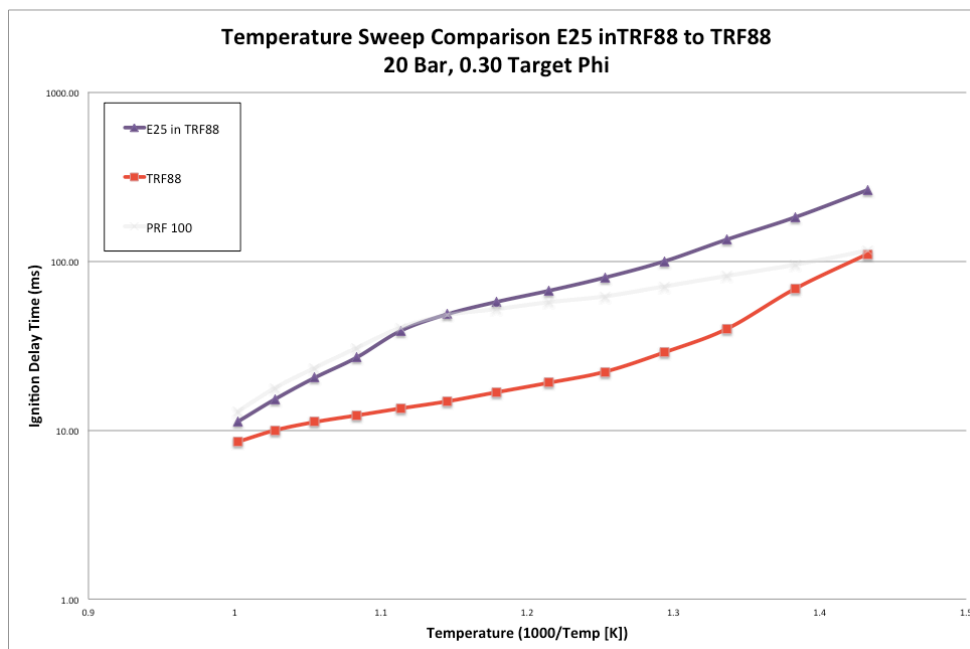


Figure 28: Temperature sweep summary of the TRF88 and E25 TRF88 (with PRF100 in the background for reference) to compare affects of ethanol, at 20 bar, with a target Φ of 0.30.
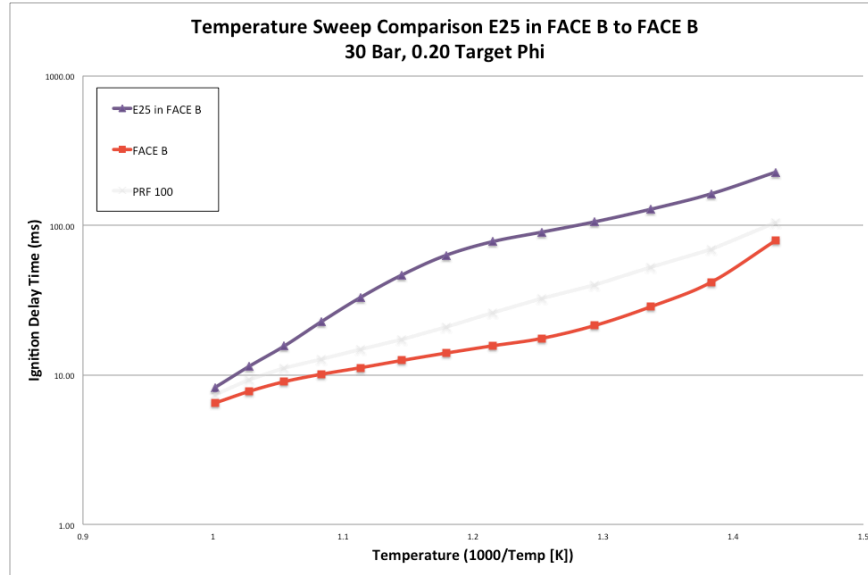
Figure 29: Temperature sweep summary of the TRF88 and E25 TRF88 (with PRF100 in the background for reference) to compare affects of ethanol, at 30 bar, with a target Φ of 0.20.

Figure 30, Figure 31, Figure 32 and Figure 33 highlight the differences between FACE B and E25 in FACE B at 5, 10, 20, and 30 bar respectively. These plots show the effects of ethanol on the temperature sweep profile at various pressures. PRF100 is shown in the background for reference. Figure 30 is missing some data for E25 FACE B at low pressures, because the ID times became to long to record. This shows there is a large difference between FACE B with, and without, ethanol. As the pressure increases, the two fuels start to exhibit different behavior at high temperatures and spread apart as they have a difference of 8.4 in S. However the Φ is changing between each pressure as well. Thus the differences in temperature sweeps for all the fuels will be partially from change in pressure and partially from changing Φ.
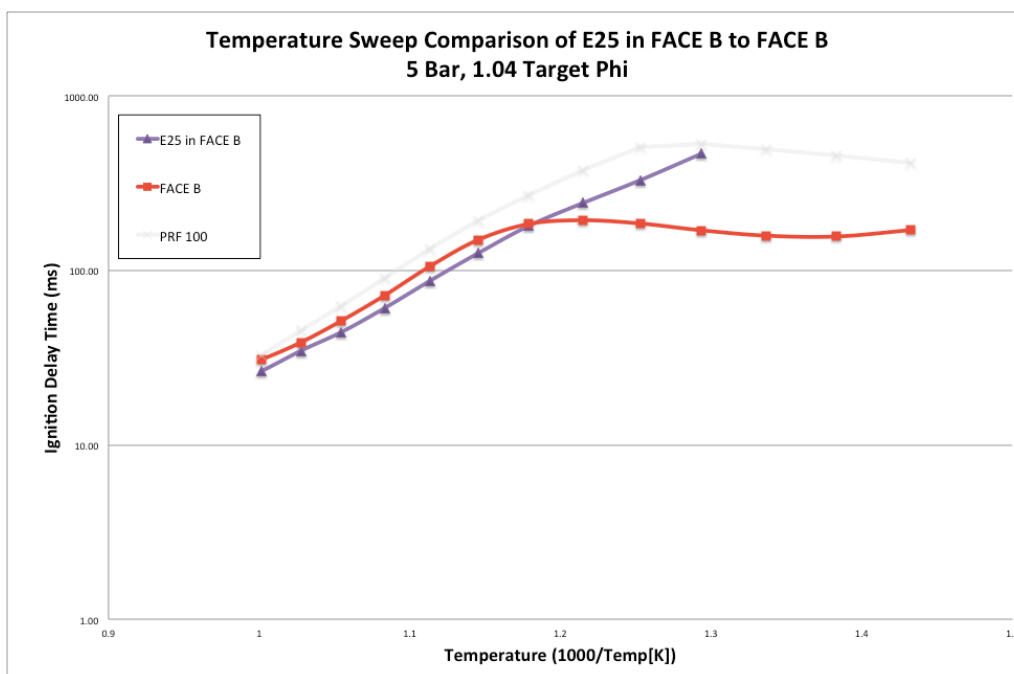
Figure 30: Temperature sweep summary of the FACE B and E25 FACE B (with PRF100 in the background for reference) to compare affects of ethanol, at 5 bar, with a target Φ of 1.04.
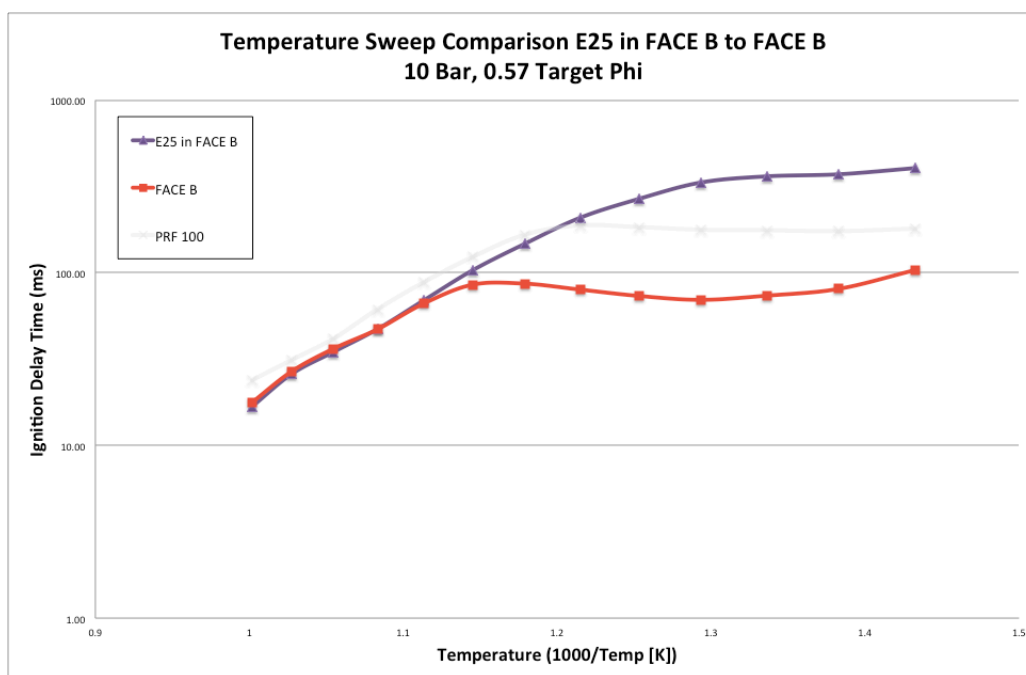


Figure 31: Temperature sweep summary of the FACE B and E25 FACE B (with PRF100 in the background for reference) to compare affects of ethanol, at 10 bar, with a target Φ of 0.57.
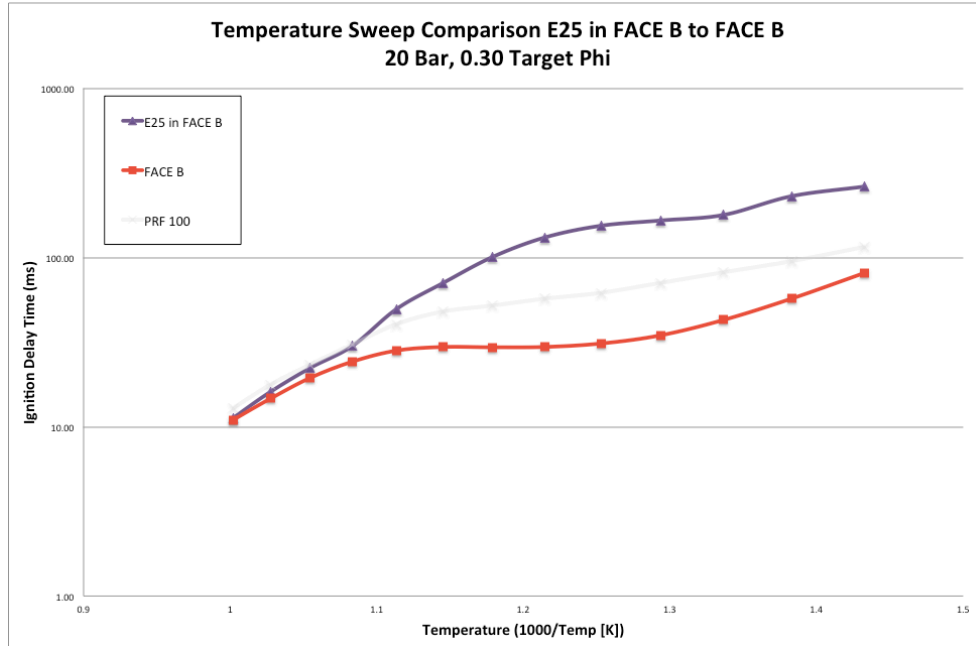
Figure 32: Temperature sweep summary of the FACE B and E25 FACE B (with PRF100 in the background for reference) to compare affects of ethanol, at 20 bar, with a target Φ of 0.30.
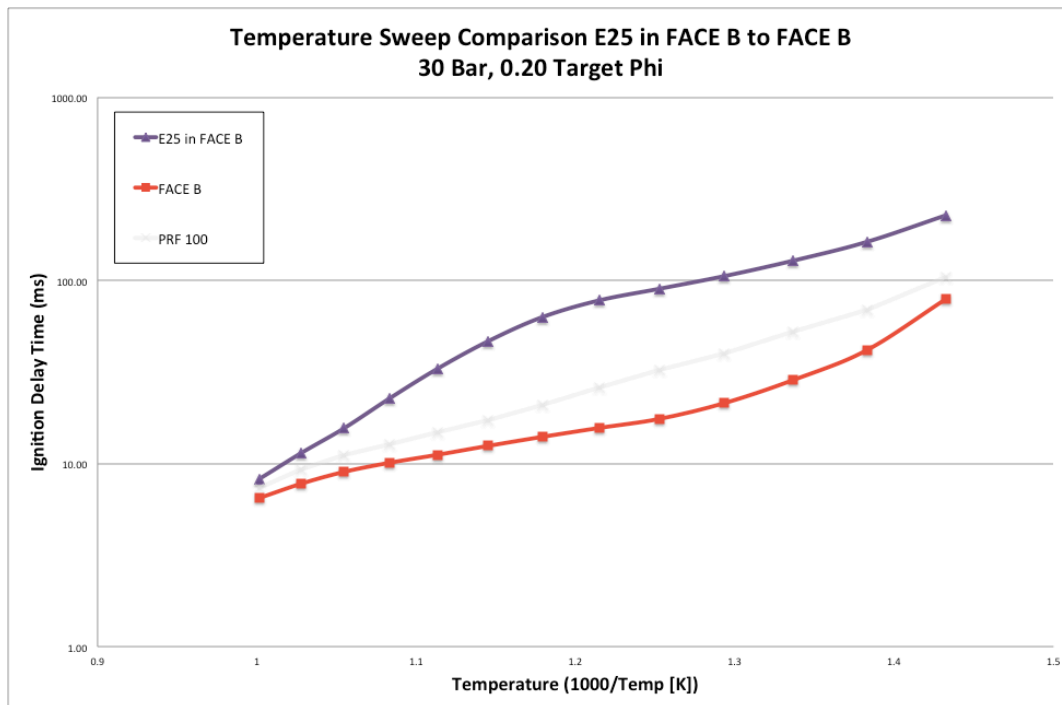


Figure 33: Temperature sweep summary of the FACE B and E25 FACE B (with PRF100 in the background for reference) to compare affects of ethanol, at 30 bar, with a target Φ of 0.20.

The results have also been plotted as generated 3D surfaces for each fuel. The surface fit equation is a 3rd order polynomial in pressure and a 4th order polynomial in temperature. 3D

surface plots can be seen in Figure 34-Figure 42 for PRF100, TRF99.8, E20 in TRF 88, E40 in

TRF71, E20 + 2% p-cresol in TRF 88, E20 + 6% anisole in TRF88, TRF88, E25 in FACE B,

and FACE B respectively. Figure 41 shows the surface of ID time as pressure and temperature

change for E25 FACE B, this surface is what a typical ID time surface should look like as a

function of temperature and pressure. ID time is expected to decrease with pressure thus the ID

time at 5 bar should be higher than 10 bar, and so on. However, in some of the surfaces the

opposite is happing, and at low temperatures the ID time is increasing as the pressure increases.

This effect can be seen in Figure 39, which is the surface for E20 plus 6% anisole in TRF88.

This abnormal behavior can be explained by the decreasing fuel-air equivalence ratio, $\Phi$. The

tests are leaner both as the pressure increases, and as the temperature decreases. At high

temperatures the fuel injected creates a rich zone and combusts before the fuel has time to

disperse, which gives the expected result despite $\Phi$ changing between pressures and

temperatures. However, at the very low temperatures and low $\Phi$ / high pressures, the rich pocket

of fuel has time to disperse before combustion, thus the fuel becomes a less rich pocket or even a

lean pocket and takes even longer to combust. At high temperatures, $\Phi$ has less of an effect on

the ID than compared to low temperatures. While this behavior is not typical of a temperature

sweep across pressures, the $\Phi$ is typically help constant, and close to 1. These results can be well

explained by the changing $\Phi$ through the temperature and pressure tests.
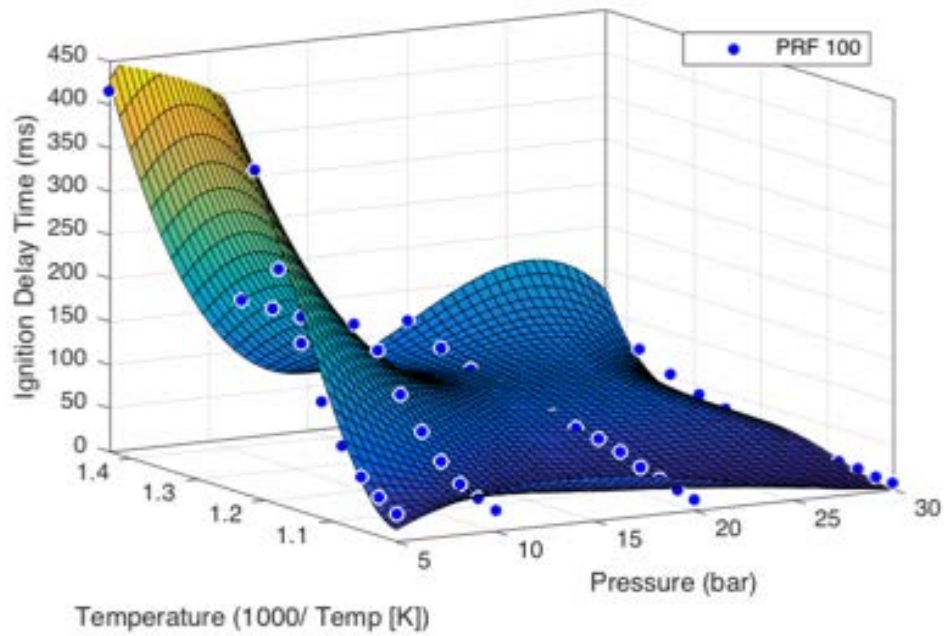
Figure 34: 3D surface of ID time as temperature and pressure change for REF 100 The surface is a 4th order polynomial in temperature and a 3rd order polynomial in pressure.
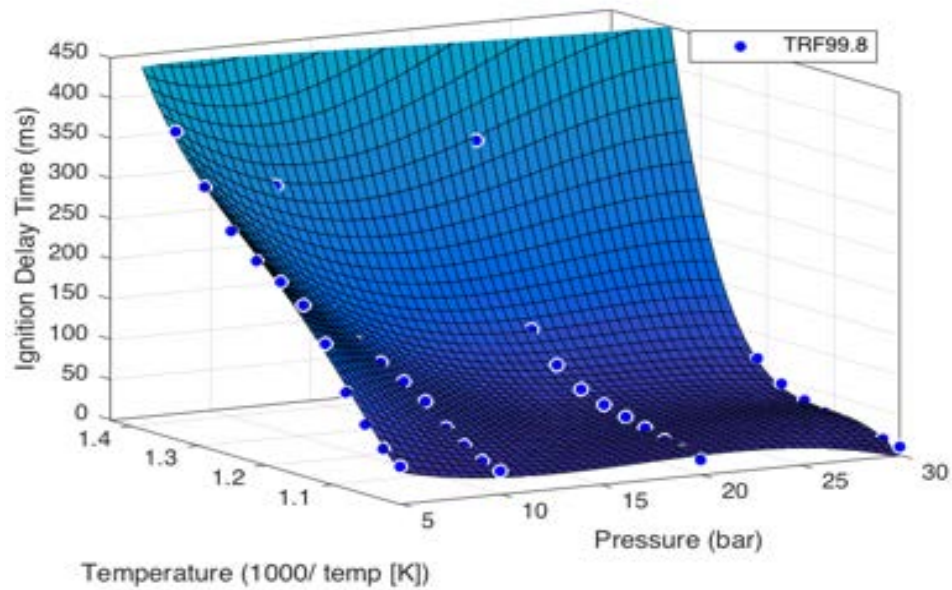


Figure 35: 3D surface of ID time as temperature and pressure change for TRF99.8. The surface is a 4th order polynomial in temperature and a 3rd order polynomial in pressure.
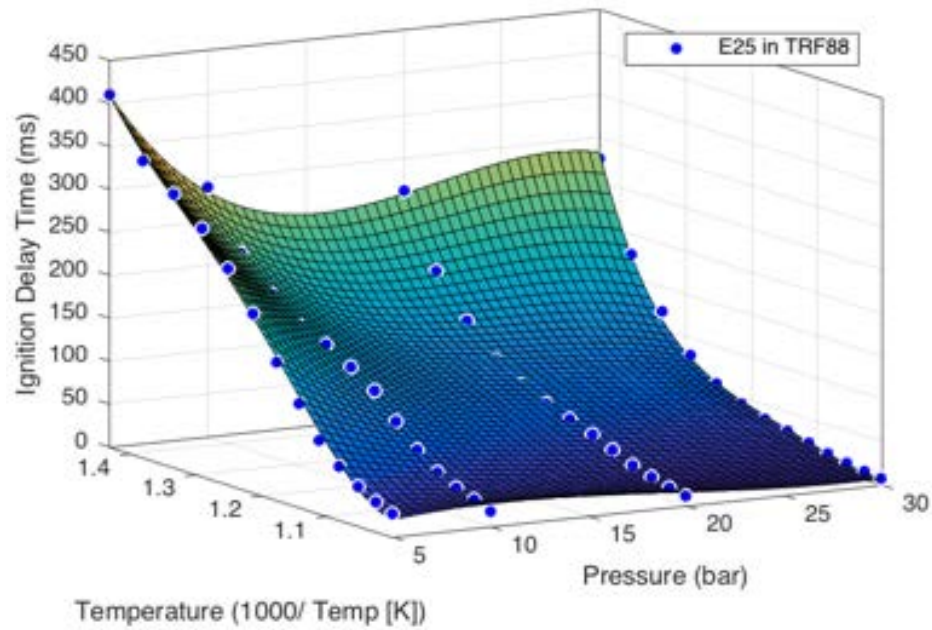
Figure 36: 3D surface of ID time as temperature and pressure change for E25 in TRF88. The surface is a 4th order polynomial in temperature and a 3rd order polynomial in pressure.
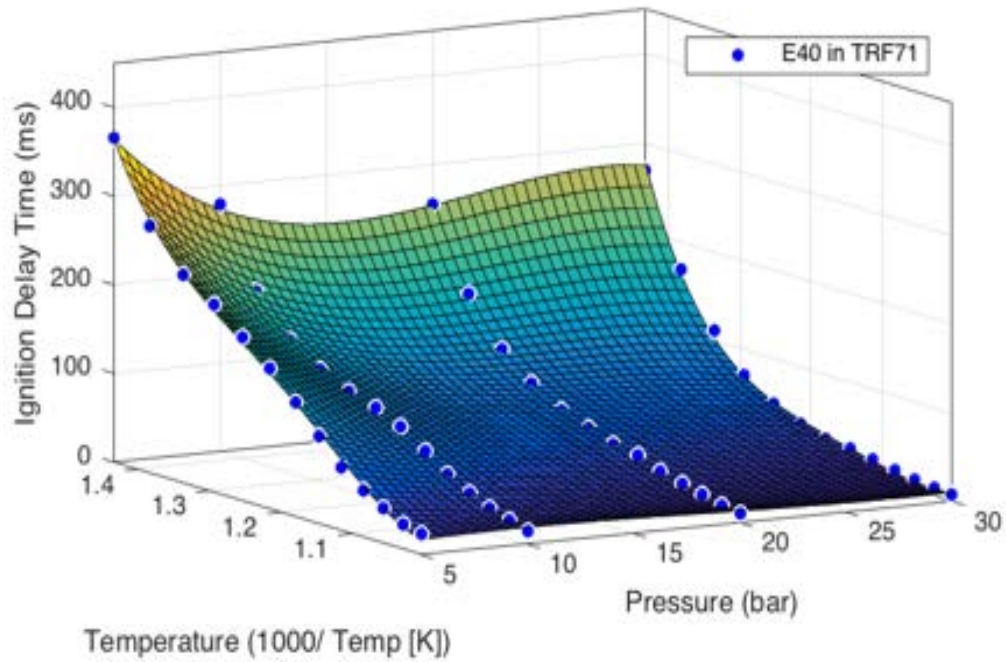


Figure 37: 3D surface of ID time as temperature and pressure change for E40 in TRF71. The surface is a 4th order polynomial in temperature and a 3rd order polynomial in pressure.
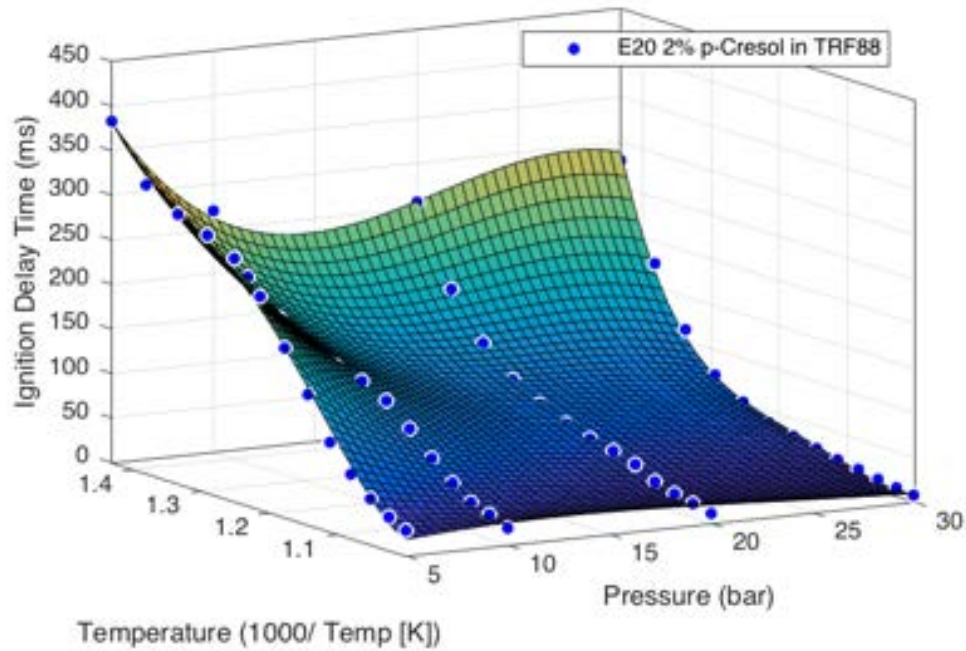
Figure 38: 3D surface of ID time as temperature and pressure change for E20 +2% p-cresol in TRF88. The surface is a 4$^{th}$ order polynomial in temperature and a 3$^{rd}$ order polynomial in pressure.
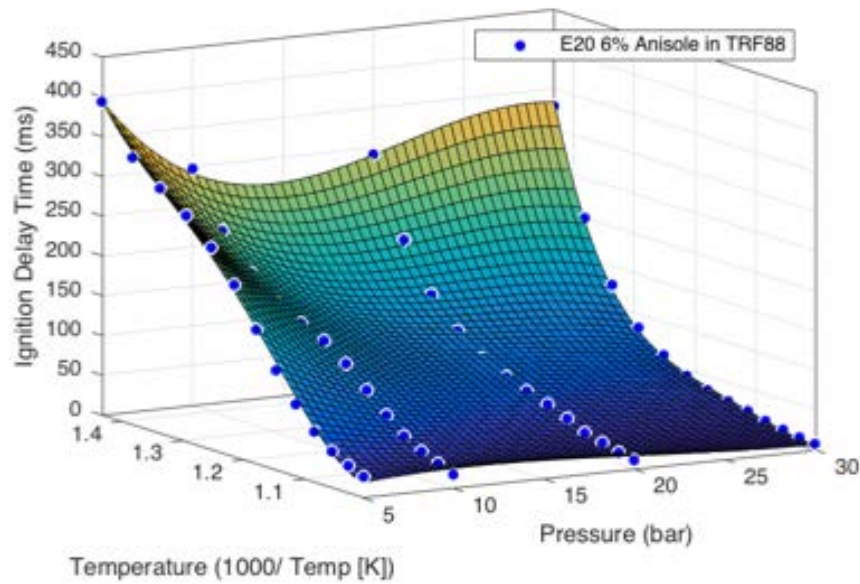


Figure 39: 3D surface of ID time as temperature and pressure change for E20 +6% anisole in TRF88. The surface is a 4$^{th}$ order polynomial in temperature and a 3$^{rd}$ order polynomial in pressure.
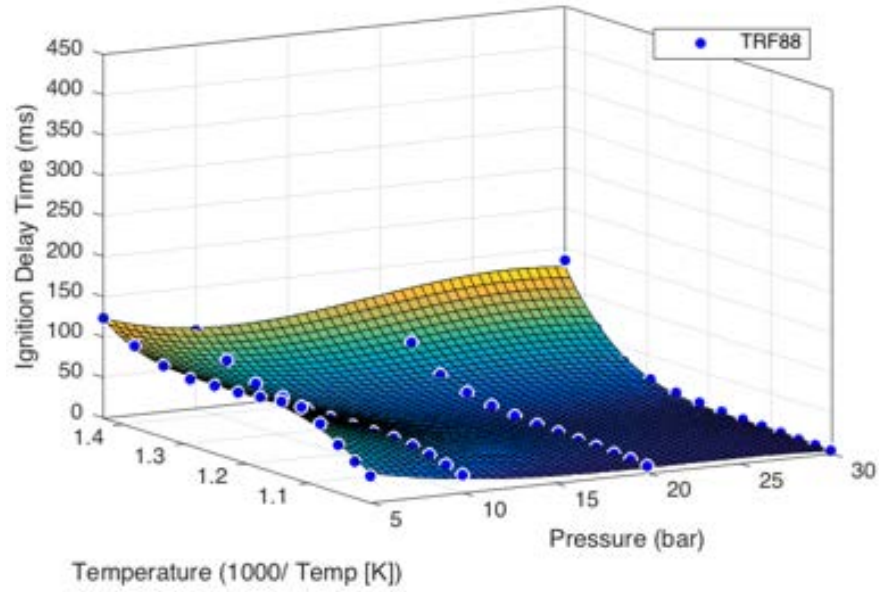
Figure 40: 3D surface of ID time as temperature and pressure change for TRF88. The surface is a 4th order polynomial in temperature and a 3rd order polynomial in pressure.
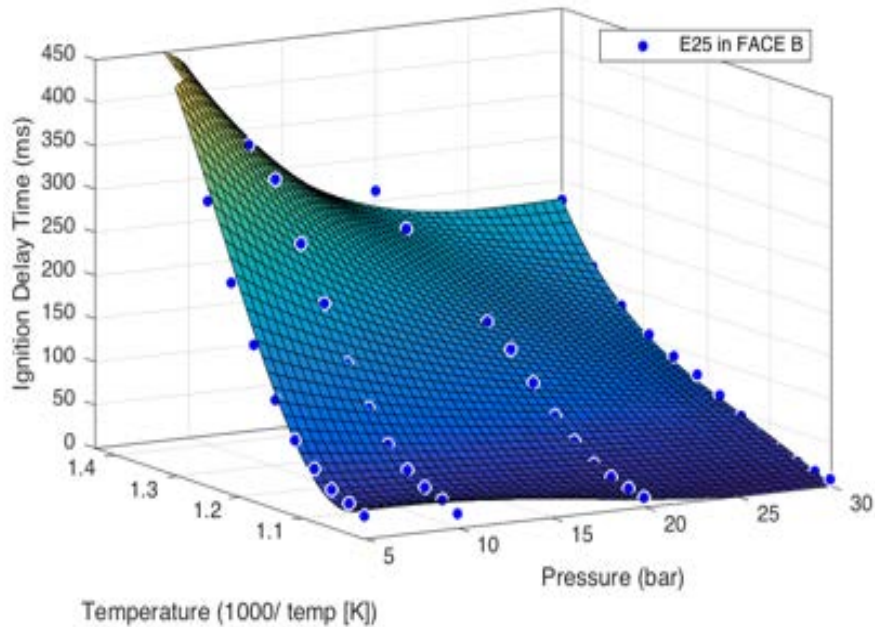


Figure 41: 3D surface of ID time as temperature and pressure change for E25 in FACE B. The surface is a 4th order polynomial in temperature and a 3rd order polynomial in pressure.
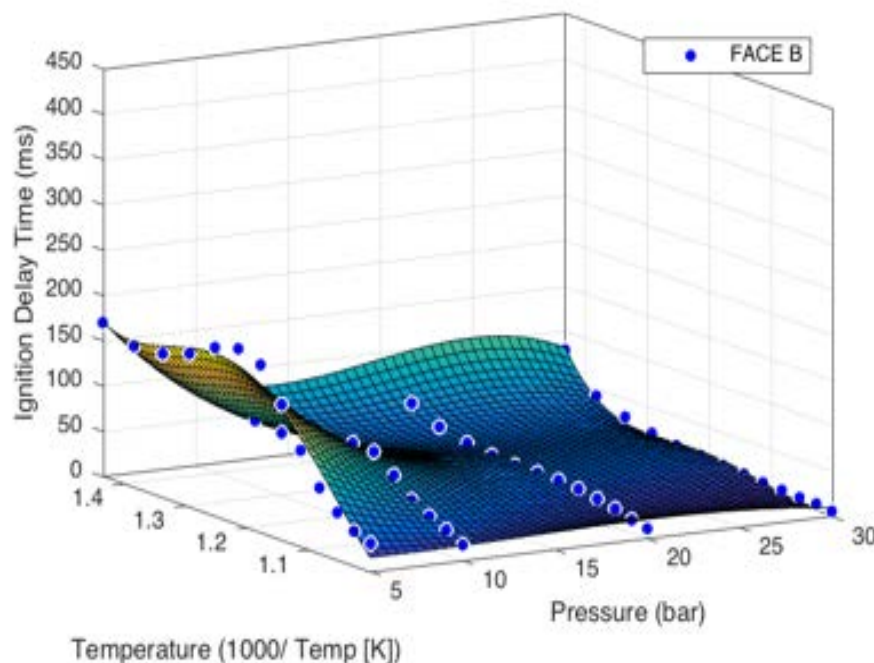
Figure 42: 3D surface of ID time as temperature and pressure change for FACE B. The surface is a 4$^{th}$ order polynomial in temperature and a 3$^{rd}$ order polynomial in pressure.

## 3.3 Correlation

The original plan for correlation with the AVFL-20 fuel set was to correlate the 3D

surface plot of ID time as a function of pressure and temperature of each fuel to the major

chemical compounds identified in the DHA. This plan was modified with the new fuel set, since

the fuels were simple blends of up to 4 components (from a palette of 7 components, as shown in

Table 8), thus making this a more tractable problem. Linear regression was preformed in

MATLAB on the fuel set in numerous ways with the assistance from Dr. Daily. Initially a linear

regression was performed between RON and weight percent of C, H, and O of each of the 9

fuels. This showed poor correlations $R^2$ of 0.31, but this result is not unexpected. Next a linear

regression was performed between RON and the composition of each of the 9 fuels (7

components in total). While this regression was perfect with an $R^2$ value of 1, it wasn't

meaningful. A point was deleted from the set, the regression performed again, and then the

deleted point was used with the regression equation to predict RON. The value was incorrect which shows this correlation is not useful for fuels outside those used in the regression. Unfortunately with such a small set of 9 fuels by 7 components, it is easy to find a perfect but meaningless correlation. Next a regression was performed on the entire set of data: temperature, pressure, $\Phi$, composition, HOV, RON, and S. Figure 43 shows the results of this regression. While the correlation between ID time and 'fit' ID time is not valuable, there is a pattern within the data. Since pressure and thus $\Phi$ changes significantly throughout the fuel set, the data was parsed by pressure, and regressed against temperature and $\Phi$. The results for 5, 10, 20, and 30 bar can be seen in Figure 44, Figure 45, Figure 46 and Figure 47 respectively. The $R^2$ values are 0.63, 0.59, 0.59, and 0.54 for 5, 10, 20, and 30 bar respectively. While the correlation still isn't significant the ID time is clearly dependent on phi and temperature for the fuels. One would not expect a meaningful correlation for this regression, as it does not account for chemical differences between the fuels at all. Finally a regression was performed at each pressure against 1000/temperature [K], phi, composition, HOV, RON and S. The regressions for 5, 10, 20, and 30 bar are shown in Figure 48, Figure 49, Figure 50 and Figure 51 respectively with $R^2$ values of 0.81, 0.77, 0.76, and 0.66. While these correlations still are not significant, and ID time cannot be predicted from the regression, the regression ID times are correlating better to the actual ID times. This is useful as there should be some correlation between composition of fuel and their parametric ID times.
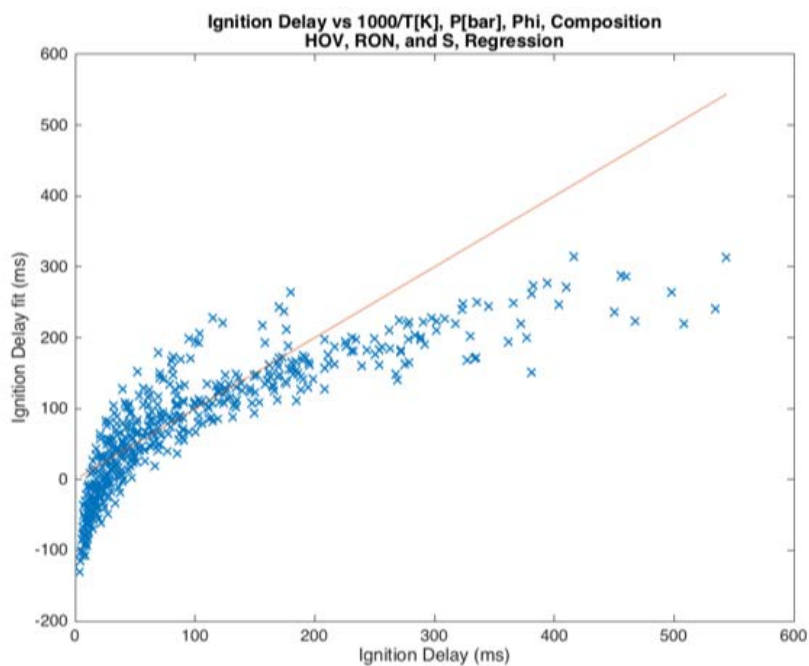
Figure 43: Linear regression of ID time versus: 1000/T [K], Pressure(bar), Φ, composition (vol.% toluene, iso-octane, n-heptane, ethanol, anisole, p-cresol, and o-xylene), HOV, RON, and S.
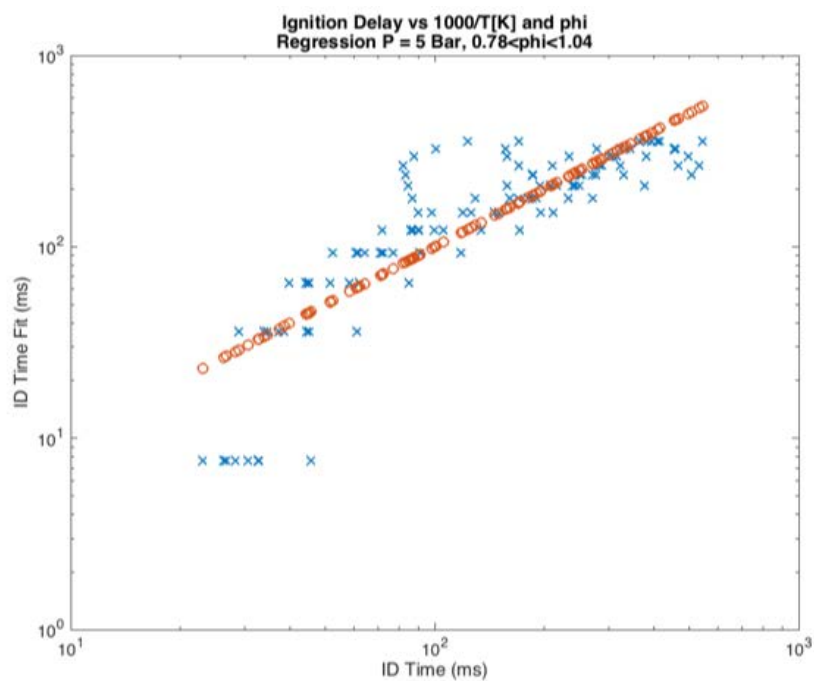


Figure 44: Linear regression of ID time versus: 1000/T [K] and Φ for fuels at 5 bar.
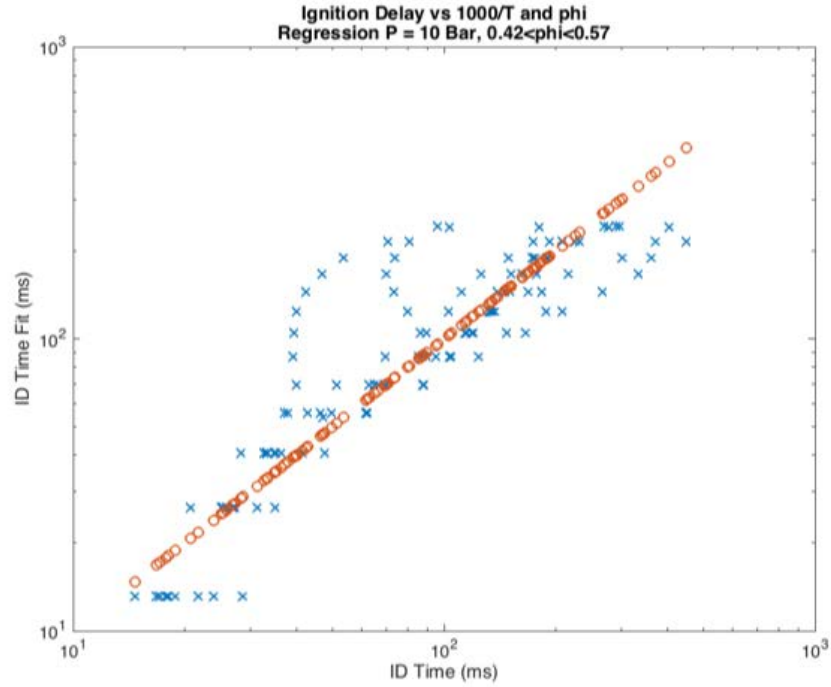
Figure 45: Linear regression of ID time versus: 1000/T [K] and Φ for fuels at 10 bar.
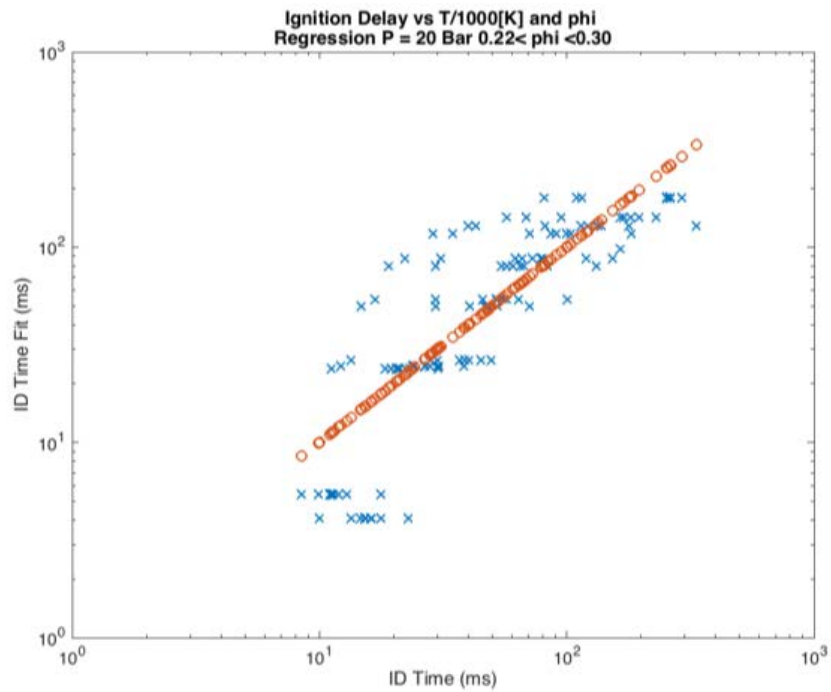


Figure 46: Linear regression of ID time versus: 1000/T [K] and Φ for fuels at 20 bar.
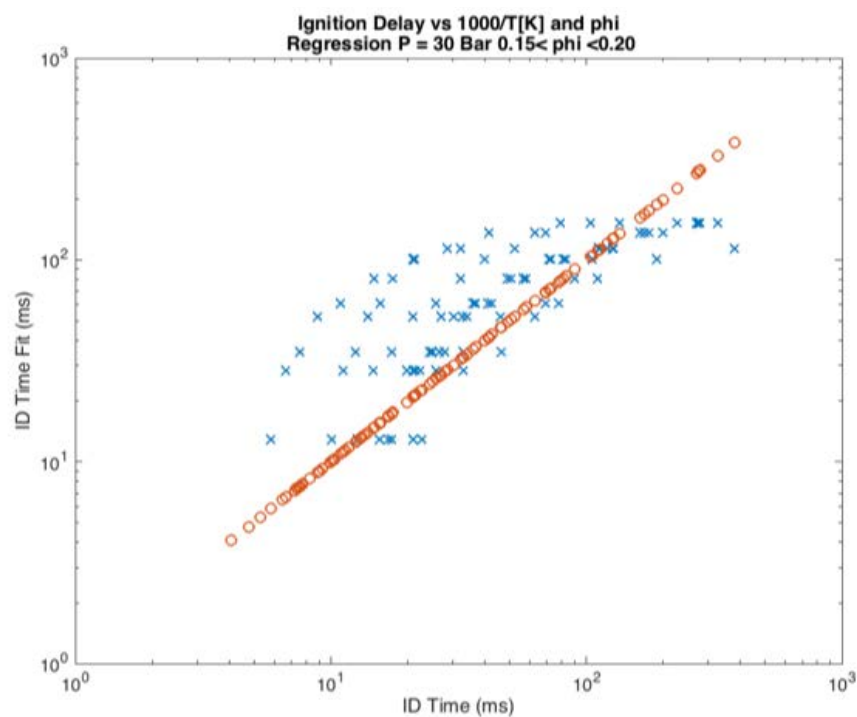
Figure 47: Linear regression of ID time versus: 1000/T [K] and Φ for fuels at 30 bar.
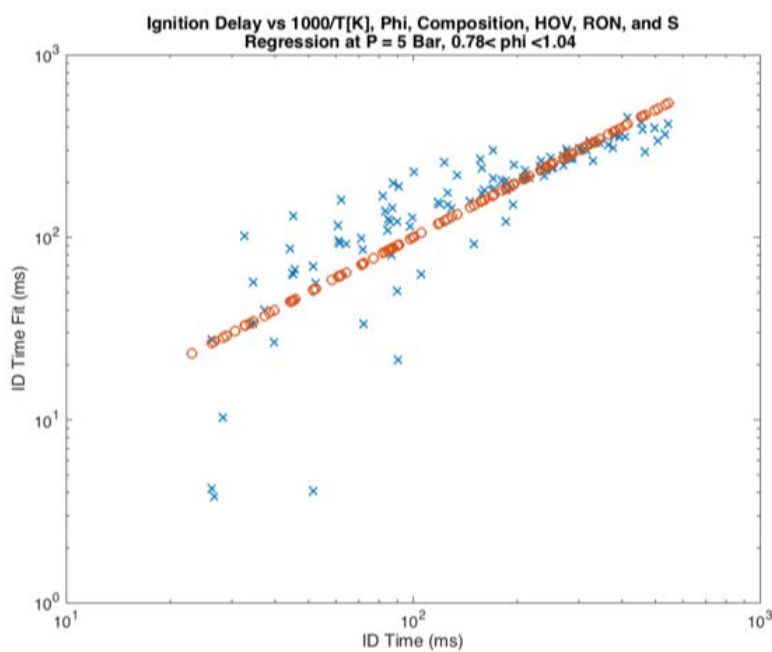


Figure 48: Linear regression of ID time versus: 1000/T [K], Φ, composition (vol.% toluene, iso-octane, n-heptane, ethanol, anisole, p-cresol, and o-xylene), HOV, RON, and S at 5 bar.
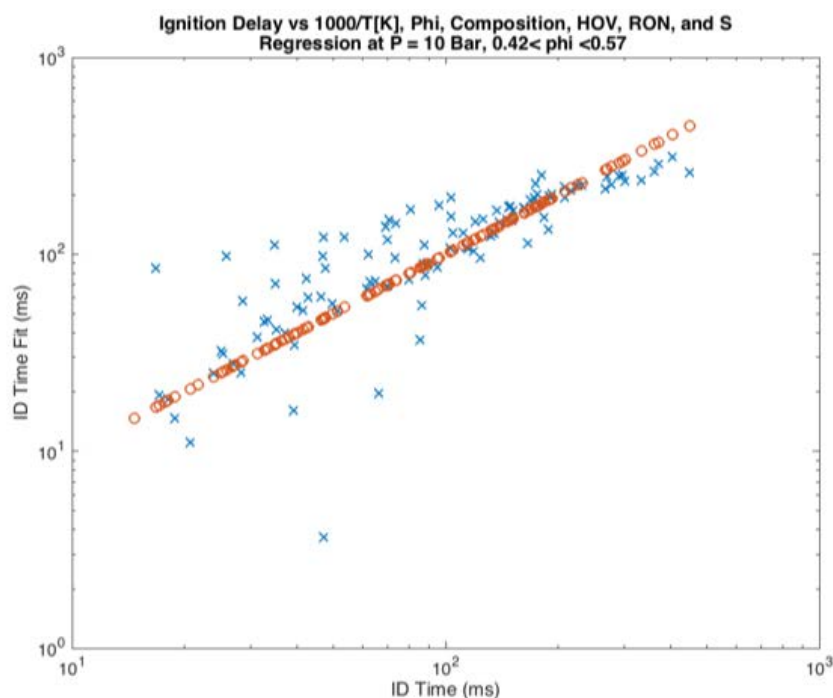
Figure 49: Linear regression of ID time versus: 1000/T [K], Φ, composition (vol.% toluene, iso-octane, n-heptane, ethanol, anisole, p-cresol, and o-xylene), HOV, RON, and S at 10 bar.
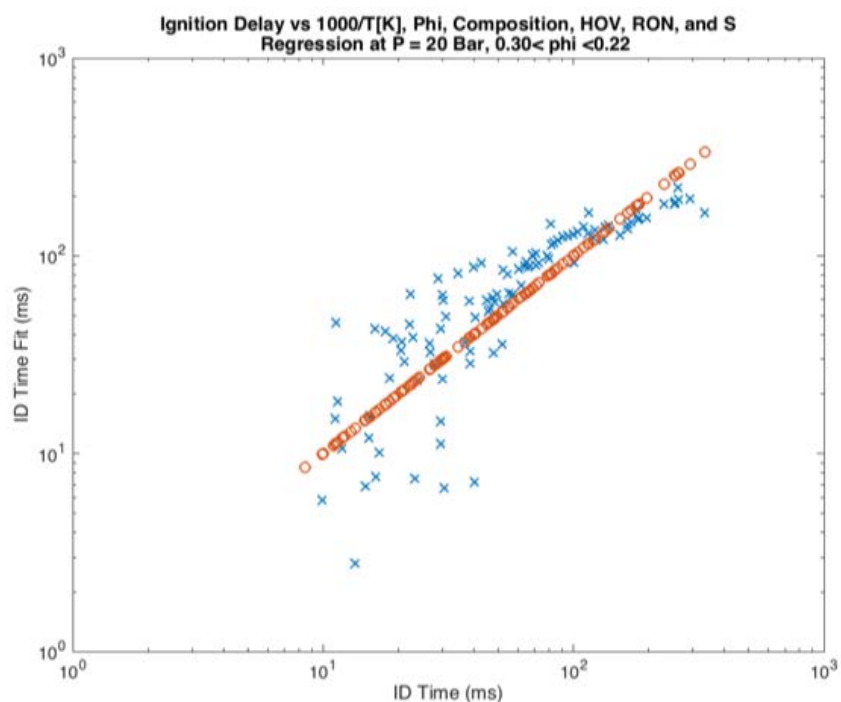


Figure 50: Linear regression of ID time versus: 1000/T [K], Φ, composition (vol.% toluene, iso-octane, n-heptane, ethanol, anisole, p-cresol, and o-xylene), HOV, RON, and S at 20 bar.
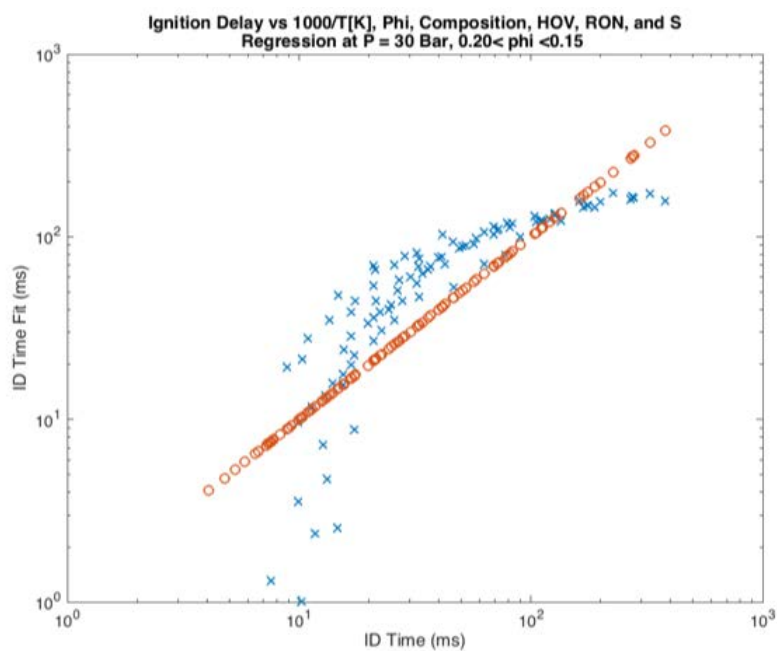
Figure 51: Linear regression of ID time versus: 1000/T [K], Φ, composition (vol.% toluene, iso-octane, n-heptane, ethanol, anisole, p-cresol, and o-xylene), HOV, RON, and S at 30 bar.

CHAPTER 4

Conclusion

## 4.1 Conclusions

Significant correlation between parametric ID and composition was not found with the regression methodologies used in this research. While the linear regression analysis on all fuel properties and composition at each pressure was an improved correlation to the previous attempts, it is clear that the data do not fit a linear model. More advanced regression work would need to be conducted to determine a consistent correlation between fuel autoignition and its composition, without resorting to building kinetic mechanisms. The ID time should relate back to the chemical composition as well as the temperature and pressure conditions of the test. Though a clear correlation was not determined, the research provided valuable information about the fuel set and 3D surfaces of fuel ID are more indicative of knock resistance that the two engine conditions run with RON and MON tests.  Most importantly, crucial information was learned about the AFIDA and progress was made in the ability to test gasoline range fuels in this new highly flexible CVCC. While the IQT has been extremely useful for the study of PRFs and other simple component blends, research was approaching the limits of its capabilities. In order to examine fuels with lower boiling fractions more reflective of gasolines, it is necessary to migrate research to the AFIDA. This study is valuable as it is the first study of its kind in the AFIDA with gasoline range fuels. It is possible a more meaningful correlation could be made with more advanced regression analysis.

## 4.2 Future Work

Going forward the surrogate blend for FACE B will be tested in the AFIDA, under the same conditions as the fuel set in this study, to determine its success in replicating FACE B. This

study was more focused on testing the fuel set, while performing simple correlation work. Future work will be conducted with these results to implement a more complex regression analysis between the ID time and the fuel composition. Currently the significant change in $\Phi$ from 1.04 to 0.20 is not desirable and adds another changing variable, which most similar studies keep relatively constant. For more studies like this to progress with gasoline range fuels in the AFIDA it will be important to modify the fuel injection system with a larger rail volume in order to reach a $\Phi$ of 1 at all desirable test conditions (up to 30 bar and down to 400 °C). Future work will also look to study more complex gasoline surrogates and blends, which are not able to be studied in tho other CVCCs, RCMs, or shock tubes that are currently used in this area of research.

# Citations

[1] Energy Information Administration, Monthly Energy Review, August 2017, Tables 2.1 and 2.5. https://www.eia.gov/totalenergy/data/monthly/archive/00351708.pdf

[2] U.S. Department of Energy, Vehicle Technologies Office, "Transportation Analysis Fact of the Week #996", September 27, 2017. https://energy.gov/eere/vehicles/articles/fact-996-september-25-2017-transportation-accounts-nearly-three-quarters

[3] Oak Ridge National Laboratory, Transportation Energy Data Book: Edition 35, October 2016, ORNL-6992, Table 1.16. http://cta.ornl.gov/data/tedb35/Edition35_Full_Doc.pdf

[4] Mittal, V., Heywood, J.B., 2009. The Shift in Relevance of Fuel RON and MON to Knock Onset in Modern SI Engines Over the Last 70 Years. SAE International Journal of Engines 2, 1–10. https://doi.org/10.4271/2009-01-2622

[5] Mittal, V., Heywood, J.B., 2008. The Relevance of Fuel RON and MON to Knock Onset in Modern SI Engines. https://doi.org/10.4271/2008-01-2414

[6] Dr, Y.A.C., Boles, M.A., 2014. Thermodynamics: An Engineering Approach, 8 edition. ed. McGraw-Hill Education, New York, NY.

[7] Tatarevic, B., n.d. The Truth About Gas! Does Premium Fuel Perform Better? – Hoonable.

[8] Szybist, J.P., Splitter, D.A., 2017. Pressure and temperature effects on fuels with varying octane sensitivity at high load in SI engines. Combustion and Flame 177, 49–66. https://doi.org/10.1016/j.combustflame.2016.12.002

[9] ASTM D2699 - 13b, Standard Test Method for Research Octane Number of Spark-Ignition Engine Fuel. Annual Book of ASTM Standards, Vol. 5.05, 2013. https://doi.org/10.1520/D2699

[10] ASTM D2700 - 13b, Standard Test Method for Motor Octane Number of Spark-Ignition Engine Fuel. Annual Book of ASTM Standards, Vol. 5.05, 2013. https://doi.org/10.1520/D2700-17

[11] Sluder, C.S., Szybist, J.P., McCormick, R.L., Ratcliff, M.A., Zigler, B.T., 2016. Exploring the Relationship Between Octane Sensitivity and Heat-of-Vaporization. SAE International Journal of Fuels and Lubricants 9, 80–90. https://doi.org/10.4271/2016-01-0836

[12] Stein, R.A., Polovina, D., Roth, K., Foster, M., Lynskey, M., Whiting, T., Anderson, J.E., Shelby, M.H., Leone, T.G., VanderGriend, S., 2012. Effect of Heat of Vaporization, Chemical Octane, and Sensitivity on Knock Limit for Ethanol - Gasoline Blends. SAE International Journal of Fuels and Lubricants 5, 823–843. https://doi.org/10.4271/2012-01-1277

[13] Anderson, J.E., Leone, T.G., Shelby, M.H., Wallington, T.J., Bizub, J.J., Foster, M., Lynskey, M.G., Polovina, D., 2012. Octane Numbers of Ethanol-Gasoline Blends: Measurements and Novel Estimation Method from Molar Composition. https://doi.org/10.4271/2012-01-1274

[14] Davidson, D.F., Haylett, D.R., Hanson, R.K., 2008. Development of an aerosol shock tube for kinetic studies of low-vapor-pressure fuels. Combustion and Flame 155, 108–117. https://doi.org/10.1016/j.combustflame.2008.01.006

[15] Shen, H.-P.S., Oehlschlaeger, M.A., 2009. The autoignition of C8H10 aromatics at moderate temperatures and elevated pressures. Combustion and Flame 156, 1053–1062. https://doi.org/10.1016/j.combustflame.2008.11.015

[16] Allen, C., Mittal, G., Sung, C.-J., Toulson, E., Lee, T., 2011. An aerosol rapid compression machine for studying energetic-nanoparticle-enhanced combustion of liquid fuels. Proceedings of the Combustion Institute 33, 3367–3374. https://doi.org/10.1016/j.proci.2010.06.007

[17] Karwat, D.M.A., Wagnon, S.W., Teini, P.D., Wooldridge, M.S., 2011. On the Chemical Kinetics of n-Butanol: Ignition and Speciation Studies. J. Phys. Chem. A 115, 4909–4921. https://doi.org/10.1021/jp200905n

[18] Fisher, B.T., Allen, J.C., Hancock, R.L., Bittle, J.A., 2017. Evaluating the Potential of a Direct-Injection Constant-Volume Combustion Chamber as a Tool to Validate Chemical-Kinetic Models for Liquid Fuels. Combustion Science and Technology 189, 1–23. https://doi.org/10.1080/00102202.2016.1193015

[19] Bogin, G., Dean, A.M., Ratcliff, M.A., Luecke, J., Zigler, B.T., 2010. Expanding the Experimental Capabilities of the Ignition Quality Tester for Autoigniting Fuels. SAE Int. J. Fuels Lubr. 3, 353–367. https://doi.org/10.4271/2010-01-0741

[20] Tekawade, A., Oehlschlaeger, M.A., 2016. An experimental study of the spray ignition of alkanes. Fuel 185, 381–393. https://doi.org/10.1016/j.fuel.2016.07.108

[21] Coordinating Research Council,. About CRC. https://crcao.org/about/index.html.

[22] Coordinating Research Council, INC, 2017. CRC ANNUAL REPORT 2017.

[23] M. A. Ratcliff, J. Burton, P. Sindler, R. L. McCormick, L. Fouts, and E. Christensen,. Effects of Heat of Vaporization and Octane Sensitivity on Knock-Limited Spark Ignition Engine Performance. under review by SAE International.

[24] Foong, T.M., Morganti, K.J., Brear, M.J., da Silva, G., Yang, Y., Dryer, F.L., 2014. The octane numbers of ethanol blended with gasoline and its surrogates. Fuel 115, 727–739. https://doi.org/10.1016/j.fuel.2013.07.105

[25] Morgan, N., Smallbone, A., Bhave, A., Kraft, M., Cracknell, R., Kalghatgi, G., 2010. Mapping surrogate gasoline compositions into RON/MON space. Combustion and Flame 157, 1122–1131. https://doi.org/10.1016/j.combustflame.2010.02.003

[26] Cannella, W., Foster, M., Gunter, G., Leppard, W., 2014. FACE GASOLINES AND BLENDS WITH ETHANOL: DETAILED CHARACTERIZATION OF PHYSICAL AND CHEMICAL PROPERTIES (No. AVFL-24). Coordinating Research Council, Inc.

[27] Allard, L.N., Webster, G.D., Hole, N.J., Ryan, T.W., Ott, D., Fairbridge, C.W., 1996. Diesel Fuel Ignition Quality as Determined in the Ignition Quality Tester (IQT). https://doi.org/10.4271/961182

[28] Allard, L.N., Hole, N.J., Webster, G.D., Ryan, T.W., Ott, D., Beregszazy, A., Fairbridge, C.W., Cooley, J., Mitchell, K., Richardson, E.K., Elliot, N.G., Rickeard, D.J., 1997. Diesel Fuel Ignition Quality as Determined in the Ignition Quality Tester (IQT) - Part II. https://doi.org/10.4271/971636

[29] Allard, L.N., Webster, G.D., Ryan, T.W., Baker, G., Beregszaszy, A., Fairbridge, C.W., Ecker, A., Rath, J., 1999. Analysis of the Ignition Behaviour of the ASTM D-613 Primary Reference Fuels and Full Boiling Range Diesel Fuels in the Ignition Quality Tester (IQT$^{TM}$) - Part III. https://doi.org/10.4271/1999-01-3591

[30] Allard, L.N., Webster, G.D., Ryan, T.W., Matheaus, A.C., Baker, G., Beregszaszy, A., Read, H., Mortimer, K., Jones, G., 2001. Diesel Fuel Ignition Quality as Determined in the Ignition Quality Tester (IQT$^{TM}$) - Part IV. https://doi.org/10.4271/2001-01-3527

[31] ASTM D6890-16e1, Standard Test Method for Determination of Ignition Delay and Derived Cetane Number (DCN) of Diesel Fuel Oils by Combustion in a Constant Volume Chamber. ASTM International. West Conshohocken, PA, 2016. https://doi.org/10.1520/D6890-16E01

[32] ASTM D613-17b, Standard Test Method for Cetane Number of Diesel Fuel Oil. ASTM International. West Conshohocken, PA, 2017. https://doi.org/10.1520/D0613-17B

[33] Bogin, G.E., Jr., Luecke, J., Ratcliff, M.A., Osecky, E., Zigler, B.T., 2016. Effects of iso-octane/ethanol blend ratios on the observance of negative temperature coefficient behavior within the Ignition Quality Tester. Fuel 186, 82–90. https://doi.org/10.1016/j.fuel.2016.08.021

[34] Webster, G., n.d. Ignition Quality Tester (IQT(tm)) [WWW Document]. URL http://aet.ca/files/resourcesmodule/@random428b4e06ecd32/1254780127_IQT_Brochure___June_18__2009_with_EN590__stainless_steel_mod.pdf

[35] Bogin, G.E., Osecky, E., Ratcliff, M.A., Luecke, J., He, X., Zigler, B.T., Dean, A.M., 2013. Ignition Quality Tester (IQT) Investigation of the Negative Temperature Coefficient Region of Alkane Autoignition. Energy Fuels 27, 1632–1642. https://doi.org/10.1021/ef301738b

[36] Seidenspinner, P., Härtl, M., Wilharm, T., and Wachtmeister, G., 2015. Cetane Number Determination by Advanced Fuel Ignition Delay Analysis in a New Constant Volume Combustion Chamber. http://doi.org/10.4271/2015-01-0798.

[37] AFIDA manual, ASG Analytik-Service Gesellschaft mbH, Germany

[38] Audi Technology Portal - Piezo-Injektoren [WWW Document], n.d. . Audi Technology Portal. URL https://www.audi-technology-portal.de/de/antrieb/tdi-motoren/piezo-injektoren?c=image:506 (accessed 11.1.17).

[39] Kolodziej, C., Kodavasal, J., Ciatti, S., Som, S. et al., 2015. Achieving Stable Engine Operation of Gasoline Compression Ignition Using 87 AKI Gasoline Down to Idle. SAE Technical Paper 2015-01-0832. http://doi.org/10.4271/2015-01-0832.

[40] Osecky, E.M., Bogin, G.E., Jr., Villano, S.M., Ratcliff, M.A., Luecke, J., Zigler, B.T., Dean, A.M., 2016. Investigation of Iso-octane Ignition and Validation of a Multizone Modeling Method in an Ignition Quality Tester. Energy and Fuels 30, 9761–9771. https://doi.org/10.1021/acs.energyfuels.6b01406

[41] Chupka, G.M., Christensen, E., Fouts, L., Alleman, T.L., Ratcliff, M.A., McCormick, R.L., 2015. Heat of Vaporization Measurements for Ethanol Blends Up To 50 Volume Percent in Several Hydrocarbon Blendstocks and Implications for Knock in SI Engines. SAE International Journal of Fuels and Lubricants 8. https://doi.org/10.4271/2015-01-0763

[42] ASTM D6729-14, Standard Test Method for Determination of Individual Components in Spark Ignition Engine Fuels by 100 Metre Capillary High Resolution Gas Chromatography, ASTM International. West Conshohocken, PA, 2014. https://doi.org/10.1520/D6729-14

[43] Morgan, N., Smallbone, A., Bhave, A., Kraft, M., Cracknell, R., Kalghatgi, G., 2010. Mapping surrogate gasoline compositions into RON/MON space. Combustion and Flame 157, 1122–1131. https://doi.org/10.1016/j.combustflame.2010.02.003

[44] Ratcliff, M.A., Burton, J., Sindler, P., Christensen, E., Fouts, L., Chupka, G.M., McCormick, R.L., 2016. Knock Resistance and Fine Particle Emissions for Several Biomass-Derived Oxygenates in a Direct-Injection Spark-Ignition Engine. SAE International Journal of Fuels and Lubricants 9, 59–70. https://doi.org/10.4271/2016-01-0705

[45] Aikawa, K., Sakurai, T., Jetter, J.J., 2010. Development of a Predictive Model for Gasoline Vehicle Particulate Matter Emissions. SAE International Journal of Fuels and Lubricants 3, 610–622. https://doi.org/10.4271/2010-01-2115

[46] October 31, 2017, Personal communication with Dr. Scott Wagnon, Lawrence Livermore National Laboratory.

## Appendix A:

## Detailed Hydrocarbon Analysis

Table A- 1: Detailed hydrocarbon analysis of FACE B summary by group, courtesy of Earl
Christensen of NREL.

| GROUP | %WGT | %VOL | %MOL | AREA | AVERAGE_ MW | AVERAGE_ SG |
|---|---|---|---|---|---|---|
| Paraffin | 6.530 | 7.476 | 10.143 | 1722.538 | 6.614 | 0.045 |
| I-Paraffins | 85.635 | 86.251 | 82.486 | 22854.648 | 86.742 | 0.592 |
| Aromatics | 7.440 | 5.936 | 7.098 | 2140.812 | 7.537 | 0.051 |
| Mono-Aromatics | 7.440 | 5.936 | 7.098 | 2140.812 | 7.537 | 0.051 |
| Naphthalenes | 0.000 | 0.000 | 0.000 | 0.000 | 0.000 | 0.000 |
| Indanes | 0.000 | 0.000 | 0.000 | 0.000 | 0.000 | 0.000 |
| Indenes | 0.000 | 0.000 | 0.000 | 0.000 | 0.000 | 0.000 |
| Naphthenes | 0.004 | 0.004 | 0.006 | 1.146 | 0.004 | 0.000 |
| Mono-Naphthenes | 0.004 | 0.004 | 0.006 | 1.146 | 0.004 | 0.000 |
| Di/Bicyclo-Naphthenes | 0.000 | 0.000 | 0.000 | 0.000 | 0.000 | 0.000 |
| Olefins | 0.025 | 0.024 | 0.019 | 6.737 | 0.025 | 0.000 |
| n-Olefins | 0.016 | 0.015 | 0.013 | 4.401 | 0.016 | 0.000 |
| Iso-Olefins | 0.009 | 0.008 | 0.006 | 2.337 | 0.009 | 0.000 |
| Naphtheno-Olefins | 0.000 | 0.000 | 0.000 | 0.000 | 0.000 | 0.000 |
| Di-Olefins | 0.000 | 0.000 | 0.000 | 0.000 | 0.000 | 0.000 |
| Oxygenates | 0.000 | 0.000 | 0.000 | 0.000 | 0.000 | 0.000 |
| Unidentified | 0.366 | 0.309 | 0.247 | 108.902 | 0.371 | 0.003 |
| Plus | 0.000 | 0.000 | 0.000 | 0.000 | 0.000 | 0.000 |

Table A- 2: Detailed hydrocarbon analysis of FACE B summary by carbon weight
percent, courtesy of Earl Christensen of NREL.

| Carbon# | Paraffin | I-Paraffins | Aromatics | Naphthenes | Olefins | Oxygenates | Plus | Total |
|---|---|---|---|---|---|---|---|---|
| 1 | -- | -- | -- | -- | -- | -- | -- | 0.000 |
| 2 | -- | -- | -- | -- | -- | -- | -- | 0.000 |
| 3 | -- | -- | -- | -- | -- | -- | -- | 0.000 |
| 4 | 3.146 | 0.070 | -- | -- | -- | -- | -- | 3.215 |
| 5 | 3.237 | 9.088 | -- | 0.004 | -- | -- | -- | 12.329 |
| 6 | 0.017 | 1.240 | -- | -- | -- | -- | -- | 1.257 |
| 7 | 0.005 | 13.501 | -- | -- | -- | -- | -- | 13.506 |
| 8 | -- | 59.626 | 7.434 | -- | -- | -- | -- | 67.060 |
| 9 | 0.100 | 1.672 | 0.006 | -- | 0.016 | -- | -- | 1.794 |
| 10 | -- | 0.388 | -- | -- | 0.009 | -- | -- | 0.397 |
| 11 | -- | 0.050 | -- | -- | -- | -- | -- | 0.050 |
| 12 | -- | -- | -- | -- | -- | -- | -- | 0.000 |
| 13 | -- | -- | -- | -- | -- | -- | -- | 0.000 |

| 14 | 0.025 | -- | -- | -- | -- | -- | -- | 0.025 |
|---|---|---|---|---|---|---|---|---|
| 15 | -- | -- | -- | -- | -- | -- | -- | 0.000 |
| | | | | | | | | |
| TOTAL | 6.530 | 85.635 | 7.440 | 0.004 | 0.025 | 0.000 | 0.000 | 99.634 |
| | | | | | | | UNKNOWNS | 0.366 |
| | | | | | | | GRAND_TOTAL | 100.000 |

Table A- 3: DHA components listed by group in weight volume and mole percent, courtesy of Earl Christensen of NREL.

| Group | Time | Ri | Component | %Wgt | %Vol | %Mol | Area | Average_MW | Average_SG |
|---|---|---|---|---|---|---|---|---|---|
| Paraffin | 10.142 | 400.00 | n-Butane | 3.146 | 3.759 | 5.482 | 826.590 | 3.186 | 0.022 |
| Paraffin | 18.046 | 500.00 | n-Pentane | 3.237 | 3.575 | 4.545 | 856.556 | 3.279 | 0.022 |
| Paraffin | 34.923 | 600.00 | n-Hexane | 0.017 | 0.018 | 0.020 | 4.580 | 0.017 | 0.000 |
| Paraffin | 55.643 | 700.00 | n-heptane | 0.005 | 0.005 | 0.005 | 1.311 | 0.005 | 0.000 |
| Paraffin | 87.368 | 900.00 | n-Nonane | 0.100 | 0.096 | 0.079 | 26.686 | 0.101 | 0.001 |
| Paraffin | 122.200 | 1400.00 | n-Tetradecane | 0.025 | 0.023 | 0.013 | 6.815 | 0.026 | 0.000 |
| I-Paraffins | 8.959 | 354.37 | i-Butane | 0.070 | 0.086 | 0.121 | 18.304 | 0.071 | 0.000 |
| I-Paraffins | 10.753 | 410.19 | 2,2-Dimethylpropane | 0.012 | 0.014 | 0.016 | 3.096 | 0.012 | 0.000 |
| I-Paraffins | 15.085 | 468.92 | i-Pentane | 9.076 | 10.131 | 12.742 | 2401.562 | 9.193 | 0.063 |
| I-Paraffins | 27.840 | 565.68 | 2,3-Dimethylbutane | 0.851 | 0.889 | 1.000 | 225.967 | 0.862 | 0.006 |
| I-Paraffins | 28.873 | 571.19 | 2-Methylpentane | 0.259 | 0.275 | 0.305 | 68.930 | 0.263 | 0.002 |
| I-Paraffins | 31.387 | 583.84 | 3-Methylpentane | 0.130 | 0.136 | 0.153 | 34.592 | 0.132 | 0.001 |
| I-Paraffins | 40.913 | 633.97 | 2,4-Dimethylpentane | 4.226 | 4.345 | 4.271 | 1127.057 | 4.280 | 0.029 |
| I-Paraffins | 41.435 | 636.69 | 2,2,3-Trimethylbutane | 0.017 | 0.017 | 0.017 | 4.587 | 0.017 | 0.000 |
| I-Paraffins | 48.803 | 671.80 | 2-Methylhexane | 9.083 | 9.257 | 9.181 | 2422.565 | 9.200 | 0.063 |
| I-Paraffins | 50.462 | 678.98 | 3-Methylhexane | 0.176 | 0.177 | 0.178 | 46.986 | 0.178 | 0.001 |
| I-Paraffins | 53.104 | 689.93 | 2,2,4-Trimethylpentane | 39.137 | 39.123 | 34.704 | 10459.763 | 39.643 | 0.271 |
| I-Paraffins | 61.933 | 736.59 | 2,2,3- | 0.673 | 0.650 | 0.596 | 179.776 | 0.681 | 0.005 |

| | | | Trimethylpentane | | | | | | |
|---|---|---|---|---|---|---|---|---|---|
| I-Paraffins | 62.192 | 738.02 | 2,5-Dimethylhexane | 1.308 | 1.304 | 1.159 | 349.470 | 1.325 | 0.009 |
| I-Paraffins | 62.503 | 739.73 | 2,4-Dimethylhexane | 1.865 | 1.842 | 1.654 | 498.519 | 1.889 | 0.013 |
| I-Paraffins | 65.393 | 755.21 | 2,3,4-Trimethylpentane | 8.645 | 8.316 | 7.666 | 2310.388 | 8.756 | 0.060 |
| I-Paraffins | 66.013 | 758.44 | 2,3,3-Trimethylpentane | 5.852 | 5.574 | 5.189 | 1564.075 | 5.928 | 0.040 |
| I-Paraffins | 67.666 | 766.91 | 2,3-Dimethylhexane | 1.735 | 1.686 | 1.539 | 463.822 | 1.758 | 0.012 |
| I-Paraffins | 67.778 | 767.47 | 2-Methyl-3-ethylpentane | 0.051 | 0.049 | 0.045 | 13.552 | 0.051 | 0.000 |
| I-Paraffins | 68.919 | 773.19 | 2-Methylheptane | 0.032 | 0.032 | 0.029 | 8.620 | 0.033 | 0.000 |
| I-Paraffins | 69.143 | 774.31 | 4-Methylheptane | 0.147 | 0.145 | 0.131 | 39.358 | 0.149 | 0.001 |
| I-Paraffins | 69.268 | 774.92 | 3,4-Dimethylhexane | 0.148 | 0.142 | 0.131 | 39.445 | 0.149 | 0.001 |
| I-Paraffins | 70.186 | 779.43 | 3-Methylheptane | 0.033 | 0.033 | 0.030 | 8.892 | 0.034 | 0.000 |
| I-Paraffins | 71.987 | 788.11 | 2,2,5-Trimethylhexane | 1.203 | 1.176 | 0.950 | 322.096 | 1.218 | 0.008 |
| I-Paraffins | 72.896 | 792.40 | 2,2,4-Trimethylhexane | 0.020 | 0.019 | 0.016 | 5.355 | 0.020 | 0.000 |
| I-Paraffins | 76.818 | 819.00 | 2,3,5-Trimethylhexane | 0.210 | 0.201 | 0.166 | 56.124 | 0.212 | 0.001 |
| I-Paraffins | 77.944 | 828.15 | 2,4-Dimethylheptane | 0.037 | 0.036 | 0.030 | 10.006 | 0.038 | 0.000 |
| I-Paraffins | 78.849 | 835.41 | 2,6-Dimethylheptane | 0.013 | 0.013 | 0.011 | 3.613 | 0.014 | 0.000 |
| I-Paraffins | 79.702 | 842.17 | 2,5-Dimethylheptane | 0.061 | 0.059 | 0.048 | 16.392 | 0.062 | 0.000 |
| I-Paraffins | 79.846 | 843.31 | 2-Methyl-4-ethylhexane | 0.006 | 0.006 | 0.005 | 1.703 | 0.006 | 0.000 |

| I-Paraffins | 81.250 | 854.27 | 3,3-Diethylpentane | 0.016 | 0.015 | 0.013 | 4.330 | 0.016 | 0.000 |
|---|---|---|---|---|---|---|---|---|---|
| I-Paraffins | 82.328 | 862.56 | 2,3-Dimethylheptane | 0.067 | 0.064 | 0.053 | 17.913 | 0.068 | 0.000 |
| I-Paraffins | 82.558 | 864.30 | 3,5-Dimethylheptane | 0.007 | 0.007 | 0.006 | 1.985 | 0.008 | 0.000 |
| I-Paraffins | 82.658 | 865.07 | 4-Ethylheptane | 0.010 | 0.010 | 0.008 | 2.795 | 0.011 | 0.000 |
| I-Paraffins | 83.321 | 870.09 | Heptane, 3-ethyl- | 0.005 | 0.005 | 0.004 | 1.379 | 0.005 | 0.000 |
| I-Paraffins | 83.448 | 871.04 | 2-Methyloctane | 0.007 | 0.006 | 0.005 | 1.746 | 0.007 | 0.000 |
| I-Paraffins | 84.240 | 876.99 | 3-Methyloctane | 0.008 | 0.008 | 0.007 | 2.241 | 0.008 | 0.000 |
| I-Paraffins | 85.206 | 884.15 | C10 - Isoparaffin - 2 | 0.104 | 0.099 | 0.074 | 27.993 | 0.106 | 0.001 |
| I-Paraffins | 85.966 | 889.74 | 2,2,4-trimethylheptane | 0.185 | 0.175 | 0.131 | 49.508 | 0.187 | 0.001 |
| I-Paraffins | 89.351 | 920.43 | 2,3,6-trimethylheptane | 0.049 | 0.034 | 0.035 | 13.208 | 0.050 | 0.000 |
| I-Paraffins | 89.553 | 922.50 | 2,2-Dimethyloctane | 0.019 | 0.018 | 0.014 | 5.111 | 0.019 | 0.000 |
| I-Paraffins | 90.321 | 930.33 | C10 - IsoParaffin - 2(1) | 0.004 | 0.004 | 0.003 | 1.084 | 0.004 | 0.000 |
| I-Paraffins | 90.849 | 935.68 | 2,4-Dimethyloctane | 0.011 | 0.011 | 0.008 | 3.019 | 0.011 | 0.000 |
| I-Paraffins | 93.326 | 960.33 | 2,3-Dimethyloctane(1) | 0.006 | 0.006 | 0.004 | 1.679 | 0.006 | 0.000 |
| I-Paraffins | 94.166 | 968.54 | C11-Isoparaffin-1 | 0.050 | 0.047 | 0.033 | 13.512 | 0.051 | 0.000 |
| I-Paraffins | 95.398 | 980.45 | C10 - IsoParaffin - 5 | 0.009 | 0.009 | 0.007 | 2.535 | 0.010 | 0.000 |
| Mono-Aromatics | 80.863 | 851.26 | Ethylbenzene | 1.125 | 0.898 | 1.074 | 323.755 | 1.140 | 0.008 |
| Mono-Aromatics | 82.011 | 860.13 | m-Xylene | 3.421 | 2.738 | 3.264 | 984.294 | 3.465 | 0.024 |
| Mono-Aromatics | 82.142 | 861.13 | p-Xylene | 1.471 | 1.182 | 1.404 | 423.287 | 1.490 | 0.010 |
| Mono-Aromatics | 84.737 | 880.68 | o-Xylene | 1.417 | 1.113 | 1.352 | 407.643 | 1.435 | 0.010 |

| Mono-Aromatics | 88.603 | 912.73 | i-Propylbenzene | 0.006 | 0.005 | 0.005 | 1.833 | 0.006 | 0.000 |
|---|---|---|---|---|---|---|---|---|---|
| Mono-Naphthenes | 27.168 | 561.98 | Cyclopentane | 0.004 | 0.004 | 0.006 | 1.146 | 0.004 | 0.000 |
| n-Olefins | 84.638 | 879.95 | C9-isoolefin | 0.009 | 0.009 | 0.007 | 2.437 | 0.009 | 0.000 |
| n-Olefins | 88.917 | 915.97 | c-Nonene-2 | 0.007 | 0.006 | 0.006 | 1.964 | 0.007 | 0.000 |
| Iso-Olefins | 87.443 | 900.66 | C10 - IsoOlefin - 1 | 0.009 | 0.008 | 0.006 | 2.337 | 0.009 | 0.000 |
| Unidentified | 75.343 | 806.81 | Unidentified | 0.050 | 0.042 | 0.034 | 14.966 | 0.051 | 0.000 |
| Unidentified | 81.039 | 852.63 | Unidentified | 0.016 | 0.014 | 0.011 | 4.799 | 0.016 | 0.000 |
| Unidentified | 88.816 | 914.93 | Unidentified | 0.007 | 0.006 | 0.005 | 2.120 | 0.007 | 0.000 |
| Unidentified | 95.771 | 984.03 | Unidentified | 0.005 | 0.004 | 0.003 | 1.416 | 0.005 | 0.000 |
| Unidentified | 133.832 | 2153.76 | Unidentified | 0.013 | 0.011 | 0.009 | 3.887 | 0.013 | 0.000 |
| Unidentified | 141.383 | 2599.19 | Unidentified | 0.275 | 0.232 | 0.186 | 81.713 | 0.278 | 0.002 |

Table A- 4: DHA for PRF100 in weight, volume and molar percent of the components; the percent carbon, hydrogen and oxygen; and particulate matter index, average density.

| COMPONENT | %WGT | %VOL | %MOL |
|---|---|---|---|
| 2-Methylhexane | 0.04 | 0.04 | 0.05 |
| 2,2,4-Trimethylpentane | 99.89 | 99.89 | 99.88 |
| 2,2-Dimethylhexane | 0.07 | 0.07 | 0.07 |
| | | | |
| %H | 15.9 | | |
| PMI | 0.19 | | |

Table A- 5: DHA for TRF99.8 in weight, volume and molar percent of the components; the percent carbon, hydrogen and oxygen; and particulate matter index, average density.

| COMPONENT | %WGT | %VOL | %MOL |
|---|---|---|---|
| n-heptane | 13.42 | 16.09 | 12.69 |
| 2,2,4-Trimethylpentane | 8.70 | 10.30 | 7.21 |
| Toluene | 77.86 | 73.59 | 80.08 |
| Ethylbenzene | 0.02 | 0.02 | 0.02 |
| | | | |
| Density (g/mL)at 15C | 0.8235 | | |
| %H | 10.4 | | |
| PMI | 0.96 | | |

Table A- 6: DHA for TRF88 in weight, volume and molar percent of the components; the percent carbon, hydrogen and oxygen; and particulate matter index, average density.

| COMPONENT | %WGT | %VOL | %MOL |
|---|---|---|---|
| n-heptane | 19.57 | 21.17 | 20.16 |
| 2-Methylhexane | 0.04 | 0.04 | 0.04 |
| 3-Methylhexane | 0.02 | 0.02 | 0.02 |
| 2,2,4-Trimethylpentane | 47.12 | 50.38 | 42.57 |
| 2,2-Dimethylhexane | 0.03 | 0.03 | 0.03 |
| Toluene | 33.13 | 28.27 | 37.11 |
| Methylcyclohexane | 0.02 | 0.02 | 0.03 |
| | | | |
| Density (g/mL) at 15C | 0.7439 | | |
| H wt% | 13.6 | | |
| C wt% | 86.4 | | |
| PMI | 0.51 | | |

Table A- 7: DHA for E25 TRF88 in weight, volume and molar percent of the components; the percent carbon, hydrogen and oxygen; and particulate matter index, average density, average molecular weight, HOV, LHV.

| COMPONENT | %WGT | %VOL |
|---|---|---|
| n-heptane | 14.76 | 16.20 |
| 2-Methylhexane | 0.03 | 0.03 |
| 3-Methylhexane | 0.02 | 0.02 |
| 2,2,4-Trimethylpentane | 35.54 | 38.55 |
| 2,2-Dimethylhexane | 0.02 | 0.03 |
| Toluene | 24.99 | 21.63 |
| Methylcyclohexane | 0.02 | 0.02 |
| Ethanol | 24.58 | 23.49 |
| | | |
| Density at 15C | 0.7583 | |
| C wt% | 78.0 | |
| H wt% | 13.4 | |
| O wt% | 8.5 | |
| PMI | 0.40 | |

Table A- 8: DHA for E40 + 2% TRF81 in weight, volume and molar percent of the components; the percent carbon, hydrogen and oxygen; and particulate matter index, average density, average molecular weight, HOV, LHV.

| COMPONENT | WT% | VOL% | MOL% |
|---|---|---|---|
| n-heptane | 21.6 | 24.45 | 14.6 |
| 2,2,4-Trimethylpentane | 10.1 | 11.23 | 5.9 |
| Toluene | 28.0 | 24.95 | 20.5 |
| Ethanol | 40.3 | 39.44 | 59.0 |
| Sum | 100.0 | 100.1 | 100.0 |
| | | | |

| | | | |
|---|---|---|---|
| C wt% | 73.2 | | |
| H wt% | 12.8 | | |
| O wt% | 14.0 | | |
| Ave MW | 67.5 | | |
| PMI | 0.41 | | |
| HOV kJ/kg | 594.6 | | |
| Density (g/mL) at 15C | 0.7725 | | |
| LHV J/g | 36213 | | |

Table A- 9: DHA for E20 + 2% p-cresol in TRF88 in weight, volume and molar percent of the components; the percent carbon, hydrogen and oxygen; and particulate matter index, average density, average molecular weight, HOV, LHV.

| COMPONENT | WT% | VOL% | MOL% |
|---|---|---|---|
| n-heptane | 14.5 | 16.1 | 11.9 |
| 2,2,4-Trimethylpentane | 35.4 | 38.8 | 25.5 |
| Toluene | 27.6 | 24.2 | 24.6 |
| Ethanol | 20.4 | 19.7 | 36.5 |
| Cresol | 2.0 | 1.5 | 1.5 |
| | | | |
| C wt% | 79.3 | | |
| H wt% | 13.3 | | |
| O wt% | 7.4 | | |
| Ave MW | 82.2 | | |
| PMI | 0.70 | | |
| HOV kJ/kg, 25C | 472.0 | | |
| Density (g/mL)at 15C | 0.7592 | | |

Table A- 10: DHA for E20 + 6% Anisole in TRF88 in weight, volume and molar percent of the components; the percent carbon, hydrogen and oxygen; and particulate matter index, average density, average molecular weight, HOV, LHV.

| COMPONENT | WT% | VOL% | MOL% |
|---|---|---|---|
| n-heptane | 13.8 | 15.5 | 11.3 |
| 2,2,4-Trimethylpentane | 33.6 | 37.3 | 24.2 |
| Toluene | 26.2 | 23.3 | 23.5 |
| ethanol | 20.3 | 19.7 | 36.3 |
| anisole | 6.2 | 4.8 | 4.7 |
| | | | |
| C wt% | 79.0 | | |
| H wt% | 13.0 | | |
| O wt% | 8.0 | | |
| Ave MW | 82.5 | | |
| PMI | 0.61 | | |
| HOV kJ/kg, 25C | 471.7 | | |
| Density at 15C | 0.7691 | | |

Appendix B:

ID Data

Table B- 1: Ignition delay time at specified pressure, temperature, and Φ for PRF 100 from the tests in the AFIDA.

| Fuel ID | PRF 100 | | | |
|---|---|---|---|---|
| Temp °C | 1000/Temp [K] | ID time (ms) | Pressure (bar) | Φ |
| 725 | 1.001853429 | 32.761 | 5 | 1.04 |
| 700 | 1.027590813 | 45.203 | 5 | 1.02 |
| 675 | 1.05468544 | 62.353 | 5 | 1.00 |
| 650 | 1.083247576 | 91.276 | 5 | 0.98 |
| 625 | 1.113399766 | 134.203 | 5 | 0.96 |
| 600 | 1.145278589 | 195.253 | 5 | 0.94 |
| 575 | 1.179036727 | 271.709 | 5 | 0.92 |
| 550 | 1.214845411 | 377.08 | 5 | 0.90 |
| 525 | 1.252897325 | 508.349 | 5 | 0.88 |
| 500 | 1.293410076 | 534.553 | 5 | 0.86 |
| 475 | 1.336630355 | 497.769 | 5 | 0.84 |
| 450 | 1.382838968 | 455.886 | 5 | 0.82 |
| 425 | 1.432356943 | 416.139 | 5 | 0.80 |
| 725 | 1.001853429 | 23.90 | 10 | 0.57 |
| 700 | 1.027590813 | 31.323 | 10 | 0.56 |
| 675 | 1.05468544 | 41.56 | 10 | 0.55 |
| 650 | 1.083247576 | 61.494 | 10 | 0.54 |
| 625 | 1.113399766 | 88.303 | 10 | 0.52 |
| 600 | 1.145278589 | 123.849 | 10 | 0.51 |
| 575 | 1.179036727 | 166.336 | 10 | 0.50 |
| 550 | 1.214845411 | 188.396 | 10 | 0.49 |
| 525 | 1.252897325 | 183.996 | 10 | 0.48 |
| 500 | 1.293410076 | 177.653 | 10 | 0.47 |
| 475 | 1.336630355 | 176.363 | 10 | 0.46 |
| 450 | 1.382838968 | 174.289 | 10 | 0.45 |
| 425 | 1.432356943 | 180.24 | 10 | 0.43 |
| 725 | 1.001853429 | 12.88 | 20 | 0.30 |
| 700 | 1.027590813 | 17.76 | 20 | 0.29 |
| 675 | 1.05468544 | 23.34 | 20 | 0.29 |
| 650 | 1.083247576 | 30.607 | 20 | 0.28 |
| 625 | 1.113399766 | 40.426 | 20 | 0.27 |
| 600 | 1.145278589 | 47.96 | 20 | 0.27 |

| 575 | 1.179036727 | 52.04 | 20 | 0.26 |
|---|---|---|---|---|
| 550 | 1.214845411 | 57.16 | 20 | 0.26 |
| 525 | 1.252897325 | 61.88 | 20 | 0.25 |
| 500 | 1.293410076 | 70.76 | 20 | 0.25 |
| 475 | 1.336630355 | 81.88 | 20 | 0.24 |
| 450 | 1.382838968 | 95.20 | 20 | 0.23 |
| 425 | 1.432356943 | 115.373 | 20 | 0.23 |
| 725 | 1.001853429 | 7.37 | 30 | 0.20 |
| 700 | 1.027590813 | 9.242 | 30 | 0.20 |
| 675 | 1.05468544 | 11.16 | 30 | 0.19 |
| 650 | 1.083247576 | 12.76 | 30 | 0.19 |
| 625 | 1.113399766 | 14.72 | 30 | 0.19 |
| 600 | 1.145278589 | 17.32 | 30 | 0.18 |
| 575 | 1.179036727 | 20.95 | 30 | 0.18 |
| 550 | 1.214845411 | 25.87 | 30 | 0.17 |
| 525 | 1.252897325 | 32.32 | 30 | 0.17 |
| 500 | 1.293410076 | 39.85 | 30 | 0.17 |
| 475 | 1.336630355 | 52.40 | 30 | 0.16 |
| 450 | 1.382838968 | 69.473 | 30 | 0.16 |
| 425 | 1.432356943 | 104.039 | 30 | 0.15 |

Table B- 2: Ignition delay time at specified pressure, temperature, and Φ for TSF 99.8 from the tests in the AFIDA.

| Fuel ID | TSF 99.8 | | | |
|---|---|---|---|---|
| Temp °C | 1000/Temp [K] | ID time (ms) | Pressure (bar) | Φ |
| 725 | 1.001853429 | 45.80 | 5 | 1.04 |
| 700 | 1.027590813 | 61.323 | 5 | 1.02 |
| 675 | 1.05468544 | 85.006 | 5 | 1.00 |
| 650 | 1.083247576 | 117.963 | 5 | 0.98 |
| 625 | 1.113399766 | 171.403 | 5 | 0.96 |
| 600 | 1.145278589 | 212.176 | 5 | 0.94 |
| 575 | 1.179036727 | 232.88 | 5 | 0.92 |
| 550 | 1.214845411 | 250.059 | 5 | 0.90 |
| 525 | 1.252897325 | 277.799 | 5 | 0.88 |
| 500 | 1.293410076 | 323.336 | 5 | 0.86 |
| 475 | 1.336630355 | 381.256 | 5 | 0.84 |
| 450 | 1.382838968 | 460.106 | 5 | 0.82 |
| 425 | 1.432356943 | 543.76 | 5 | 0.80 |
| 725 | 1.001853429 | 28.74 | 10 | 0.57 |
| 700 | 1.027590813 | 35.13 | 10 | 0.56 |
| 675 | 1.05468544 | 47.80 | 10 | 0.55 |

| 650 | 1.083247576 | 62.36 | 10 | 0.54 |
|---|---|---|---|---|
| 625 | 1.113399766 | 87.72 | 10 | 0.52 |
| 600 | 1.145278589 | 104.536 | 10 | 0.51 |
| 575 | 1.179036727 | 120.00 | 10 | 0.50 |
| 550 | 1.214845411 | 136.796 | 10 | 0.49 |
| 525 | 1.252897325 | 168.88 | 10 | 0.48 |
| 500 | 1.293410076 | 216.52 | 10 | 0.47 |
| 475 | 1.336630355 | 301.52 | 10 | 0.46 |
| 450 | 1.382838968 | 450.16 | 10 | 0.45 |
| 725 | 1.001853429 | 17.70 | 20 | 0.30 |
| 700 | 1.027590813 | 22.89 | 20 | 0.29 |
| 675 | 1.05468544 | 30.38 | 20 | 0.29 |
| 650 | 1.083247576 | 38.51 | 20 | 0.28 |
| 625 | 1.113399766 | 45.04 | 20 | 0.27 |
| 600 | 1.145278589 | 52.28 | 20 | 0.27 |
| 575 | 1.179036727 | 63.80 | 20 | 0.26 |
| 550 | 1.214845411 | 84.08 | 20 | 0.26 |
| 525 | 1.252897325 | 119.52 | 20 | 0.25 |
| 500 | 1.293410076 | 182.24 | 20 | 0.25 |
| 475 | 1.336630355 | 334.853 | 20 | 0.24 |
| 725 | 1.001853429 | 10.324 | 30 | 0.20 |
| 700 | 1.027590813 | 13.56 | 30 | 0.20 |
| 675 | 1.05468544 | 16.84 | 30 | 0.19 |
| 650 | 1.083247576 | 21.03 | 30 | 0.19 |
| 625 | 1.113399766 | 25.86 | 30 | 0.19 |
| 600 | 1.145278589 | 33.05 | 30 | 0.18 |
| 575 | 1.179036727 | 46.16 | 30 | 0.18 |
| 550 | 1.214845411 | 69.04 | 30 | 0.17 |
| 525 | 1.252897325 | 111.12 | 30 | 0.17 |
| 500 | 1.293410076 | 188.24 | 30 | 0.17 |
| 475 | 1.336630355 | 381.236 | 30 | 0.16 |

Table B- 3: Ignition delay time at specified pressure, temperature, and Φ for E25 in TSF 88 from the tests in the AFIDA.

| Fuel ID | E25 in TRF88 | | | |
|---|---|---|---|---|
| Temp °C | 1000/Temp [K] | ID time (ms) | Pressure (bar) | Φ |
| 725 | 1.001853429 | 26.32 | 5 | 1.04 |
| 700 | 1.027590813 | 34.655 | 5 | 1.02 |
| 675 | 1.05468544 | 45.08 | 5 | 1.00 |
| 650 | 1.083247576 | 61.643 | 5 | 0.98 |
| 625 | 1.113399766 | 85.766 | 5 | 0.96 |

| 600 | 1.145278589 | 119.626 | 5 | 0.94 |
|-----|-------------|---------|----|------|
| 575 | 1.179036727 | 160.989 | 5 | 0.92 |
| 550 | 1.214845411 | 208.079 | 5 | 0.90 |
| 525 | 1.252897325 | 250.613 | 5 | 0.88 |
| 500 | 1.293410076 | 288.52 | 5 | 0.86 |
| 475 | 1.336630355 | 317.526 | 5 | 0.84 |
| 450 | 1.382838968 | 345.163 | 5 | 0.82 |
| 425 | 1.432356943 | 410.08 | 5 | 0.80 |
| 725 | 1.001853429 | 18.070 | 10 | 0.57 |
| 700 | 1.027590813 | 25.345 | 10 | 0.56 |
| 675 | 1.05468544 | 32.704 | 10 | 0.55 |
| 650 | 1.083247576 | 42.92 | 10 | 0.54 |
| 625 | 1.113399766 | 62.776 | 10 | 0.52 |
| 600 | 1.145278589 | 87.399 | 10 | 0.51 |
| 575 | 1.179036727 | 115.013 | 10 | 0.50 |
| 550 | 1.214845411 | 134.739 | 10 | 0.49 |
| 525 | 1.252897325 | 150.68 | 10 | 0.48 |
| 500 | 1.293410076 | 162.88 | 10 | 0.47 |
| 475 | 1.336630355 | 189.52 | 10 | 0.46 |
| 450 | 1.382838968 | 225.946 | 10 | 0.45 |
| 425 | 1.432356943 | 290.719 | 10 | 0.44 |
| 725 | 1.001853429 | 11.16 | 20 | 0.30 |
| 700 | 1.027590813 | 15.24 | 20 | 0.29 |
| 675 | 1.05468544 | 20.42 | 20 | 0.29 |
| 650 | 1.083247576 | 26.88 | 20 | 0.28 |
| 625 | 1.113399766 | 38.66 | 20 | 0.27 |
| 600 | 1.145278589 | 48.52 | 20 | 0.27 |
| 575 | 1.179036727 | 57.40 | 20 | 0.26 |
| 550 | 1.214845411 | 66.84 | 20 | 0.26 |
| 525 | 1.252897325 | 79.84 | 20 | 0.25 |
| 500 | 1.293410076 | 99.609 | 20 | 0.25 |
| 475 | 1.336630355 | 134.40 | 20 | 0.24 |
| 450 | 1.382838968 | 181.52 | 20 | 0.23 |
| 425 | 1.432356943 | 263.12 | 20 | 0.23 |
| 725 | 1.001853429 | 7.39 | 30 | 0.20 |
| 700 | 1.027590813 | 9.95 | 30 | 0.20 |
| 675 | 1.05468544 | 12.713 | 30 | 0.19 |
| 650 | 1.083247576 | 17.28 | 30 | 0.19 |
| 625 | 1.113399766 | 22.41 | 30 | 0.19 |
| 600 | 1.145278589 | 27.92 | 30 | 0.18 |
| 575 | 1.179036727 | 34.00 | 30 | 0.18 |

| 550 | 1.214845411 | 42.68 | 30 | 0.17 |
|---|---|---|---|---|
| 525 | 1.252897325 | 56.76 | 30 | 0.17 |
| 500 | 1.293410076 | 81.04 | 30 | 0.17 |
| 475 | 1.336630355 | 120.88 | 30 | 0.16 |
| 450 | 1.382838968 | 176.40 | 30 | 0.16 |
| 425 | 1.432356943 | 275.44 | 30 | 0.15 |

Table B- 4: Ignition delay time at specified pressure, temperature, and Φ for E40 in TRF71 from the tests in the AFIDA.

| Fuel ID | E40 TRF71 | | | |
|---|---|---|---|---|
| Temp °C | 1000/Temp [K] | ID time (ms) | Pressure (bar) | Φ |
| 725 | 1.001853429 | 23.09 | 5 | 1.04 |
| 700 | 1.027590813 | 28.90 | 5 | 1.02 |
| 675 | 1.05468544 | 39.85 | 5 | 1.00 |
| 650 | 1.083247576 | 52.513 | 5 | 0.98 |
| 625 | 1.113399766 | 71.859 | 5 | 0.96 |
| 600 | 1.145278589 | 98.283 | 5 | 0.94 |
| 575 | 1.179036727 | 129.499 | 5 | 0.92 |
| 550 | 1.214845411 | 158.473 | 5 | 0.90 |
| 525 | 1.252897325 | 185.24 | 5 | 0.88 |
| 500 | 1.293410076 | 211.08 | 5 | 0.86 |
| 475 | 1.336630355 | 234.64 | 5 | 0.84 |
| 450 | 1.382838968 | 278.84 | 5 | 0.82 |
| 425 | 1.432356943 | 365.736 | 5 | 0.80 |
| 725 | 1.001853429 | 14.72 | 10 | 0.57 |
| 700 | 1.027590813 | 20.72 | 10 | 0.56 |
| 675 | 1.05468544 | 28.364 | 10 | 0.55 |
| 650 | 1.083247576 | 37.12 | 10 | 0.54 |
| 625 | 1.113399766 | 51.306 | 10 | 0.52 |
| 600 | 1.145278589 | 69.509 | 10 | 0.51 |
| 575 | 1.179036727 | 89.625 | 10 | 0.50 |
| 550 | 1.214845411 | 102.843 | 10 | 0.49 |
| 525 | 1.252897325 | 111.44 | 10 | 0.48 |
| 500 | 1.293410076 | 125.64 | 10 | 0.47 |
| 475 | 1.336630355 | 149.44 | 10 | 0.46 |
| 450 | 1.382838968 | 192.20 | 10 | 0.45 |
| 425 | 1.432356943 | 278.093 | 10 | 0.43 |
| 725 | 1.001853429 | 9.90 | 20 | 0.30 |
| 700 | 1.027590813 | 13.48 | 20 | 0.29 |
| 675 | 1.05468544 | 18.43 | 20 | 0.29 |
| 650 | 1.083247576 | 23.92 | 20 | 0.28 |

| 625 | 1.113399766 | 30.08 | 20 | 0.27 |
| 600 | 1.145278589 | 40.76 | 20 | 0.27 |
| 575 | 1.179036727 | 45.959 | 20 | 0.26 |
| 550 | 1.214845411 | 54.536 | 20 | 0.26 |
| 525 | 1.252897325 | 66.133 | 20 | 0.25 |
| 500 | 1.293410076 | 86.52 | 20 | 0.25 |
| 475 | 1.336630355 | 114.60 | 20 | 0.24 |
| 450 | 1.382838968 | 165.16 | 20 | 0.23 |
| 425 | 1.432356943 | 254.28 | 20 | 0.23 |
| 725 | 1.001853429 | 7.20 | 30 | 0.20 |
| 700 | 1.027590813 | 9.28 | 30 | 0.20 |
| 675 | 1.05468544 | 11.744 | 30 | 0.19 |
| 650 | 1.083247576 | 15.52 | 30 | 0.19 |
| 625 | 1.113399766 | 19.78 | 30 | 0.19 |
| 600 | 1.145278589 | 24.42 | 30 | 0.18 |
| 575 | 1.179036727 | 27.02 | 30 | 0.18 |
| 550 | 1.214845411 | 36.02 | 30 | 0.17 |
| 525 | 1.252897325 | 49.04 | 30 | 0.17 |
| 500 | 1.293410076 | 71.60 | 30 | 0.17 |
| 475 | 1.336630355 | 111.36 | 30 | 0.16 |
| 450 | 1.382838968 | 168.88 | 30 | 0.16 |
| 425 | 1.432356943 | 269.32 | 30 | 0.15 |

Table B- 5: Ignition delay time at specified pressure, temperature, and Φ for E20 + 2% p-cresol in TRF88 from the tests in the AFIDA.

| Fuel ID | E20 2%pCresol in TRF88 | | | |
|---|---|---|---|---|
| Temp °C | 1000/Temp [K] | ID time (ms) | Pressure (bar) | Φ |
| 725 | 1.001853429 | 28.319 | 5 | 1.04 |
| 700 | 1.027590813 | 37.290 | 5 | 1.02 |
| 675 | 1.05468544 | 51.64 | 5 | 1.00 |
| 650 | 1.083247576 | 71.183 | 5 | 0.98 |
| 625 | 1.113399766 | 99.583 | 5 | 0.96 |
| 600 | 1.145278589 | 146.413 | 5 | 0.94 |
| 575 | 1.179036727 | 190.516 | 5 | 0.92 |
| 550 | 1.214845411 | 239.769 | 5 | 0.90 |
| 525 | 1.252897325 | 272.326 | 5 | 0.88 |
| 500 | 1.293410076 | 288.383 | 5 | 0.86 |
| 475 | 1.336630355 | 301.913 | 5 | 0.84 |
| 450 | 1.382838968 | 323.709 | 5 | 0.82 |
| 425 | 1.432356943 | 382.929 | 5 | 0.80 |
| 725 | 1.001853429 | 18.858 | 10 | 0.57 |

| | | | | |
|---|---|---|---|---|
| 700 | 1.027590813 | 27.100 | 10 | 0.56 |
| 675 | 1.05468544 | 35.23 | 10 | 0.55 |
| 650 | 1.083247576 | 49.72 | 10 | 0.54 |
| 625 | 1.113399766 | 69.803 | 10 | 0.52 |
| 600 | 1.145278589 | 94.979 | 10 | 0.51 |
| 575 | 1.179036727 | 119.029 | 10 | 0.50 |
| 550 | 1.214845411 | 132.04 | 10 | 0.49 |
| 525 | 1.252897325 | 139.383 | 10 | 0.48 |
| 500 | 1.293410076 | 151.76 | 10 | 0.47 |
| 475 | 1.336630355 | 173.24 | 10 | 0.46 |
| 450 | 1.382838968 | 208.719 | 10 | 0.45 |
| 425 | 1.432356943 | 270.80 | 10 | 0.44 |
| 725 | 1.001853429 | 11.96 | 20 | 0.30 |
| 700 | 1.027590813 | 16.32 | 20 | 0.29 |
| 675 | 1.05468544 | 21.10 | 20 | 0.29 |
| 650 | 1.083247576 | 27.94 | 20 | 0.28 |
| 625 | 1.113399766 | 38.64 | 20 | 0.27 |
| 600 | 1.145278589 | 46.56 | 20 | 0.27 |
| 575 | 1.179036727 | 52.60 | 20 | 0.26 |
| 550 | 1.214845411 | 60.64 | 20 | 0.26 |
| 525 | 1.252897325 | 72.88 | 20 | 0.25 |
| 500 | 1.293410076 | 90.989 | 20 | 0.25 |
| 475 | 1.336630355 | 121.48 | 20 | 0.24 |
| 450 | 1.382838968 | 169.84 | 20 | 0.23 |
| 425 | 1.432356943 | 256.12 | 20 | 0.23 |
| 725 | 1.001853429 | 7.70 | 30 | 0.20 |
| 700 | 1.027590813 | 10.27 | 30 | 0.20 |
| 675 | 1.05468544 | 13.27 | 30 | 0.19 |
| 650 | 1.083247576 | 16.80 | 30 | 0.19 |
| 625 | 1.113399766 | 20.96 | 30 | 0.19 |
| 600 | 1.145278589 | 25.09 | 30 | 0.18 |
| 575 | 1.179036727 | 30.18 | 30 | 0.18 |
| 550 | 1.214845411 | 37.021 | 30 | 0.17 |
| 525 | 1.252897325 | 50.88 | 30 | 0.17 |
| 500 | 1.293410076 | 72.48 | 30 | 0.17 |
| 475 | 1.336630355 | 112.64 | 30 | 0.16 |
| 450 | 1.382838968 | 175.32 | 30 | 0.16 |
| 425 | 1.432356943 | 279.223 | 30 | 0.15 |

Table B- 6: Ignition delay time at specified pressure, temperature, and Φ for E20 + 6% anisole in TRF88 from the tests in the AFIDA.

| Fuel ID | E20 6% anisole in TRF88 | | | |
|---|---|---|---|---|
| Temp °C | 1000/Temp [K] | ID time (ms) | Pressure (bar) | Φ |
| 725 | 1.001853429 | 26.78 | 5 | 1.04 |
| 700 | 1.027590813 | 33.95 | 5 | 1.02 |
| 675 | 1.05468544 | 45.20 | 5 | 1.00 |
| 650 | 1.083247576 | 64.109 | 5 | 0.98 |
| 625 | 1.113399766 | 90.156 | 5 | 0.96 |
| 600 | 1.145278589 | 125.929 | 5 | 0.94 |
| 575 | 1.179036727 | 169.219 | 5 | 0.92 |
| 550 | 1.214845411 | 216.763 | 5 | 0.90 |
| 525 | 1.252897325 | 253.829 | 5 | 0.88 |
| 500 | 1.293410076 | 283.979 | 5 | 0.86 |
| 475 | 1.336630355 | 308.566 | 5 | 0.84 |
| 450 | 1.382838968 | 335.76 | 5 | 0.82 |
| 425 | 1.432356943 | 394.28 | 5 | 0.80 |
| 725 | 1.001853429 | 17.15 | 10 | 0.57 |
| 700 | 1.027590813 | 25.158 | 10 | 0.56 |
| 675 | 1.05468544 | 33.39 | 10 | 0.55 |
| 650 | 1.083247576 | 46.376 | 10 | 0.54 |
| 625 | 1.113399766 | 64.923 | 10 | 0.52 |
| 600 | 1.145278589 | 89.503 | 10 | 0.51 |
| 575 | 1.179036727 | 113.92 | 10 | 0.50 |
| 550 | 1.214845411 | 133.52 | 10 | 0.49 |
| 525 | 1.252897325 | 146.303 | 10 | 0.48 |
| 500 | 1.293410076 | 162.24 | 10 | 0.47 |
| 475 | 1.336630355 | 190.56 | 10 | 0.46 |
| 450 | 1.382838968 | 231.48 | 10 | 0.45 |
| 425 | 1.432356943 | 297.36 | 10 | 0.44 |
| 725 | 1.001853429 | 11.47 | 20 | 0.30 |
| 700 | 1.027590813 | 15.36 | 20 | 0.29 |
| 675 | 1.05468544 | 20.630 | 20 | 0.29 |
| 650 | 1.083247576 | 26.595 | 20 | 0.28 |
| 625 | 1.113399766 | 36.840 | 20 | 0.27 |
| 600 | 1.145278589 | 47.52 | 20 | 0.27 |
| 575 | 1.179036727 | 55.40 | 20 | 0.26 |
| 550 | 1.214845411 | 64.80 | 20 | 0.26 |
| 525 | 1.252897325 | 78.836 | 20 | 0.25 |
| 500 | 1.293410076 | 103.60 | 20 | 0.25 |
| 475 | 1.336630355 | 138.44 | 20 | 0.24 |

| 450 | 1.382838968 | 196.28 | 20 | 0.23 |
|---|---|---|---|---|
| 425 | 1.432356943 | 292.04 | 20 | 0.23 |
| 725 | 1.001853429 | 7.50 | 30 | 0.20 |
| 700 | 1.027590813 | 9.90 | 30 | 0.20 |
| 675 | 1.05468544 | 12.99 | 30 | 0.19 |
| 650 | 1.083247576 | 16.86 | 30 | 0.19 |
| 625 | 1.113399766 | 21.55 | 30 | 0.19 |
| 600 | 1.145278589 | 26.74 | 30 | 0.18 |
| 575 | 1.179036727 | 32.84 | 30 | 0.18 |
| 550 | 1.214845411 | 41.156 | 30 | 0.17 |
| 525 | 1.252897325 | 58.24 | 30 | 0.17 |
| 500 | 1.293410076 | 83.056 | 30 | 0.17 |
| 475 | 1.336630355 | 126.993 | 30 | 0.16 |
| 450 | 1.382838968 | 199.036 | 30 | 0.16 |
| 425 | 1.432356943 | 327.423 | 30 | 0.15 |

Table B- 7: Ignition delay time at specified pressure, temperature, and $\Phi$ for TRF88 from the tests in the AFIDA.

| Fuel ID | TRF88 | | | |
|---|---|---|---|---|
| Temp | 1000/Temp | ID time (ms) | Pressure | Phi |
| 725 | 1.001853429 | 32.90 | 5 | 1.04 |
| 700 | 1.027590813 | 44.44 | 5 | 1.02 |
| 675 | 1.05468544 | 58.24 | 5 | 1.00 |
| 650 | 1.083247576 | 76.88 | 5 | 0.98 |
| 625 | 1.113399766 | 90.709 | 5 | 0.96 |
| 600 | 1.145278589 | 90.193 | 5 | 0.94 |
| 575 | 1.179036727 | 86.92 | 5 | 0.92 |
| 550 | 1.214845411 | 84.68 | 5 | 0.90 |
| 525 | 1.252897325 | 83.48 | 5 | 0.88 |
| 500 | 1.293410076 | 82.16 | 5 | 0.86 |
| 475 | 1.336630355 | 87.80 | 5 | 0.84 |
| 450 | 1.382838968 | 100.733 | 5 | 0.82 |
| 425 | 1.432356943 | 123.179 | 5 | 0.80 |
| 725 | 1.001853429 | 21.72 | 10 | 0.57 |
| 700 | 1.027590813 | 27.36 | 10 | 0.56 |
| 675 | 1.05468544 | 33.299 | 10 | 0.55 |
| 650 | 1.083247576 | 38.008 | 10 | 0.54 |
| 625 | 1.113399766 | 39.938 | 10 | 0.52 |
| 600 | 1.145278589 | 39.197 | 10 | 0.51 |
| 575 | 1.179036727 | 39.421 | 10 | 0.50 |
| 550 | 1.214845411 | 40.042 | 10 | 0.49 |

| | | | | |
|---|---|---|---|---|
| 525 | 1.252897325 | 42.429 | 10 | 0.48 |
| 500 | 1.293410076 | 46.949 | 10 | 0.47 |
| 475 | 1.336630355 | 53.720 | 10 | 0.46 |
| 450 | 1.382838968 | 70.727 | 10 | 0.45 |
| 425 | 1.432356943 | 96.16 | 10 | 0.44 |
| 725 | 1.001853429 | 8.50 | 20 | 0.30 |
| 700 | 1.027590813 | 9.98 | 20 | 0.29 |
| 675 | 1.05468544 | 11.16 | 20 | 0.29 |
| 650 | 1.083247576 | 12.22 | 20 | 0.28 |
| 625 | 1.113399766 | 13.44 | 20 | 0.27 |
| 600 | 1.145278589 | 14.80 | 20 | 0.27 |
| 575 | 1.179036727 | 16.75 | 20 | 0.26 |
| 550 | 1.214845411 | 19.06 | 20 | 0.26 |
| 525 | 1.252897325 | 22.14 | 20 | 0.25 |
| 500 | 1.293410076 | 28.78 | 20 | 0.25 |
| 475 | 1.336630355 | 39.85 | 20 | 0.24 |
| 450 | 1.382838968 | 68.52 | 20 | 0.23 |
| 425 | 1.432356943 | 110.08 | 20 | 0.23 |
| 725 | 1.001853429 | 4.08 | 30 | 0.20 |
| 700 | 1.027590813 | 4.77 | 30 | 0.20 |
| 675 | 1.05468544 | 5.29 | 30 | 0.19 |
| 650 | 1.083247576 | 5.85 | 30 | 0.19 |
| 625 | 1.113399766 | 6.67 | 30 | 0.19 |
| 600 | 1.145278589 | 7.57 | 30 | 0.18 |
| 575 | 1.179036727 | 8.86 | 30 | 0.18 |
| 550 | 1.214845411 | 10.95 | 30 | 0.17 |
| 525 | 1.252897325 | 14.77 | 30 | 0.17 |
| 500 | 1.293410076 | 20.92 | 30 | 0.17 |
| 475 | 1.336630355 | 32.228 | 30 | 0.16 |
| 450 | 1.382838968 | 62.793 | 30 | 0.16 |
| 425 | 1.432356943 | 135.036 | 30 | 0.15 |

Table B- 8: Ignition delay time at specified pressure, temperature, and Φ for E25 FACE B from the tests in the AFIDA.

| Fuel ID | E25 in FACE B | | | |
|---|---|---|---|---|
| Temp °C | 1000/Temp [K] | ID time (ms) | Pressure (bar) | Phi |
| 725 | 1.001853429 | 26.37 | 5 | 1.04 |
| 700 | 1.027590813 | 34.62 | 5 | 1.02 |
| 675 | 1.05468544 | 44.40 | 5 | 1.00 |
| 650 | 1.083247576 | 60.886 | 5 | 0.98 |
| 625 | 1.113399766 | 87.319 | 5 | 0.96 |

| 600 | 1.145278589 | 125.676 | 5 | 0.94 |
|---|---|---|---|---|
| 575 | 1.179036727 | 180.633 | 5 | 0.92 |
| 550 | 1.214845411 | 243.833 | 5 | 0.90 |
| 525 | 1.252897325 | 329.96 | 5 | 0.88 |
| 500 | 1.293410076 | 467.56 | 5 | 0.86 |
| 725 | 1.001853429 | 16.80 | 10 | 0.57 |
| 700 | 1.027590813 | 25.943 | 10 | 0.56 |
| 675 | 1.05468544 | 34.80 | 10 | 0.55 |
| 650 | 1.083247576 | 47.20 | 10 | 0.53 |
| 625 | 1.113399766 | 69.32 | 10 | 0.52 |
| 600 | 1.145278589 | 103.68 | 10 | 0.51 |
| 575 | 1.179036727 | 147.360 | 10 | 0.50 |
| 550 | 1.214845411 | 208.28 | 10 | 0.49 |
| 525 | 1.252897325 | 267.76 | 10 | 0.48 |
| 500 | 1.293410076 | 333.463 | 10 | 0.47 |
| 475 | 1.336630355 | 362.04 | 10 | 0.46 |
| 450 | 1.382838968 | 371.96 | 10 | 0.45 |
| 425 | 1.432356943 | 403.76 | 10 | 0.43 |
| 725 | 1.001853429 | 11.28 | 20 | 0.30 |
| 700 | 1.027590813 | 16.11 | 20 | 0.29 |
| 675 | 1.05468544 | 22.29 | 20 | 0.29 |
| 650 | 1.083247576 | 29.98 | 20 | 0.28 |
| 625 | 1.113399766 | 49.56 | 20 | 0.27 |
| 600 | 1.145278589 | 70.76 | 20 | 0.27 |
| 575 | 1.179036727 | 100.84 | 20 | 0.26 |
| 550 | 1.214845411 | 131.56 | 20 | 0.26 |
| 525 | 1.252897325 | 154.08 | 20 | 0.25 |
| 500 | 1.293410076 | 165.48 | 20 | 0.24 |
| 475 | 1.336630355 | 178.56 | 20 | 0.24 |
| 450 | 1.382838968 | 230.20 | 20 | 0.23 |
| 425 | 1.432356943 | 262.40 | 20 | 0.23 |
| 725 | 1.001853429 | 8.25 | 30 | 0.20 |
| 700 | 1.027590813 | 11.38 | 30 | 0.20 |
| 675 | 1.05468544 | 15.57 | 30 | 0.19 |
| 650 | 1.083247576 | 22.66 | 30 | 0.19 |
| 625 | 1.113399766 | 32.94 | 30 | 0.19 |
| 600 | 1.145278589 | 46.60 | 30 | 0.18 |
| 575 | 1.179036727 | 62.96 | 30 | 0.18 |
| 550 | 1.214845411 | 77.76 | 30 | 0.17 |
| 525 | 1.252897325 | 90.08 | 30 | 0.17 |
| 500 | 1.293410076 | 105.52 | 30 | 0.17 |

| | | | | |
|---|---|---|---|---|
| 475 | 1.336630355 | 128.12 | 30 | 0.16 |
| 450 | 1.382838968 | 162.32 | 30 | 0.16 |
| 425 | 1.432356943 | 226.52 | 30 | 0.15 |

Table B- 9: Ignition delay time at specified pressure, temperature, and Φ for FACE B from the tests in the AFIDA.

| Fuel ID | FACE B | | | |
|---|---|---|---|---|
| Temp °C | 1000/Temp [K] | ID time (ms) | Pressure (bar) | Phi |
| 725 | 1.001853429 | 30.75 | 5 | 1.04 |
| 700 | 1.027590813 | 38.66 | 5 | 1.02 |
| 675 | 1.05468544 | 51.56 | 5 | 1.00 |
| 650 | 1.083247576 | 72.00 | 5 | 0.98 |
| 625 | 1.113399766 | 105.819 | 5 | 0.96 |
| 600 | 1.145278589 | 149.919 | 5 | 0.94 |
| 575 | 1.179036727 | 185.086 | 5 | 0.92 |
| 550 | 1.214845411 | 194.28 | 5 | 0.90 |
| 525 | 1.252897325 | 186.153 | 5 | 0.88 |
| 500 | 1.293410076 | 170.12 | 5 | 0.86 |
| 475 | 1.336630355 | 158.48 | 5 | 0.84 |
| 450 | 1.382838968 | 156.676 | 5 | 0.82 |
| 425 | 1.432356943 | 170.579 | 5 | 0.80 |
| 725 | 1.001853429 | 17.777 | 10 | 0.57 |
| 700 | 1.027590813 | 26.88 | 10 | 0.56 |
| 675 | 1.05468544 | 36.35 | 10 | 0.55 |
| 650 | 1.083247576 | 47.08 | 10 | 0.53 |
| 625 | 1.113399766 | 66.40 | 10 | 0.52 |
| 600 | 1.145278589 | 85.40 | 10 | 0.51 |
| 575 | 1.179036727 | 86.52 | 10 | 0.50 |
| 550 | 1.214845411 | 79.92 | 10 | 0.49 |
| 525 | 1.252897325 | 73.456 | 10 | 0.48 |
| 500 | 1.293410076 | 69.72 | 10 | 0.47 |
| 475 | 1.336630355 | 73.76 | 10 | 0.46 |
| 450 | 1.382838968 | 80.72 | 10 | 0.45 |
| 425 | 1.432356943 | 103.60 | 10 | 0.43 |
| 725 | 1.001853429 | 10.99 | 20 | 0.30 |
| 700 | 1.027590813 | 14.69 | 20 | 0.29 |
| 675 | 1.05468544 | 19.48 | 20 | 0.29 |
| 650 | 1.083247576 | 24.25 | 20 | 0.28 |
| 625 | 1.113399766 | 28.187 | 20 | 0.27 |
| 600 | 1.145278589 | 29.62 | 20 | 0.27 |
| 575 | 1.179036727 | 29.50 | 20 | 0.26 |

| | | | | |
|---|---|---|---|---|
| 550 | 1.214845411 | 29.64 | 20 | 0.26 |
| 525 | 1.252897325 | 31.04 | 20 | 0.25 |
| 500 | 1.293410076 | 34.68 | 20 | 0.25 |
| 475 | 1.336630355 | 42.80 | 20 | 0.24 |
| 450 | 1.382838968 | 57.12 | 20 | 0.23 |
| 425 | 1.432356943 | 80.88 | 20 | 0.23 |
| 725 | 1.001853429 | 6.48 | 30 | 0.20 |
| 700 | 1.027590813 | 7.746 | 30 | 0.20 |
| 675 | 1.05468544 | 9.00 | 30 | 0.19 |
| 650 | 1.083247576 | 10.09 | 30 | 0.19 |
| 625 | 1.113399766 | 11.16 | 30 | 0.19 |
| 600 | 1.145278589 | 12.48 | 30 | 0.18 |
| 575 | 1.179036727 | 13.97 | 30 | 0.18 |
| 550 | 1.214845411 | 15.63 | 30 | 0.17 |
| 525 | 1.252897325 | 17.54 | 30 | 0.17 |
| 500 | 1.293410076 | 21.36 | 30 | 0.17 |
| 475 | 1.336630355 | 28.56 | 30 | 0.16 |
| 450 | 1.382838968 | 41.599 | 30 | 0.16 |
| 425 | 1.432356943 | 79.00 | 30 | 0.15 |

<div align="center">

Appendix C:

MATLAB Code

</div>

**C-1: MATLAB Code To Create Surface Plot And Polynomial Curve Fit To Data.**

```matlab
%%% importing data
%clear workspace
clear

%import data from excel sheets
Fuel = xlsread('Summary_E40_TRF6x.xlsx');

%assign data to specific arrays for each pressure
pressure = Fuel(1:52,4);
pressure = pressure(:);
ignition_delay = Fuel(1:52,3);
ignition_delay = ignition_delay(:);
temperature = Fuel(1:52,2);
temperature = temperature(:);

%% find polynomial surface fit

[xData, yData, zData] = prepareSurfaceData( pressure, temperature,
ignition_delay );

% Set up fittype and options.
ft = fittype( 'poly34' );

% Fit model to data.
[fitresult, gof] = fit( [xData, yData], zData, ft );

% Create a figure for the plots.
figure( 'Name', 'untitled fit 1' );

% Plot fit with data.
subplot( 2, 1, 1 );
h = plot( fitresult, [xData, yData], zData );
legend( 'E40 in TRF71', 'Location', 'NorthEast' );
% Label axes
xlabel 'Pressure (bar)'
ylabel 'Temperature (1000/ Temp [K])'
zlabel 'Ignition Delay Time (ms)'
grid on
zlim([0 450])
view( -30, 15 );;

% Plot residuals.
subplot( 2, 1, 2 );
h = plot( fitresult, [xData, yData], zData, 'Style', 'Residual' );
legend( h, 'untitled fit 1 - residuals', 'Location', 'NorthEast' );
```

```matlab
% Label axes
xlabel 'Temperature (1000/ temp [K])'
ylabel 'Pressure (bar)'
zlabel 'Ignition Delay Time (ms)'
grid on
view( -83.5, 13.2 );

%% outputt fitt coefficents

p00 = fitresult.p00
p10 = fitresult.p10
p01 = fitresult.p01
p20 = fitresult.p20
p02 = fitresult.p02
p30 = fitresult.p30
p03 = fitresult.p03
p04 = fitresult.p04
p11 = fitresult.p11
p12 = fitresult.p12
p21 = fitresult.p21
p31 = fitresult.p31
p13 = fitresult.p13
p22 = fitresult.p22

E40_TRF6x_coef = [p00, p01, p10, p20, p02, p03, p30, p04, p11, p12, p22, p21,
p13]
```

C-2: MATLAB Code To Apply Linear Regression of ID time to Temperature 1000/T [K] and Φ.

```matlab
Linear regression with the help of Dr. Daily
% Examine Drew's data

close all;clear all;clc;

filedata = 'data/FuelDatathesisall';

load(filedata)


Tinvp5 = Tinv(P==5,:);
phip5 = phi(P==5,:);
IDp5 = ID(P==5,:);


%set up regression wrt 1000/T and phi

x = [ones(size(Tinvp5)) Tinvp5 phip5 ];
y = IDp5;

[b bint,r,rint,stats] = regress(y, x)
stats5=stats

%yfit = b(1)+b(2)*Tinvp5;
```

```matlab
yfit = b(1)+b(2)*Tinvp5+ b(3)*phip5;

figure
loglog(y,yfit,'x',y,y,'o')
xlabel('ID Time (ms)','fontsize',12)
ylabel('ID Time Fit (ms)', 'fontsize',12)
title({'Ignition Delay vs 1000/T[K] and phi',' Regression P = 5 Bar,
0.78<phi<1.04 '}, 'fontsize',14)

% plot and regress P = 10 atm and narrow phi range

Tinvp10 = Tinv(P==10,:);
phip10 = phi(P==10,:);
IDp10 = ID(P==10,:);

% set up regression wrt 1000/T

x = [ones(size(Tinvp10)) Tinvp10 phip10 ];
y = IDp10;

[b bint,r,rint,stats] = regress(y, x)
stats10=stats

%yfit = b(1)+b(2)*Tinvp10;
yfit = b(1)+b(2)*Tinvp10+ b(3)*phip10;

figure
loglog(y,yfit,'x',y,y,'o')
xlabel('ID Time (ms)','fontsize',12)
ylabel('ID Time Fit (ms)', 'fontsize',12)
title({'Ignition Delay vs 1000/T and phi',' Regression P = 10 Bar,
0.42<phi<0.57 '},'fontsize',14)

% plot and regress P = 20 atm and narrow phi range

Tinvp20 = Tinv(P==20,:);
phip20 = phi(P==20,:);
IDp20 = ID(P==20,:);

% set up regression wrt 1000/T

x = [ones(size(Tinvp20)) Tinvp20 phip20 ];
y = IDp20;

[b bint,r,rint,stats] = regress(y, x)
stats20=stats

%yfit = b(1)+b(2)*Tinvp20;
yfit = b(1)+b(2)*Tinvp20+ b(3)*phip20;

figure
loglog(y,yfit,'x',y,y,'o')
xlabel('ID Time (ms)','fontsize',12)
ylabel('ID Time Fit (ms)', 'fontsize',12)
title({'Ignition Delay vs T/1000[K] and phi ','Regression P = 20 Bar 0.22<
```

```matlab
phi <0.30'},'fontsize',14)

% plot and regress P = 30 atm and narrow phi range

Tinvp30 = Tinv(P==30,:);
phip30 = phi(P==30,:);
IDp30 = ID(P==30,:);

% set up regression wrt 1000/T

x = [ones(size(Tinvp30)) Tinvp30 phip30];
y = IDp30;

[b bint,r,rint,stats] = regress(y, x)
stats30=stats

yfit = b(1)+b(2)*Tinvp30+ b(3)*phip30;

figure
loglog(y,yfit,'x',y,y,'o')
xlabel('ID Time (ms)','fontsize',12)
ylabel('ID Time Fit (ms)', 'fontsize',12)
title({'Ignition Delay vs 1000/T[K] and phi',' Regression P = 30 Bar 0.15<
phi <0.20'}, 'fontsize',14)
```

## C-3: MATLAB Code To Apply Linear Regression of ID time to temperature (1000/T[K]), Φ, composition, HOV, RON, and S.

```matlab
close all;clear all;clc;

filedata = 'data/FuelDatathesisall';

load(filedata)

Tinvp5 = Tinv(P==5,:);
phip5 = phi(P==5,:);
IDp5 = ID(P==5,:);
C1p5 = C1(P==5,:);
C2p5 = C2(P==5,:);
C3p5 = C3(P==5,:);
C4p5 = C4(P==5,:);
C5p5 = C5(P==5,:);
C6p5 = C6(P==5,:);;
C7p5 = C7(P==5,:);
HOVp5 = HOV(P==5,:);
RONp5 = RON(P==5,:);
Sp5 = S(P==5,:);

% set up regression wrt 1000/T and phi

x = [ones(size(Tinvp5)) Tinvp5 phip5 C1p5 C2p5 C3p5 C4p5 C5p5 C6p5 C7p5 HOVp5
RONp5 Sp5 ];
y = IDp5;
```

```
[b bint,r,rint,stats] = regress(y, x)
stats5=stats

    % Removes NaN data

yfit =
b(1)+b(2)*Tinvp5+b(3)*phip5+b(4)*C1p5+b(5)*C2p5+b(6)*C3p5+b(7)*C4p5+b(8)*C5p5
+b(9)*C6p5+b(10)*C7p5+b(11)*HOVp5+b(12)*RONp5+b(13)*Sp5;

figure
loglog(y,yfit,'x',y,y,'o')
xlabel('ID Time (ms)','fontsize',12)
ylabel('ID Time Fit (ms)', 'fontsize',12)
title( {'Ignition Delay vs 1000/T[K], Phi, Composition, HOV, RON, and S',
'Regression at P = 5 Bar, 0.78< phi <1.04 '},'fontsize',14)

% plot and regress P = 10 atm and narrow phi range

Tinvp10 = Tinv(P==10,:);
phip10 = phi(P==10,:);
IDp10 = ID(P==10,:);
C1p10 = C1(P==10,:);
C2p10 = C2(P==10,:);
C3p10 = C3(P==10,:);
C4p10 = C4(P==10,:);
C5p10 = C5(P==10,:);
C6p10 = C6(P==10,:);
C7p10 = C7(P==10,:);
HOVp10 = HOV(P==10,:);
RONp10 = RON(P==10,:);
Sp10 = S(P==10,:);

% set up regression wrt 1000/T

x = [ones(size(Tinvp10)) Tinvp10 phip10 C1p10 C2p10 C3p10 C4p10 C5p10 C6p10
C7p10 HOVp10 RONp10 Sp10 ];
y = IDp10;

[b,bint,r,rint,stats]= regress(y,x)    % Removes NaN data
stats10=stats

yfit =
b(1)+b(2)*Tinvp10+b(3)*phip10+b(4)*C1p10+b(5)*C2p10+b(6)*C3p10+b(7)*C4p10+b(8
)*C5p10+b(9)*C6p10+b(10)*C7p10+b(11)*HOVp10+b(12)*RONp10+b(13)*Sp10;

figure
loglog(y,yfit,'x',y,y,'o')
xlabel('ID Time (ms)','fontsize',12)
ylabel('ID Time Fit (ms)', 'fontsize',12)
title({'Ignition Delay vs 1000/T[K], Phi, Composition, HOV, RON, and S',
'Regression at P = 10 Bar, 0.42< phi <0.57 '}, 'fontsize', 14)

% plot and regress P = 20 atm and narrow phi range
Tinvp20 = Tinv(P==20,:);
phip20 = phi(P==20,:);
IDp20 = ID(P==20,:);
```

```matlab
C1p20 = C1(P==20,:);
C2p20 = C2(P==20,:);
C3p20 = C3(P==20,:);
C4p20 = C4(P==20,:);
C5p20 = C5(P==20,:);
C6p20 = C6(P==20,:);
C7p20 = C7(P==20,:);
HOVp20 = HOV(P==20,:);
RONp20 = RON(P==20,:);
Sp20 = S(P==20,:);

% set up regression wrt 1000/T

x = [ones(size(Tinvp20)) Tinvp20 phip20 C1p20 C2p20 C3p20 C4p20 C5p20 C6p20
C7p20 HOVp20 RONp20 Sp20 ];

y = IDp20;

[b,bint,r,rint,stats] = regress(y,x)    % Removes NaN data
stats20=stats

yfit =
b(1)+b(2)*Tinvp20+b(3)*phip20+b(4)*C1p20+b(5)*C2p20+b(6)*C3p20+b(7)*C4p20+b(8
)*C5p20+b(9)*C6p20+b(10)*C7p20+b(11)*HOVp20+b(12)*RONp20+b(13)*Sp20;

figure
loglog(y,yfit,'x',y,y,'o')
xlabel('ID Time (ms)','fontsize',12)
ylabel('ID Time Fit (ms)', 'fontsize',12)
title({'Ignition Delay vs 1000/T[K], Phi, Composition, HOV, RON, and S',
'Regression at P = 20 Bar, 0.30< phi <0.22 '}, 'fontsize', 14)

% plot and regress P = 30 atm and narrow phi range

Tinvp30 = Tinv(P==30,:);
phip30 = phi(P==30,:);
IDp30 = ID(P==30,:);
C1p30 = C1(P==30,:);
C2p30 = C2(P==30,:);
C3p30 = C3(P==30,:);
C4p30 = C4(P==30,:);
C5p30 = C5(P==30,:);
C6p30 = C6(P==30,:);
C7p30 = C7(P==30,:);
HOVp30 = HOV(P==30,:);
RONp30 = RON(P==30,:);
Sp30 = S(P==30,:);

% set up regression wrt 1000/T

x = [ones(size(Tinvp30)) Tinvp30 phip30 C1p30 C2p30 C3p30 C4p30 C5p30 C6p30
C7p30 HOVp30 RONp30 Sp30];

y = IDp30;

[b,bint,r,rint,stats] = regress(y,x)    % Removes NaN data
```

```
stats30=stats

yfit =
b(1)+b(2)*Tinvp30+b(3)*phip30+b(4)*C1p30+b(5)*C2p30+b(6)*C3p30+b(7)*C4p30+b(8
)*C5p30+b(9)*C6p30+b(10)*C7p30+b(11)*HOVp30+b(12)*RONp30+b(13)*Sp30;

figure
loglog(y,yfit,'x',y,y,'o')
xlabel('ID Time (ms)','fontsize',12)
ylabel('ID Time Fit (ms)', 'fontsize',12)
title({'Ignition Delay vs 1000/T[K], Phi, Composition, HOV, RON, and S',
'Regression at P = 30 Bar, 0.20< phi <0.15 '}, 'fontsize', 14)
```